Metabolic and Immuno-Reprogramming in Genitourinary Tumors
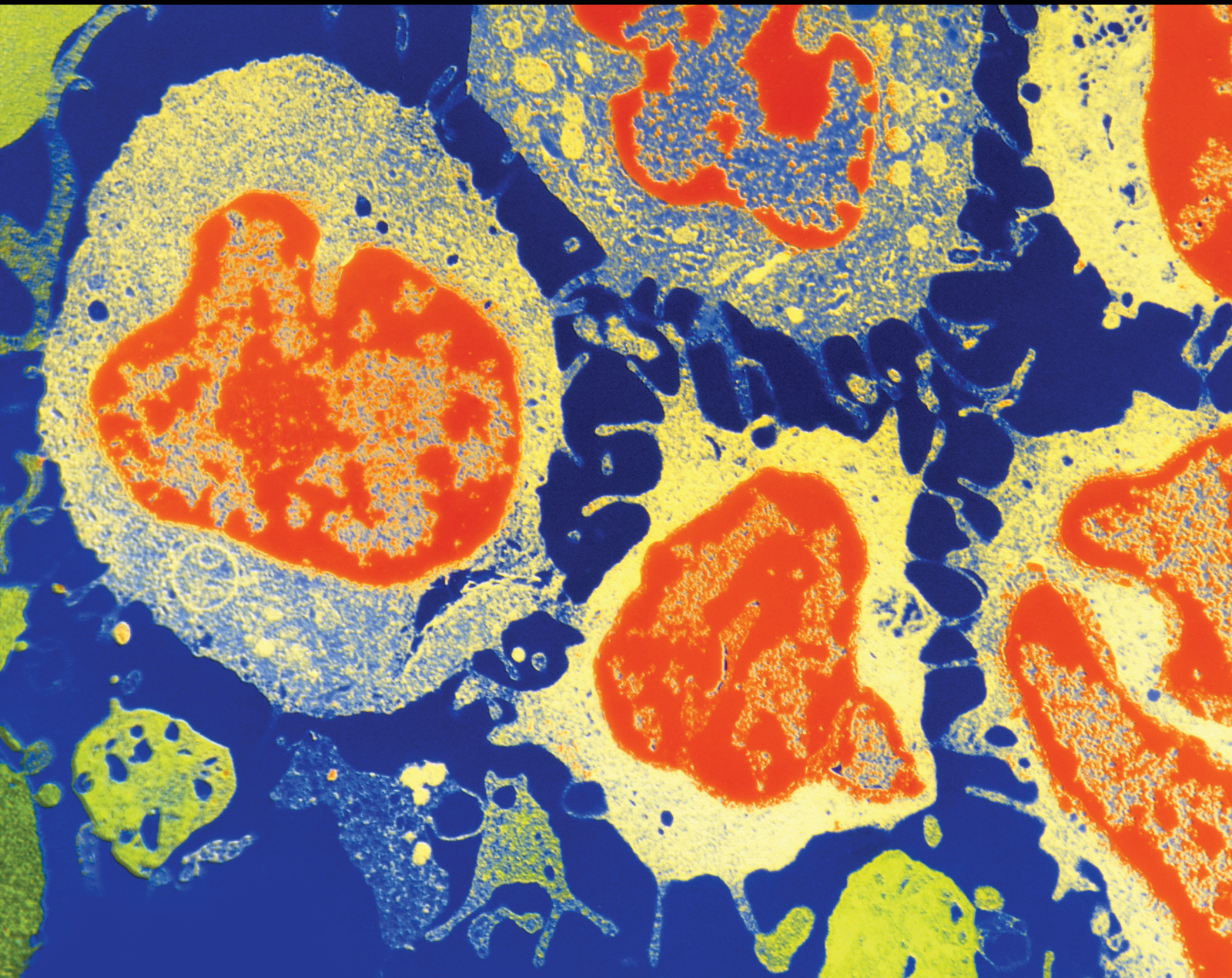
Lead Guest Editor: Yingming Sun
Guest Editors: Shuang-Zheng Jia, Eshan Khan, and Qin Xu

Metabolic and Immuno-Reprogramming in Genitourinary Tumors

Metabolic and Immuno-Reprogramming in Genitourinary Tumors

Lead Guest Editor: Yingming Sun
Guest Editors: Shuang-Zheng Jia, Eshan Khan, and Qin Xu

Contents

Hindawi

Research Article

A 20-Gene Signature Predicting Survival in Patients with Clear Cell Renal Cell Carcinoma Based on Basement Membrane

Zhenjie Yin [ID],[1] **Yu Zhao** [ID],[2] **Weiwen Zhou** [ID],[1] **Chengcheng You** [ID],[3] **Yuanyuan Bai** [ID],[1] **Bingyong You** [ID],[1] **Dongming Lu** [ID],[1] **Shangfan Liao** [ID],[1] **Luoping Zheng** [ID],[1] **Yingming Sun** [ID],[2] **and Yongyang Wu** [ID][1]

[1]*Department of Urology, Affiliated Sanming First Hospital, Fujian Medical University, Sanming, Fujian 365001, China*
[2]*Department of Medical and Radiation Oncology, Affiliated Sanming First Hospital, Fujian Medical University, Sanming, Fujian 365001, China*
[3]*Hubei Key Laboratory of Tumor Microenvironment and Immunotherapy, China Three Gorges University, Yichang, Hubei 443002, China*

Correspondence should be addressed to Yingming Sun; yingmingsun@fjmu.edu.cn and Yongyang Wu; wuyyfj@fjmu.edu.cn

Objectives. The most common subtype of renal cell carcinoma, clear cell renal cell carcinoma (ccRCC), has a high heterogeneity and aggressive nature. The basement membrane (BM) is known to play a vital role in tumor metastasis. BM-related genes remain untested in ccRCC, however, in terms of their prognostic significance. *Methods.* BM-related genes were gleaned from the most recent cutting-edge research. The RNA-seq and clinical data of the ccRCC were obtained from TCGA and GEO databases, respectively. The multigene signature was constructed using the univariate Cox regression and the LASSO regression algorithm. Then, clinical features and prognostic signatures were combined to form a nomogram to predict individual survival probabilities. Using functional enrichment analysis and immune-correlation analysis, we investigated potential enrichment pathways and immunological characteristics associated with BM-related-gene signature. *Results.* In this study, we built a model of 20 BM-related genes and classified them as high-risk or low-risk, with each having its anticipated risk profile. Patients in the high-risk group showed significantly reduced OS compared with patients in the low-risk group in the TCGA cohort, as was confirmed by the testing dataset. Functional analysis showed that the BM-based model was linked to cell-substrate adhesion and tumor-related signaling pathways. Comparative analysis of immune cell infiltration degrees and immune checkpoints reveals a central role for BM-related genes in controlling the interplay between the immune interaction and the tumor microenvironment of ccRCC. *Conclusions.* We combined clinical characteristics known to predict the prognosis of ccRCC patients to create a gene signature associated with BM. Our findings may also be useful for forecasting how well immunotherapies would work against ccRCC. Targeting BM may be a therapeutic alternative for ccRCC, but the underlying mechanism still needs further exploration.

1. Introduction

Approximately 2%–3% of all adult urinary malignancies are renal cell carcinomas (RCC), which are cancers of the kidneys [1]. By 2022, It is estimated that 79,000 additional cases of RCC will be detected in the United States [2]. Clear cell RCC (ccRCC), which accounts for approximately 70%, is the most frequent subtype. Despite advancements in urology technology, the prognosis of advanced RCC remains

unfavorable [3]. Therefore, exploring new biomarkers for prognosis prediction and immunotherapy for ccRCC is crucial.

The tumor microenvironment (TME), which consists of an extracellular matrix (ECM), is strongly associated with cancer development [4]. Basement membrane (BM), a widely distributed ECM, plays an important role in biological systems, such as resisting mechanical stress, dictating tissue shape, and creating diffusion barriers [5]. The

main structural backbone of BM is laminin, collagen IV, nidogens, proteoglycans, and growth factors. As reported in existing studies, abnormalities in the chemical and mechanical properties of the BMs are associated with various diseases including malignant tumors [6–9]. The effect of ECM components on various RCC cell lines is heterogeneous [10], in which BM integrity can serve as a good prognostic marker in RCC [11]. Jayadev R et al. defined and created an extensive network of 224 BM-related genes and further identified their growing association with human disease [12]. Although many studies have investigated prognostic risk signatures of ccRCC previously, none have attempted to develop a prognostic risk signature with BMs in ccRCC, and it is still unclear if these BM-related genes affect patient prognosis.

In this investigation, this bioinformatics analysis was carried out in this work by creating a separate prognostic BM-related gene signature in ccRCC utilizing The Cancer Genome Atlas (TCGA) database and confirming it in the Gene Expression Omnibus (GEO) database. Then, by combining clinical data and prognostic signatures, a novel nomogram was created to predict individual survival rates. Using functional enrichment analysis and immune-correlation analysis, we investigated potential enrichment pathways and immunological characteristics linked with BM-related-gene signature.

2. Methods

2.1. Data Collection.
RNA-Seq data profiles and corresponding clinical information for kidney renal clear cell carcinoma (KIRC) were downloaded from the TCGA dataset (https://portal.gdc.cancer.gov/) [13]. We also downloaded GSE29609 consisting of 39 KIRC tissues from the GEO database (https://www.ncbi.nlm.nih.gov/geo/) for validation. The RCC dataset contained 541 cancerous and 72 normal tissues, accompanied by clinical information. After that, genes associated with BM were culled from the existing literature [12] and listed in Supplementary Table S1.

2.2. Construction of a Prognostic BM-Related Gene Signature.
To identify BM-related DEGs in the TCGA cohort in tumor and paracancer tissues, we used the limma package. To identify potentially predictive genes associated with BM, we performed a univariate Cox analysis of overall survival (OS) and displayed the results with forest plots. By performing automatic feature selection, LASSO Cox regression analysis, a method for screening signatures with generally effective prognostication performance, reduces estimated variance and avoids overfitting while providing an interpretable final model [14]. The R package glmnet was utilized for the analysis, while LASSO regression was utilized for feature selection. Using gene expression and the appropriate Cox regression coefficient, a patient's risk score was determined. $Score = e^{sum(expression \, of \, each \, gene \times corresponding \, coefficient)}$ was the formula developed. The patients were then classified into high- and low-risk categories based on the median risk score. To further examine the difference in OS between high- and low-risk groups,

a Kaplan–Meier (KM) curve was constructed. To evaluate the predictive power of the gene signature and risk score, the time ROC (v0.4) analysis was performed.

2.3. Nomogram Establishment and Subgroup Analysis.
The nomogram was built and calibrated using the survival and rms packages in R version 4.1.0 using the multivariable model coefficients. Harrell's concordance index (C-index) was used to evaluate the nomogram's discriminatory performance. To compile the clinical data, each participant's age, gender, race, pathological grade, T stage, N stage, M stage, and survival information were documented. We performed dichotomies based on clinical information for subgroup analysis. For continuous variables, the ROC curve is utilized to pick the appropriate cut-off value. For categorical variables, we classified them based on the AJCC stage [15], WHO/ISUP classification [16], and current research.

2.4. Protein-Protein Interaction (PPI) and Functional Enrichment Analyses.
To learn more about the protein-protein interactions among the shared prognostic DEGs, we consulted the STRING database (http://www.string-db.org/). Moreover, gene ontology (GO) and kyoto encyclopedia of genes and genomes (KEGG) enrichment analyses were performed on the DEGs using the cluster profiler program.

2.5. Correlation Analysis with Immune Infiltration.
Using the TIMER, CIBERSORT, XCELL, and EPIC algorithms, we explored the correlation between BM-related genes and the degree of immune infiltration. We also utilized violin plots to assess the association between the expression of high- and low-risk groups and immune checkpoints (PDCD1, CD274, CTLA-4, TIGIT, LAG3, and CD28).

3. Results

3.1. Identification of Prognostic BM-Related Genes in the TCGA Cohort.
As part of the TCGA-KIRC cohort, 541 people with ccRCC were enrolled. We collected 224 BM-related genes. 106 BM-related genes were identified as DEGs between ccRCC samples and paracancer samples (FDR < 0.05; Figure 1(a)). The univariate Cox regression analysis showed that 30 BM-related DEGs were correlated with OS (Figure 1(b)). Interactions of BM-related genes were visualized with the PPI networks of the differentially expressed BMs comprising 30 nodes and 82 edges (Figure 1(c)).

3.2. Construction of a Prognostic Model for BM-Related Risk Score.
With the expression profiles of the 30 genes mentioned above, we identified a 20-gene prognostic model by LASSO Cox regression analysis (Supplementary Figure S1 A-B). According to the median of the risk score (Risk score = (0.0143) ∗ ADAMTS2 + (0.0070) ∗ ADAMTS4 + (0.0135) ∗ ADAMTS8 + (−0.0027) ∗ COL15A1 + (−0.03) 35 ∗ COL4A4 + (0.1376) ∗ COL4A6 + (0.0038) ∗ DCN + (0 .1922) ∗ GPC2 + (−0.1173) ∗ HMCN1 + (0.0026) ∗ ITGA5
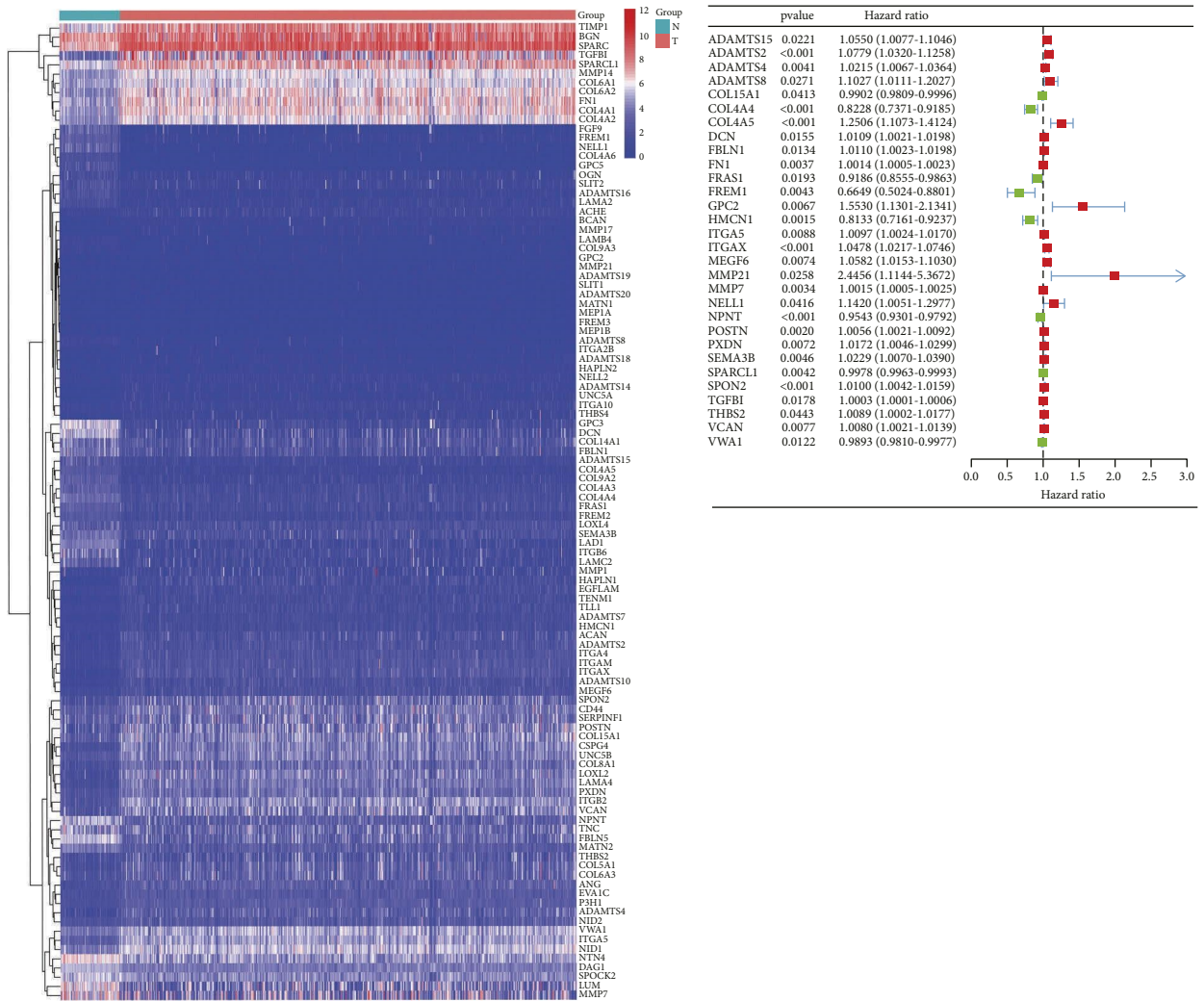
(a)

(b)
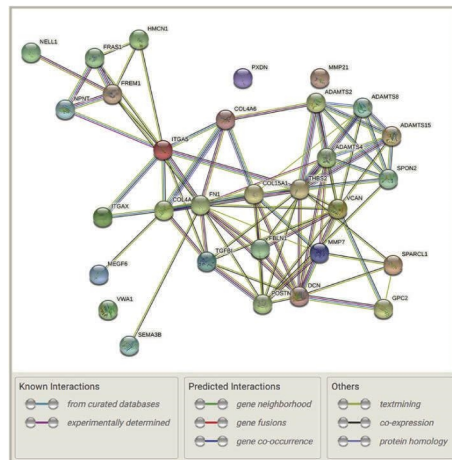
(c)

FIGURE 1: Identification of the candidate BM-related genes in the TCGA cohort. (a) Differentially expressed genes associated with BM are shown using a heatmap. (b) BM-related genes having significant predictive value based on OS are visualized in a forest plot. (c) Candidate gene interactions are mapped out by the PPI network retrieved from the STRING database.

(a)

(b)

(c)

(d)

(e)

(f)

(g)

(h)
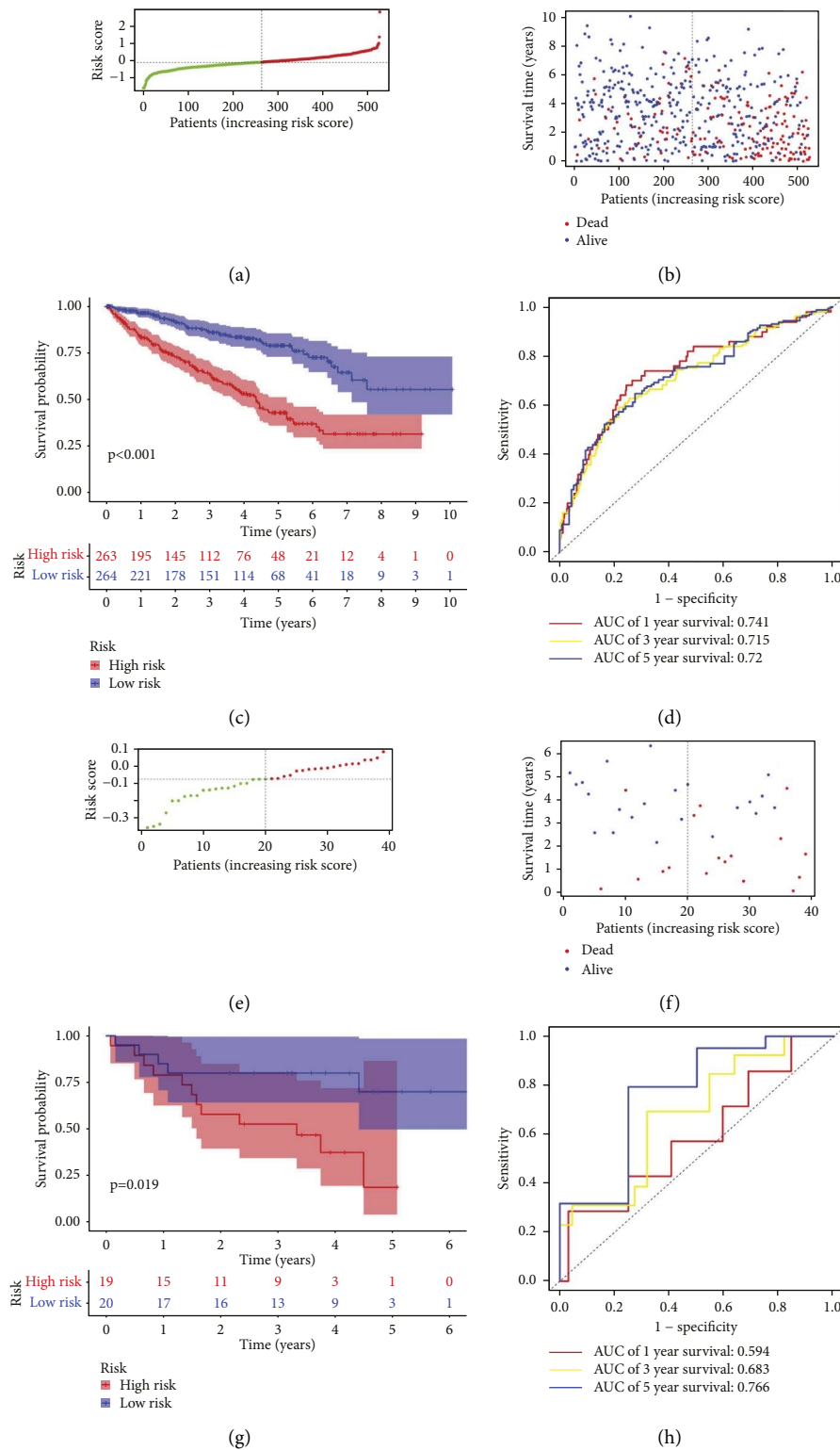
FIGURE 2: Distribution and prognostic analyses of the 20-gene signature in the TCGA cohort and GSE29609 cohort. (a, b) The distributions of the risk scores and corresponding survival status of KIRC patients in the TCGA cohort. (c) KM curves for the OS of ccRCC patients in the high- and low-risk group in the TCGA cohort. (d) The AUC of time-dependent ROC curves confirmed the risk score's prognostic efficacy in the TCGA cohort. (e, f) The distributions of the risk scores and corresponding survival status of the GSE29609 dataset. (g) KM curves for the OS of patients in the high- and low-risk groups in the GSE29609 dataset. (h) The AUC of time-dependent ROC curves confirmed the risk score's prognostic efficacy in the GSE29609 dataset.

	pvalue	Hazard ratio
Age	<0.001	1.8286 (1.3204-2.5325)
Sex	0.6997	0.9389 (0.6814-1.2936)
Race	0.7404	1.0556 (0.7663-1.4542)
Grade	<0.001	1.6120 (1.3519-1.9221)
T	<0.001	1.8481 (1.5767-2.1661)
M	<0.001	4.4503 (3.2348-6.1225)
N	<0.001	3.3957 (1.7869-6.4531)
Riskscore	<0.001	3.2158 (2.2781-4.5395)

(a)

	pvalue	Hazard ratio
Age	0.0116	1.5343 (1.1003-2.1394)
Grade	0.1192	1.1660 (0.9612-1.4144)
T	0.0055	1.3062 (1.0818-1.5771)
M	<0.001	2.7052 (1.8709-3.9115)
N	0.1864	1.5677 (0.8046-3.0547)
Riskscore	<0.001	2.5433 (1.7703-3.6537)

(b)

(c)

(d)

FIGURE 3: Results of Cox regression for risk factors for ccRCC. (a) Outcomes from a univariate Cox regression study of OS in a cohort of patients with ccRCC based on risk signature score and clinical factors. (b) Results of stepwise multivariate cox regression analysis. (c, d) Correlation of risk group and clinical traits.

+ (0.0101) ∗ ITGAX + (0.0137) ∗ MEGF6 + (0.2590) ∗ MMP21 + (0.0003) ∗ MMP7 + (0.0244) ∗ NELL1 + (−0.0181) ∗ NPNT + (0.0109) ∗ PXDN + (0.0022) ∗ SEMA3B + (0.0013) ∗ VCAN + (−0.0048) ∗ VWA1), patients were stratified into high-risk group ($n = 263$) and low-risk groups ($n = 264$) (Figure 2(a)). As shown in Figures 2(b)–2(c), prognosis and risk score were negatively correlated ($p < 0.001$). The defined 20-gene signature was found to be highly effective at predicting the OS for ccRCC patients, as shown by the AUC (AUC = 0.741, 0.715, and 0.720; at 1, 3, and 5 years, respectively, Figure 2(d)). The BM-related genes signature's predictive significance was further verified in the GSE29609 dataset (Figures 2(e)–2(h)). The survival curve confirmed that patients at high risk had a poor prognosis ($p = 0.019$; Figure 2(g)). The AUCs were 0.594, 0.683, and 0.766 at 1, 3, and 5 years, according to the time-dependent ROC curve (Figure 2(g)). Particularly, in the high-risk group, the expression of the 14 risk genes rose, whereas the expression of the six protective genes increased in the low-risk group (Supplementary Figure S2).

3.3. Independent Prognostic Value of the 20-Gene Signature and Subgroup Analysis. The independent predictive significance of the 20-gene signature for OS in the risk model was evaluated using multivariate and univariate Cox regression analysis. Univariate cox analysis revealed that risk score, age, grade, and TNM stage are the prognosis-associated factors ($p < 0.001$; Figure 3(a)). In the multivariable competing-risks regression model predicting OS, the risk score is still an independent predictor for OS (Figure 3(b)). Moreover, we stared into whether the prognostic signature was linked to the onset and progression of KIRC. Grade, T stage, N stage, and M stage were all significantly different between high- and low-risk groups (all $p < 0.001$). However, age and gender were not significantly different ($p > 0.05$) (Figures 3(c)–3(d)). Moreover, their prognostic significance in subgroups was also examined by a stratification study. Our research demonstrated that the BM-based signature performed exceptionally well at predicting outcomes in age ≥ 60, age <60, male, female, white, Grade I-II, Grade III-IV, T1-T2, stage T3-T4 stage, N0-NX stage, M0 stage, and M1 stage (all $p < 0.05$). However, BM-related genes have a poor predictive track record in the N1 and not-white
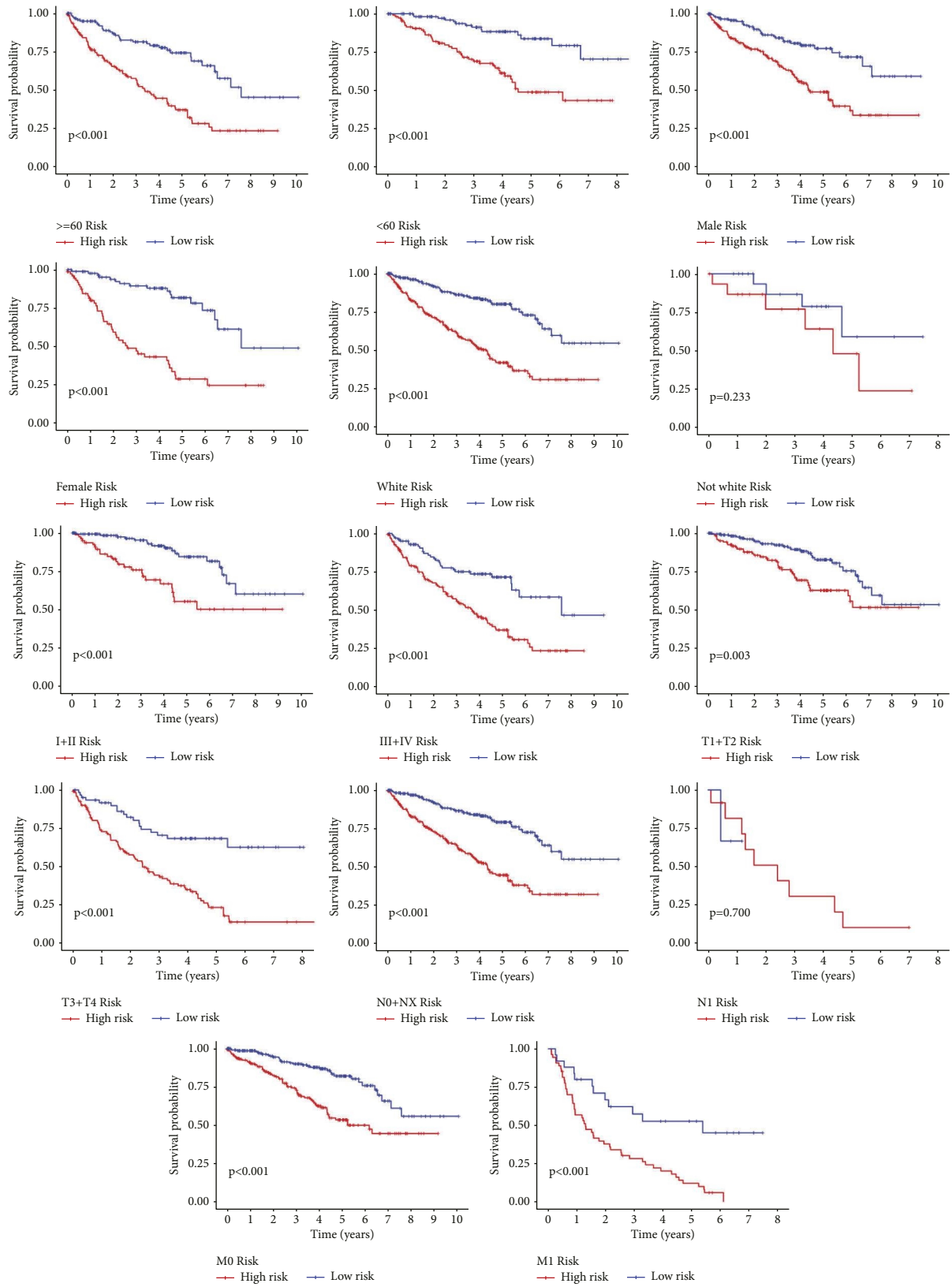
FIGURE 4: Stratified by age, gender, race, grade, T stage, N stage, or M stage, KM curves demonstrate OS disparities between high- and low-risk groups.

(a)

(b)
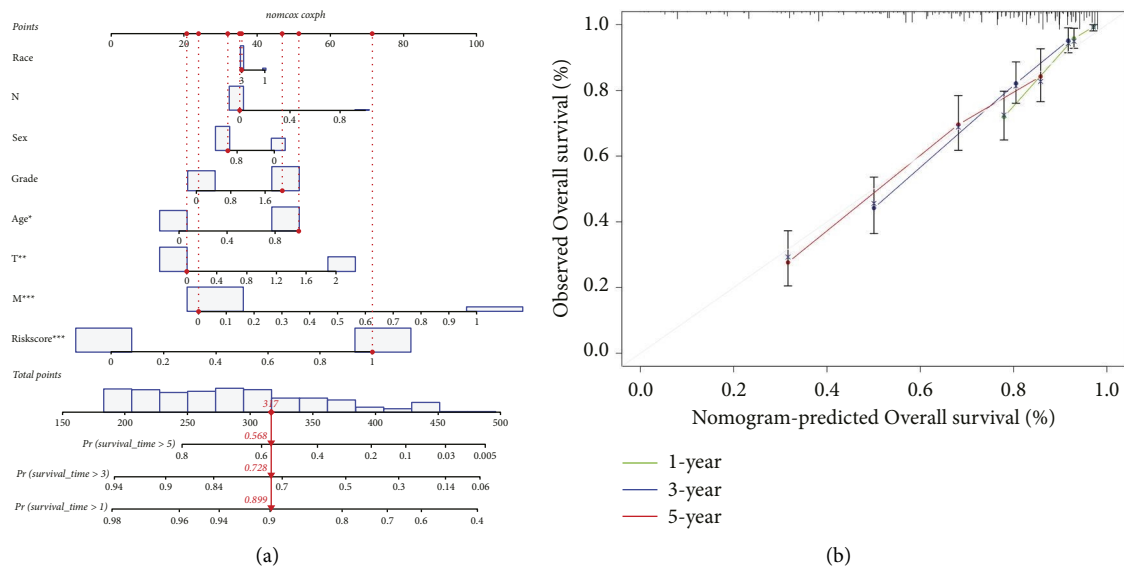
FIGURE 5: Building a nomogram of 20 BM-related genes. (a) A predictive nomogram for predicting 1, 3, and 5 years OS in ccRCC patients. (b) The calibration plots for predicting 1, 3, 5 years OS.

(a)

(b)
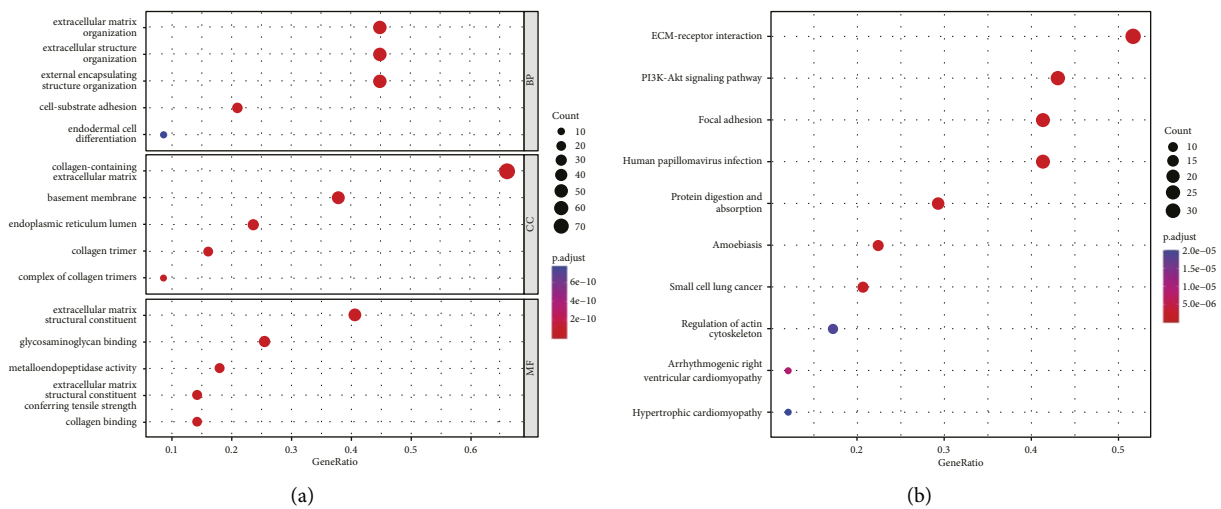
FIGURE 6: Analyses of GO and KEGG with typical findings. (a) Top 5 significant BP, MF, and CC terms in GO analyses. (b) Top 10 significant KEGG signaling pathways.

populations ($p > 0.05$; Figure 4). All independent predictors of OS in the training cohort were integrated to create the nomogram. The inclusion criteria in the nomogram included risk score, age, gender, race, grade, T stage, N stage, and M stage, as shown in Figure 5(a). The C-indexes for the nomogram predictions were 0.776 (95% CI: 0.742–0.810) for the OS. As indicated by the OS calibration plots, the nomogram might accurately estimate the mortality (Figure 5(b)).

3.4. Functional Enrichment Analysis.
20 genes between the high- and low-risk groups were used for GO and KEGG analysis, which shed light on the relationship between risk scores and biological pathways and functions. GO enrichment analysis of the biological process (BP) and molecular functions (MF) showed that DEGs were involved in the

tumor cell migration, including cell-substrate adhesion, extracellular matrix structural constituent, and metallopeptidase activity ($p < 0.05$; Figure 6(a)). Additionally, KEGG enrichment analysis revealed that elements related to tumor invasiveness and metastasis, such as ECM-receptor interaction, focal adhesion, and PI3K-Akt signaling pathway, were significantly enriched ($p < 0.05$; Figure 6(b)).

3.5. Association between BM-Related Genes and Immune Cells.
We used TIMER, CIBERSORT, XCELL, and EPIC to investigate the correlation between 20 genes and immune cell infiltration (Figure 7(a)). By CIBERSORT, CD4+ T cells, CD8+ T cells, NK T cells, regulatory T cells (Tregs), B cells, monocytes, macrophages, and dendritic cells had higher immunocyte infiltration degrees in the high-risk group,

(a)

(b)
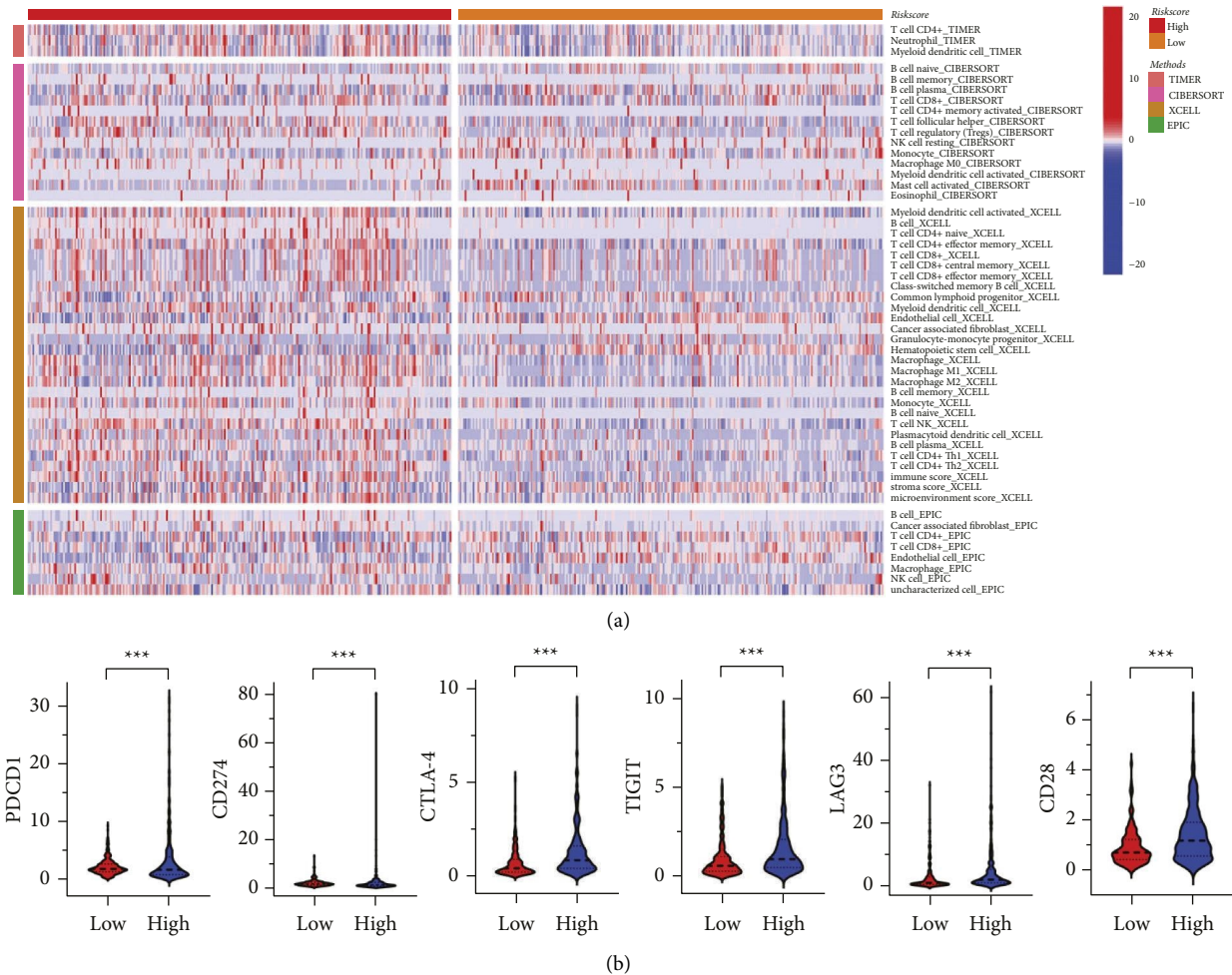
FIGURE 7: The correlation between BM-related DEGs and immune. (a) Immune cell infiltration between high- and low-risk groups. (b) The connection between prognostic signature and immune checkpoints.

whereas endothelial cells, mast cells, and hematopoietic stem cells had lower immunocyte infiltration degrees in the low-risk groups. Blocking immune checkpoint pathways is currently thought to be a promising approach to achieving antitumor immunity. We discovered that the expression of PDCD1, CD274, TIGIT, CTLA-4, LAG3, and CD28 was significantly different between the two groups of ccRCC patients (Figure 7(b)). The findings suggest that BM-related genes are actively involved in controlling how the immune system interacts with ccRCC and how their TME develops.

4. Discussion

There were 224 BM-related genes examined, and of those, 30 DEGs were shown to be connected with ccRCC prognosis. We used LASSO Cox regression to examine data from the TCGA dataset to identify a 20-gene signature (ADAMTS2, ADAMTS4, ADAMTS8, COL15A1, COL4A4, COL4A6, DCN, GPC2, HMCN1, ITGA5, ITGAX, MEGF6, MMP21, MMP7, NELL1, NPNT, PXDN, SEMA3B, VCAN, and VWA1) in ccRCC patients. In the meanwhile, we used the GSE29609 dataset to validate our risk score and showed that

it was effective for predicting ccRCC patients' outcomes. The most important takeaway from our research is the development of a novel BM-based predictive risk profile for ccRCC. This provides a more precise estimation method and a more personalized treatment strategy for the prognosis of ccRCC patients. The risk score is closely related to some clinical features, such as pathological grade and TNM stage. In different subgroups, the vast majority of high-risk groups had worse survival prognoses than lower-risk groups, which reflects the representativeness of BM-related risk scores and has important guiding significance in clinical practice.

In our model, all 20 genes are involved in human cancer occurrence and development, half of which are closely related to RCC (ADAMTS2 [17], COL15A1 [18], COL4A4 [19], DCN [19], ITGA5 [20], ITGAX [21], MMP7 [22], NELL1 [23], SEMA3B [24], and VCAN [25]). The remaining 10 genes still have some papers on their roles in other types of tumors. Cancer development and progression are linked to ADAMTS (a disintegrin and metalloproteinase with thrombospondin motifs) family genes, among which ADAMTS2, 4, and 8 have been shown to have antitumor angiogenesis effects [26–28]. MMP-7 also affects progression

by regulating angiogenesis, making it a potential target for RCC [22]. Moreover, the depletion of VCAN also markedly reduced the invasion and migration of cells, which was correlated with MMP7 reduction [25]. It has been reported that deletion of COL15A1 modulates the tumor ECM and leads to increased tumor growth in the mouse mammary carcinoma model [29]. The transcript levels of COL4A4 and 6 could act as potential indicators for early disease progression in ccRCC [30]. Yongcan et al. defined that DCN deficiency promotes RCC growth and metastasis through the downregulation of P21 and E-cadherin [19]. Guoming et al. verified that GPC2, associated with most immune-infiltrating cells, is highly expressed in pan-cancer [31]. ITGA5 and ITGAX are members of the integrin family, commonly used as receptors for the ECM and can be used as a predictor of the prognosis of the RCC in other models. In vitro and in vivo experiments have revealed ccRCC inhibition of SEMA3B associated with methylation through promoter and intronic CpG islands [24]. It is yet unknown how 20-gene signatures play a role in ccRCC.

GO enrichment analysis uncovered that BM-related genes were mainly related to tumor cell migration, such as cell-substrate adhesion, extracellular matrix structural constituent, and metallopeptidase activity. The result of KEGG enrichment analysis indicated that BM-related genes were mostly implicated in focal adhesion, PI3K-Akt signaling pathway, and ECM-receptor interaction. The epithelial-to-mesenchymal transition (EMT), tumor angiogenesis, and changes in the TME are only a few of the multiple mechanisms that contribute to the evolution of mRCC, which is crucially characterized by tumor cell infiltration and metastasis. Cellular signaling pathways, such as PI3K-Akt-mTOR, play a prominent role in pathological conditions of ccRCC. The PI3K-Akt-mTOR pathway could regulate cell proliferation, growth, cell size, metabolism, and motility [32]. EMT is a self-regulated biological process essential for tissue healing in which cells shed their epithelial cell identity and acquire properties of mesenchymal cells. Not only is EMT essential for development and wound healing but it also plays a key role in tumor formation and metastasis.

Although the effects of tumors on the ECM, especially the BM, have been the focus of research over the recent decades, it remains unclear whether tumor immunity is modulated by BM-related genes. We discovered that CD4+ T cells, CD8+ T cells, Tregs, and macrophages were highly enriched in both groups using risk group-based immunological annotation analysis, which may indicate a potential fundamental regulation between tumor immunity and BM. T cells are major players in immune-mediated cancer control and response to immunotherapy. Endothelial BM on the blood and lymphatic vessels is a limiting step for T cell entry into the TME. Besides its well-documented functions in promoting tumor neoangiogenesis, BMs have also been proposed to regulate the function of T cells. BM not only regulates T cell adhesion and migration but also directly regulates T cell activation, function, proliferation, and survival. Evidence suggests that Tregs have antitumor immunity, and an increased density of macrophages is related to poor clinical prognosis in ccRCC. M2-like macrophages can degrade the tumor ECM, destroy the BM, and recruit immunosuppressor cells, all of which further promote tumor progression and distal metastasis. Currently, a variety of innovative immunotherapies based on targeting immune checkpoint inhibitors (ICIs) are in clinical development and are used to treat mRCC patients, which was consistent with our results that the expression of PD-1, PD-L1, CTLA-4, TIGIT, LAG3, and CD28 have a prominent difference between the two groups. Despite multiple lines of evidence elucidating the functions of diverse immune cells and ICIs in cancer, the underlying mechanisms remain poorly characterized in ccRCC and are lacking in the field of BMs.

In the present study, we shed light on the involvement of BMs in ccRCC and developed a promising risk-prognostic signature. In both the derivation and validation cohorts, this model was found to be independently linked with OS. Research in the molecular underpinnings of tumor immunity in ccRCC has been hampered by a lack of knowledge about the relationship between tumor-associated BM genes and the immune system.

Data Availability

Data are available from the corresponding author upon reasonable request.

Conflicts of Interest

The authors declare that they have no conflicts of interest.

Authors' Contributions

Zhenjie Yin conceptualized and designed the study. Yongyang Wu and Yingming Sun (III) provided the administrative support. Yuanyuan Bai and Chengcheng You (IV) provided the study materials. Dongming Lu, Shangfan Liao, and Luoping Zheng (V) collected and assembled the data. Weiwen Zhou and Bingyong You (VI) carried out data analysis and interpretation. Zhenjie Yin and Yu Zhao (VII) wrote the manuscript. All authors approved the final manuscript.

Acknowledgments

Supplementary Materials

Figure S1 Construction of a BM-related genes risk signature. (A) LASSO coefficient profiles of the 30 DEGs. (B) Ten-foldcross-validation was used to select tuning parameters (λ) in the lasso model. Figure S2 Heatmap for the differences of 20 BM-related genes between high- and low-risk patients.

(A) The TCGA cohort's differences in 20 BM-related genes between high- and low-risk patients. (B) The GSE29609 cohort's differences in 20 BM-related genes between high- and low-risk patients. Table S1. BM-related genes. (*Supplementary Materials*)

References

[1] Cancer Today, "Global cancer observatory: cancer today. International Agency for Research on Cancer," 2021, https://gco.iarc.fr/today.

[2] R. L. Siegel, K. D. Miller, H. E. Fuchs, and A. Jemal, "Cancer statistics, 2022," *CA: A Cancer Journal for Clinicians*, vol. 72, no. 1, pp. 7–33, 2022.

[3] P. C. Barata and B. I. Rini, "Treatment of renal cell carcinoma: current status and future directions," *CA: A Cancer Journal for Clinicians*, vol. 67, no. 6, pp. 507–524, 2017.

[4] C. Roma-Rodrigues, R. Mendes, P. V. Baptista, and A. R. Fernandes, "Targeting tumor microenvironment for cancer therapy," *International Journal of Molecular Sciences*, vol. 20, no. 4, p. 840, 2019.

[5] P. D. Yurchenco, "Basement membranes: cell scaffoldings and signaling platforms," *Cold Spring Harbor Perspectives in Biology*, vol. 3, no. 2, Article ID a004911, 2011.

[6] J. Chang and O. Chaudhuri, "Beyond proteases: basement membrane mechanics and cancer invasion," *Journal of Cell Biology*, vol. 218, no. 8, pp. 2456–2469, 2019.

[7] S. Morgan, D. Dodington, J. M. Wu, and G. Turashvili, "Solid papillary carcinoma and encapsulated papillary carcinoma of the breast: clinical-pathologic features and basement membrane studies of 50 cases," *Pathobiology*, vol. 88, no. 5, pp. 359–373, 2021.

[8] K. Koikawa, K. Ohuchida, Y. Ando et al., "Basement membrane destruction by pancreatic stellate cells leads to local invasion in pancreatic ductal adenocarcinoma," *Cancer Letters*, vol. 425, pp. 65–77, 2018.

[9] M. Klobučar, M. Sedić, P. Gehrig et al., "Basement membrane protein ladinin-1 and the MIF-CD44-β1 integrin signaling axis are implicated in laryngeal cancer metastasis," *Biochimica et Biophysica Acta - Molecular Basis of Disease*, vol. 1862, no. 10, pp. 1938–1954, 2016.

[10] S. Majo, S. Courtois, W. Souleyreau, A. Bikfalvi, and P. Auguste, "Impact of extracellular matrix components to renal cell carcinoma behavior," *Frontiers in Oncology*, vol. 10, p. 625, 2020.

[11] L. Morell-Quadreny, J. Rubio, J. A. Lopez-Guerrero et al., "Disruption of basement membrane, extracellular matrix metalloproteinases and E-cadherin in renal-cell carcinoma," *Anticancer Research*, vol. 23, no. 6d, pp. 5005–5010, 2003.

[12] R. Jayadev, M. R. P. T. Morais, J. M. Ellingford et al., "A basement membrane discovery pipeline uncovers network complexity, regulators, and human disease associations," *Science Advances*, vol. 8, no. 20, Article ID eabn2265, 2022.

[13] J. Liu, T. Lichtenberg, K. A. Hoadley et al., "An integrated TCGA pan-cancer clinical data resource to drive high-quality survival outcome analytics," *Cell*, vol. 173, no. 2, pp. 400–416.e11, 2018.

[14] R. Tibshirani, "The lasso method for variable selection in the Cox model," *Statistics in Medicine*, vol. 16, no. 4, pp. 385–395, 1997.

[15] H. Moch, W. Artibani, B. Delahunt et al., "Reassessing the current UICC/AJCC TNM staging for renal cell carcinoma," *European Urology*, vol. 56, no. 4, pp. 636–643, 2009.

[16] B. Delahunt, J. N. Eble, L. Egevad, and H. Samaratunga, "Grading of renal cell carcinoma," *Histopathology*, vol. 74, no. 1, pp. 4–17, 2019.

[17] A. Roemer, L. Schwettmann, M. Jung et al., "Increased mRNA expression of ADAMs in renal cell carcinoma and their association with clinical outcome," *Oncology Reports*, vol. 11, no. 2, pp. 529–536, 2004.

[18] M. R. Morris, C. Ricketts, D. Gentle et al., "Identification of candidate tumour suppressor genes frequently methylated in renal cell carcinoma," *Oncogene*, vol. 29, no. 14, pp. 2104–2117, 2010.

[19] Y. Xu, Q. Xia, Q. Rao et al., "DCN deficiency promotes renal cell carcinoma growth and metastasis through down-regulation of P21 and E-cadherin," *Tumor Biology*, vol. 37, no. 4, pp. 5171–5183, 2016.

[20] J. Boguslawska, H. Kedzierska, P. Poplawski, B. Rybicka, Z. Tanski, and A. Piekielko-Witkowska, "Expression of genes involved in cellular adhesion and extracellular matrix remodeling correlates with poor survival of patients with renal cancer," *The Journal of Urology*, vol. 195, no. 6, pp. 1892–1902, 2016.

[21] Y. Sui, K. Lu, and L. Fu, "Prediction and analysis of novel key genes ITGAX, LAPTM5, SERPINE1 in clear cell renal cell carcinoma through bioinformatics analysis," *PeerJ*, vol. 9, Article ID e11272, 2021.

[22] Y. Miyata, T. Iwata, K. Ohba, S. Kanda, M. Nishikido, and H. Kanetake, "Expression of matrix metalloproteinase-7 on cancer cells and tissue endothelial cells in renal cell carcinoma: prognostic implications and clinical significance for invasion and metastasis," *Clinical Cancer Research*, vol. 12, no. 23, pp. 6998–7003, 2006.

[23] R. Nakamura, T. Oyama, R. Tajiri et al., "Expression and regulatory effects on cancer cell behavior of NELL1 and NELL2 in human renal cell carcinoma," *Cancer Science*, vol. 106, no. 5, pp. 656–664, 2015.

[24] V. I. Loginov, A. A. Dmitriev, V. N. Senchenko et al., "Tumor suppressor function of the SEMA3B gene in human lung and renal cancers," *PLoS One*, vol. 10, no. 5, Article ID e0123369, 2015.

[25] Y. Mitsui, H. Shiina, T. Kato et al., "Versican promotes tumor progression, metastasis and predicts poor prognosis in renal carcinoma," *Molecular Cancer Research*, vol. 15, no. 7, pp. 884–895, 2017.

[26] J. Dubail, F. Kesteloot, C. Deroanne et al., "ADAMTS-2 functions as anti-angiogenic and anti-tumoral molecule independently of its catalytic activity," *Cellular and Molecular Life Sciences*, vol. 67, no. 24, pp. 4213–4232, 2010.

[27] N. Rao, Z. Ke, H. Liu et al., "ADAMTS4 and its proteolytic fragments differentially affect melanoma growth and angiogenesis in mice," *International Journal of Cancer*, vol. 133, no. 2, pp. 294–306, 2013.

[28] Y. Zhang, K. Hu, Z. Qu, Z. Xie, and F. Tian, "ADAMTS8 inhibited lung cancer progression through suppressing VEGFA," *Biochemical and Biophysical Research Communications*, vol. 598, pp. 1–8, 2022.

[29] G. Martínez-Nieto, R. Heljasvaara, A. Heikkinen et al., "Deletion of Col15a1 modulates the tumour extracellular matrix and leads to increased tumour growth in the MMTV-PyMT mouse mammary carcinoma model," *International Journal of Molecular Sciences*, vol. 22, no. 18, p. 9978, 2021.

[30] B. Tu, Y. Zhang, Y. Jia et al., "Prognostic values of COL4As transcriptional expressions in clear cell renal cell carcinoma patients," *Combinatorial Chemistry & High Throughput Screening*, 2022.

[31] G. Chen, D. Luo, N. Zhong et al., "GPC2 is a potential diagnostic, immunological, and prognostic biomarker in pancancer," *Frontiers in Immunology*, vol. 13, Article ID 857308, 2022.

[32] A. S. Alzahrani, "PI3K/Akt/mTOR inhibitors in cancer: at the bench and bedside," *Seminars in Cancer Biology*, vol. 59, pp. 125–132, 2019.

Hindawi

Research Article

CDCA3 Predicts Poor Prognosis and Affects CD8⁺ T Cell Infiltration in Renal Cell Carcinoma

Yuanyuan Bai [ID], **Shangfan Liao** [ID], **Zhenjie Yin** [ID], **Bingyong You** [ID], **Dongming Lu** [ID], **Yongmei Chen** [ID], **Daoxun Chen** [ID], and **Yongyang Wu** [ID]

Department of Urology, Affiliated Sanming First Hospital, Fujian Medical University, Sanming, 365100 Fujian, China

Correspondence should be addressed to Yongyang Wu; wuyyfj@fjmu.edu.cn

Background. Cell division cycle associated 3 (CDCA3) mediates the ubiquitination WEE1 kinase at G2/M phase. However, its contribution to cancer immunity remains uncertain. *Methods.* We first evaluated the effect of CDCA3 on the prognosis of patients with renal cell carcinoma (RCC). The results of bioinformatics analysis were verified by the tissue microarray, immunofluorescence (IF) staining, CCK-8 assay, colony formation, cell cycle, and Western blot. *Results.* Bioinformatics analysis predicated CDCA3 was an independent predictor of poor prognosis in RCC and was associated with poor TNM stage and grade. CDCA3 was related to the infiltration of CD8⁺ T cells and Tregs. Tissue microarray demonstrated that CDCA3 was strongly associated with poor prognosis and positively relevant to CD8⁺ T infiltration. In vitro experiments showed that exgenomic interference of CDCA3 could attenuate cellular proliferation, arrest cell cycle, and blockade accumulation of CDK4, Bub3, and Cdc20 in mitosis process. *Conclusion.* CDCA3 presents as a good biomarker candidate to predict the prognosis of RCC patients and potentiates the immune tumor microenvironment (TME) of RCC.

1. Introduction

Renal cell carcinoma (RCC) is a malignancy from the kidney epithelium and the mobility has steadily increased globally in recent years [1]. The first-line antiangiogenic therapies such as tyrosine kinase inhibitors (TKI) have presented the certain effect for RCC patients, however, the response is discontinued in short time for the majorities [2]. Immune checkpoint inhibitors (ICIs) usher a new time of cancer therapeutic strategies via sparking anticancer immunity [3]. CD8⁺ T cells serve as an essential effector and partially relevant to the effect of ICI [4]. Traditionally, RCC is considered as an immunogenic cancer, and immunotherapy has shown a certain effect of RCC [5, 6]. In clinical practices, we observe the effect of ICIs is diversified, however, scholars fail to find a good candidate to predicate the response and adverse effects (AEs) of ICI in RCC treatment. The biomarkers will also help identify subgroups that respond to immunotherapy and avoid severe AEs.

Cell division malfunctions trigger tumor development and antitumor immune response [7]. CDCA3 has been shown to be a poor prognostic factor for renal papillary cell carcinoma, nonsmall cell lung cancer, etc. [8–10]. Scholars reveal that CDCA3 was upregulated in RCC and promote tumor progression and sunitinib resistance [11] via activating the NF-κB/cyclin D1 signaling axis [12]. There are data indicating that CDCA3 can serve as an important biomarker to evaluate the therapeutic sensitivity of TKI and therefore it would be appropriate to underline this aspect also in light of the possible associations of immunological therapies and TKI in various types of malignant tumors [13]. Moreover it should be very interesting to test the role of CDCA3 as a predictive biomarker of toxicity related to a prolonged use of these novel agents in combination therapy of RCC [14]. However, the immune impact of CDCA3 has also not been well reported.

In this paper, we try to evaluate the predicable performance of CDCA3 in RCC and figure out the attribution of

(a)

(b)

(c)

(d)

(e)

(f)

(g)

(h)
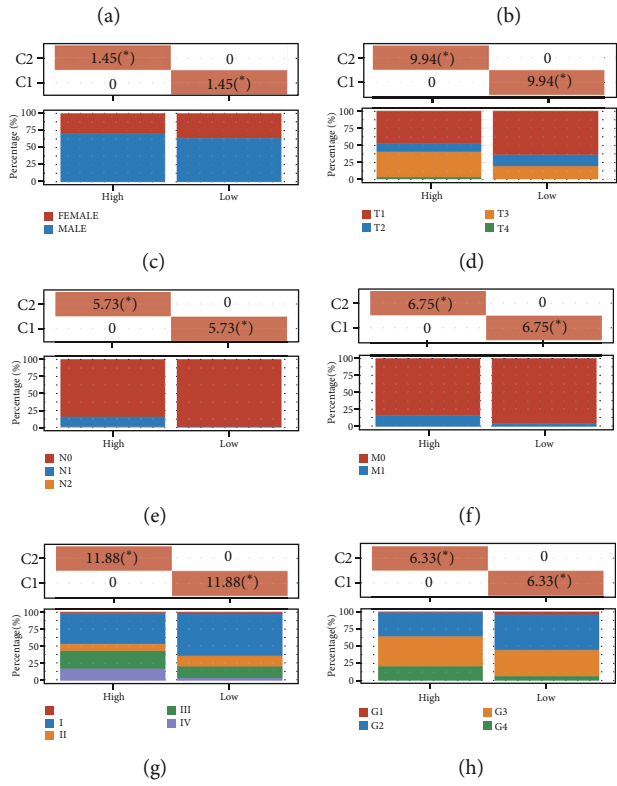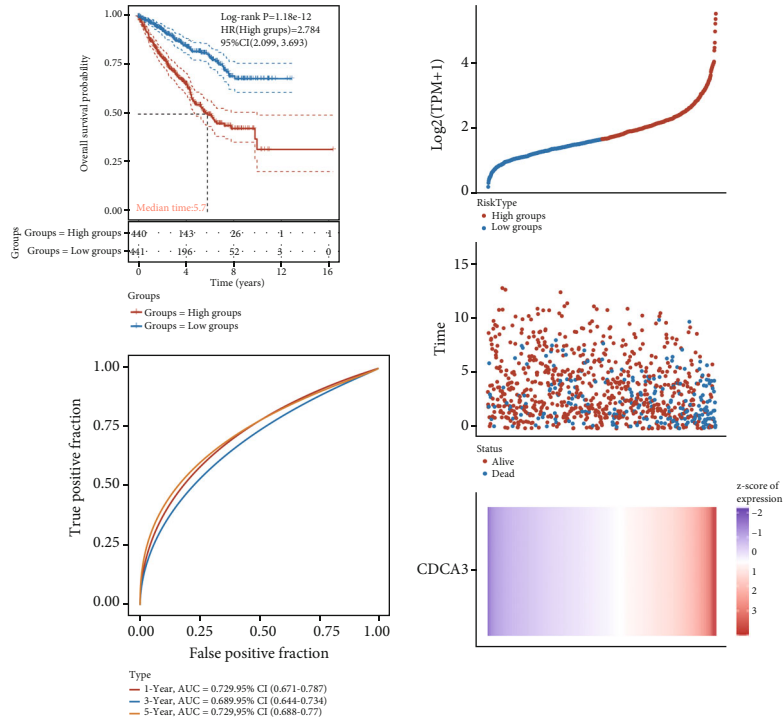
FIGURE 1: Continued.

(i)

(j)

(k)
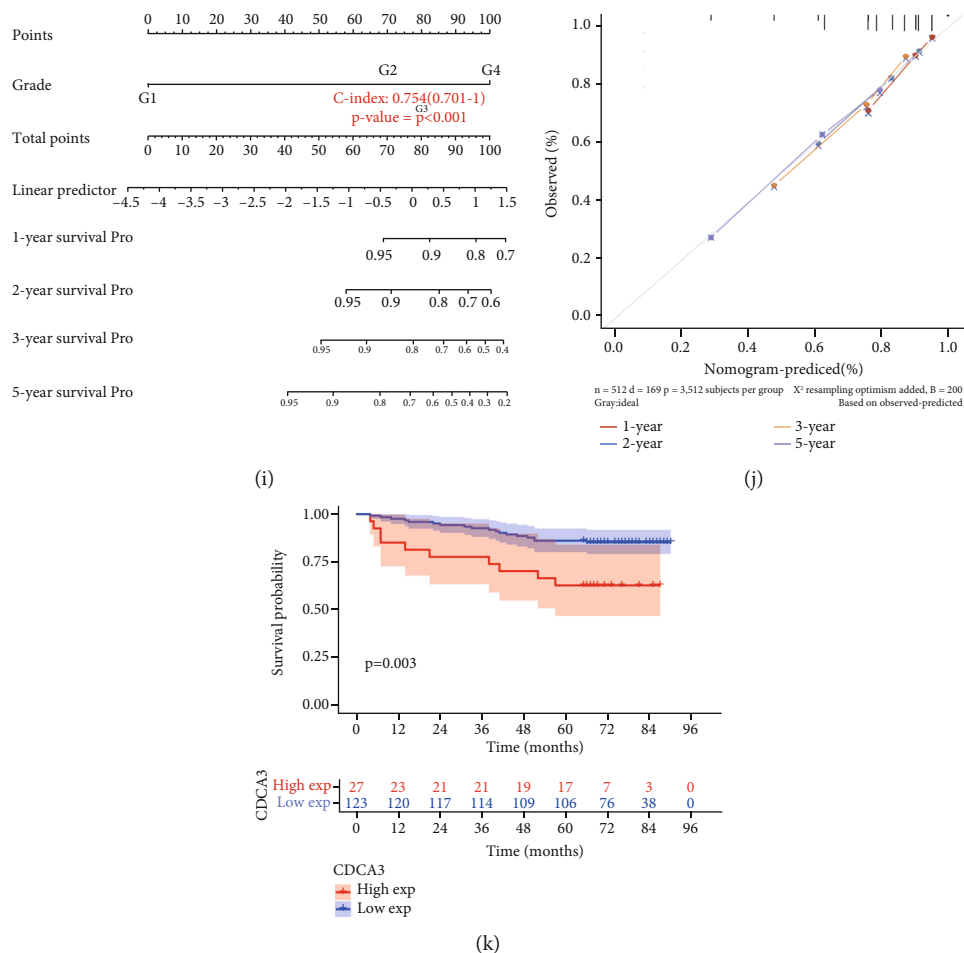
Figure 1: CDCA3 may be an independent prognostic factor for RCC. Survival curves, ROC curves (a), and mortality risk curves (b) of patients with different CDCA3 expression levels. (c–h) Comparison of distribution of gender, T, N, M stage, clinical stage, and grade among patients with different CDCA3 expression. CDCA3-related nomogram (i) and calibration curve (j) predict OS of the RCC patients. (k) Survival curve of patients with different CDCA3 expression in tissue microarray.($^*p < 0.05$, $^{**}p < 0.01$, $^{***}p < 0.001$).

Table 1: Univariate and multivariate COX regression analysis.

Uni-COX	p value	Hazard ratio (95% CI)	Multi-COX	p value	Hazard ratio (95% CI)
CDCA3	< 0.0001	2.34698 (2.0353, 2.70639)	CDCA3	< 0.0001	1.71293 (1.41056, 2.08011)
Age	< 0.0001	1.028 (1.01694, 1.03918)	Age	< 0.0001	1.03039 (1.01629, 1.04468)
Gender	0.4682	0.9037 (0.68738, 1.1881)			
Race	0.5979	1.10877 (0.75541, 1.62743)			
Clinical stage	< 0.0001	2.01609 (1.79567, 2.26356)	Clinical stage	< 0.0001	1.52842 (1.31228, 1.78016)
Grade	< 0.0001	2.29073 (1.86981, 2.80639)	Grade	0.0029	1.41708 (1.12665, 1.78237)

CDCA3 to TME of RCC. Finally, we endorse that targeting CDCA3 would be a potential therapeutic way to flight RCC.

2. Methods and Materials

2.1. Data Collection and Preprocessing. The RNA-seq data, clinical information, somatic mutation data, and microsatellite instability (MSI) status of 881 RCC were all from The Cancer Genome Atlas (TCGA, https://portal.gdc.cancer.gov/) portal. Patients were divided into high expression

group and low expression group based on the median of gene expression. We first drew Kaplan-Meier (KM) survival curve, receiver operating characteristic (ROC) curve, and risk curve to study the prognosis of patients in terms of overall survival (OS). Next, we analyzed the differences in clinical data including gender, clinical stage, TNM stage, and grade among different expression groups of CDCA3. In addition, we used univariate and multivariate COX regression to analyze the prognostic significance of CDCA3 expression and clinical data. At the same time, we drew a nomogram

Table 2: CDCA3 expression and demographic and clinicopathological characteristics.

| | CDCA3 | | N | p value |
	Low	High		
Age				
≥57	58	16	74	
<57	65	11	76	0.666
Gender				
Female	33	10	43	
Male	90	17	107	0.408
Size(cm^3)				
≤175	62	13	75	
>175	61	14	75	1.000
T				
T1-2	116	23	139	0.215
T3	7	4	11	
N				
N0	121	26	147	
N1-2	2	1	3	1.000

diagram and calibration curve to better interpret the prognostic significance of CDCA3. Moreover, fold change = 2 was used to compare the differences of gene expression among different expression groups of CDCA3, and a heat map of differentially expressed genes was drawn to show the expression trend in different groups. Finally, considering that CDCA3 can be used as an oncogene to affect the progression of tumor, we performed Gene Ontology (GO) and Kyoto Encyclopedia of Genes and Genomes (KEGG) enrichment analysis on the upregulated genes of CDCA3 in different expression groups to identify CDCA3 functional pathway localization in tumors.

2.2. Correlation between Tumor Immune Cell Infiltration and CDCA3 Gene Expression. Cell type Identification By Estimating Relative Subsets Of RNA Transcripts (CIBER-SORT) algorithm was used to estimate the infiltration proportion of 22 kinds of immune cells in normal kidney and RCC samples to describe the profile of immune cell infiltration in RCC. The abundance of immune cells infiltration and the expression of 8 important immune checkpoints (CD274, CTLA4, HAVCR2, LAG3, PDCD1, PDCD1LG2, TIGIT, and SIGLEC15) among different CDCA3 expression groups were compared. Finally, we also analyzed the correlation between CDCA3 expression with tumor mutation burden (TMB) and MSI. Tumor Immune Single-cell Hub (TISCH, http://tisch.comp-genomics.org/) is a scRNA-seq database focusing on TME. We obtained the relationship between CDCA3 and RCC TME at single-cell level in TISCH.

2.3. Cell Culture and Transfection of Lentivirus. Caki-1 and 786-O were purchased from the Type Culture Collection (Chinese Academy of Sciences, Shanghai, China). Cells were cultured in RPMI-1640 medium (HyClone, USA) with 10% fetal bovine serum (Gibco, Grand Island, NY, USA). The culture was maintained in a humidified incubator with 37°C, 5% CO_2. CDCA3 knockdown lentivirus was designed by Obio Technology Corp (Shanghai, China). Then, Caki-1 and 786-O were transfected with the lentivirus, according to the manufacturer's instructions. Two days later, puromycin was added for screening. Knockdown efficiencies of CDCA8 were assessed by Western blot.

2.4. Western Blotting. Cultured cell lysates were prepared using a Column Tissue & Cell Protein Extraction Kit (Epizyme, Shanghai, China; # PC201PLUS). Then total proteins were then separated on 10% SDS polyacrylamide gels. After overnight incubation with various primary antibodies, including anti-CDCA3 (Proteintech, 15594-1-AP), CDK4 (Proteintech, 11026-1-AP), Cdc20 (Proteintech, 10252-1-AP), Bub3 (Proteintech, 27073-1-AP), and anti-GADPH (CST, #5174) at 4°C, membranes were washed thrice for 5 min each time, using TBST (in 0.1% Tween20). Then, they were incubated in the presence of a secondary rabbit antibody (1 : 1000, LF102, Epizyme) for 1 h and washed thrice using TBST for 5 min each time. Signals were detected using the chemiluminescence system.

2.5. Cell Proliferation Assay. The cells were seeded in 96-well plates (1,000 cells/well) and cultured for 1, 2, and 3 days. After adding 10 μl CCK-8 (Dojindo, Japan) to each well and incubating at 37°C for 2 h, the absorbance at 450 nm was measured by the Rayto-6000 system (Rayto, China).

2.6. Colony Formation Assay. For cell proliferation, we seeded 200 cells to each well of 6-well plates for 14 days, then fixed with 4% paraformaldehyde (PFA) and stained with crystal violet. The cells were photographed, and the numbers of colonies were counted.

2.7. Flow Cytometry. Cell cycle analysis was performed using a Cell Cycle Staining Kit (MultiSciences, Hangzhou, China), as instructed by the manufacturer. Cells were washed using PBS, after which 1 ml of DNA staining solution and 10 μl of permeate were added to the cell suspension and vortexed to mix. Finally, cells were stained in the dark at 4°C for 30 min and analyzed by flow cytometry. The stained cells were assessed by flow cytometry (BD FACSCanto [TM] II, USA), and analysed by FlowJo vX.0.7 software.

2.8. Tissue Microarray. The RCC tissue microarray was purchased from Outdo (Shanghai, China) and contains 150 RCC tissues and 30 paired paracancer tissues along with their survival, clinical information, etc. Samples were collected from the National Human Genetic Resources Sharing Service platform (2005DKA21300). All points on the chip were detected by Immunofluorescence (IF). The expression of CDCA3, CD8, CD4, CD68, FOXP3, and PD-1 was detected by intensity and positive number of IF. We divided 150 RCC patients into two groups based on the optimal CDCA3 cut-off value and plotted survival curves to identify their prognostic significance. Finally, we analyzed the correlation between CDCA3 and CD8, CD4, FOXP3, CD68, and PD-1.

(a)

(b)

(c)

(d)

(e)

(f)

FIGURE 2: Continued.

(g)

(h)
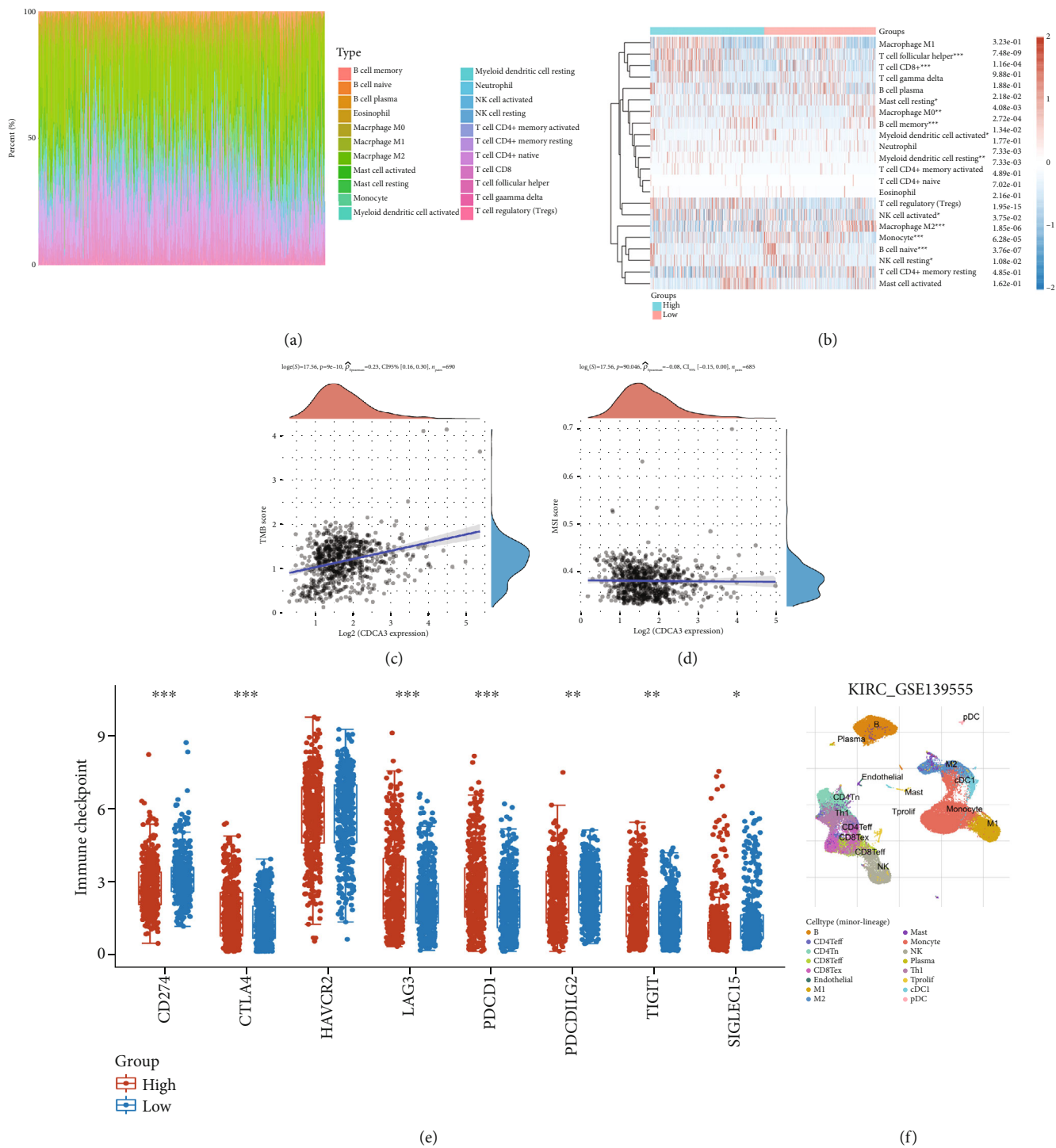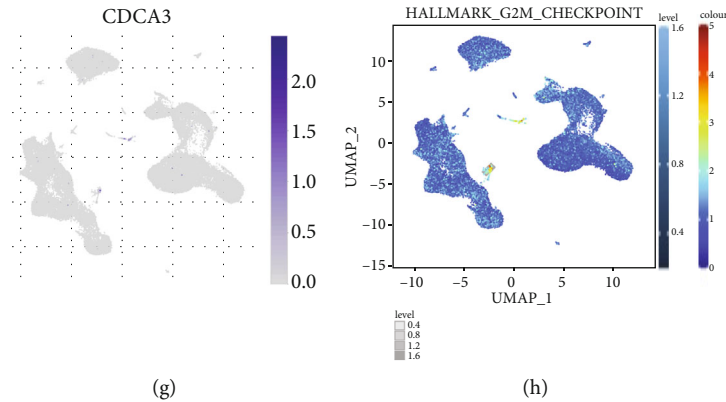
FIGURE 2: CDCA3 affects immune infiltration in RCC. (a) The distribution of immune cells infiltration in RCC. (b) Comparison of immune cells infiltration between different CDCA3 expression groups. (c) Correlation analysis between CDCA3 and TMB. (d) Correlation analysis between CDCA3 expression and MSI. (e) Comparison of 8 immune checkpoints in different expression groups of CDCA3. (f) Single-cell level distribution of immune cells in RCC. (g) Expression of CDCA3 in immune cells. (h) The relationship between CDCA3 and the G2/M checkpoint in immune cells. ($^*p < 0.05$, $^{**}p < 0.01$, $^{***}p < 0.001$).

2.9. Immunofluorescence Staining. Tissue microarray were deparaffinized by graded alcohol and then washed three times with phosphate-buffered saline (PBS), permeabilized with 0.4% Triton X-100 for 30 min, and blocked with goat serum working liquid (Wuhan Boster Biological Technology, Wuhan, China) for 2 hours after antigen retrieval. The sections were then incubated overnight with mixed primary antibodies at 4°C, washed in PBS to remove unbound primary antibodies, and incubated with secondary antibodies in the dark at room temperature (RT) for 1 hour. The sections were counterstained with $4'$, 6 diamidino-2-phenylindole (Sigma-Aldrich) for 5 minutes and washed with PBS. The primary antibodies included CDCA3 (Proteintech, 15594-1-AP). The fluorophore-conjugated secondary antibodies used were goat anti-rabbit Alexa Fluor 488 (1: 500; Abbkine, Wuhan, China) and goat anti-mouse Alexa Fluor 549 (1: 500; Abbkine, Wuhan, China). Images were captured by confocal laser scanning microscopy (Nikon A1 + R, Japan). The fluorescence intensity was analyzed by using the ImageJ software.

2.10. Statistical Analysis. In this study, R (version 4.0.2), GraphPad Prism 8, and SPSS 20.0 software were used to analyze the data. Survival, survminer, timeROC, rms, Limma, ggplot2, pheatmap, and ClusterProfiler R package were used in this study. The significance of differences between groups was assessed by the student T test. Chi-square test was used for categorical variables, and Wilcoxon test was used for continuous data. Survival differences were calculated using Kaplan-Meier and logarithmic rank tests.

3. Results

3.1. Prognostic Significance of CDCA3 in RCC. First, KM survival analysis of TCGA-RCC revealed a shorter survival time in the high-CDCA3 expression group versus the low-CDCA3 expression group ($p < 0.001$, $n = 881$). ROC curves suggested a good accuracy of CDCA3 expression in predicting RCC prognosis ($AUC = 0.729$, Figure 1(a)). The risk

curve showed higher mortality in high-CDCA3 patients than low-CDCA3 patients (Figure 1(b)). Among the patients with different CDCA3 expression groups, gender, TNM stage, clinical stage, and grade showed differences in distribution (Figures 1(c)–1(h)). Univariate and multivariate COX analysis showed that CDCA3, age, TNM stage, and grade could be used as prognostic factors of RCC, and CDCA3 could independently predict the prognosis of RCC (Table 1). We also constructed the prognostic nomogram and calibration curve of RCC, and the 5-year overall survival rate could be estimated according to the total score ($C - index = 0.754$, Figures 1(i) and 1(j)). Demographic characteristics and pathological baseline of tissue microarray were listed in Table 2, showing that high CDCA3 expression levels predicted shorter survival ($p = 0.003$, Figure 1(k)), which proves the bioinformatics analysis. In summary, CDCA3 can be an independent prognostic factor and reflect the rate of tumor progression tumor progression in RCC.

3.2. CDCA3 Is Related to Immune Infiltration. Figure 2(a) showed the infiltration of immune cells in RCC. On this basis, we further analyzed the different abundance of immune cell infiltration among different CDCA3 expression groups (Figure 2(b)). The infiltration of $CD8^+$ T cell ($p < 0.001$), Tregs ($p < 0.001$), memory B cell ($p < 0.001$), follicular helper T cell ($p < 0.001$), activated NK cell ($p < 0.05$), and M0 macrophage ($p < 0.01$) was upregulated in the patients with high expression of CDCA3, while naive B cell ($p < 0.001$), resting NK cell ($p < 0.05$), Monocyte ($p < 0.001$), and M2 macrophage ($p < 0.001$) was downregulated. TMB and MSI levels reflect tumor surface neoantigen abundance and can stimulate antitumor immune response. CDCA3 was also positively correlated with TMB ($p < 0.001$, $r = 0.23$, Figure 2(c)) and negatively correlated with MSI ($p = 0.046$, $r = -0.08$, Figure 2(d)). CD274 (PD-L1, $p < 0.001$), PDCD1LG2 (PD-L2, $p < 0.01$), and SIGLEC15 ($p < 0.05$) were downregulated in patients with high expression of CDCA3, while CTLA4 ($p < 0.001$), LAG3 ($p < 0.001$), PDCD1 (PD-1, $p < 0.001$), and TIGIT ($p < 0.01$) were
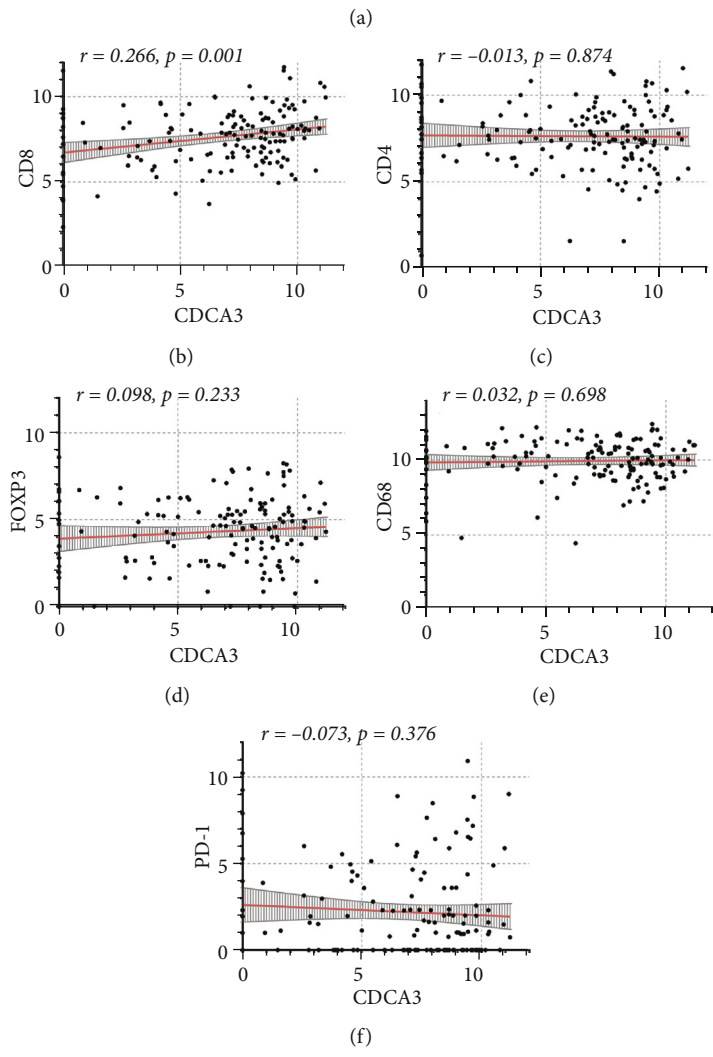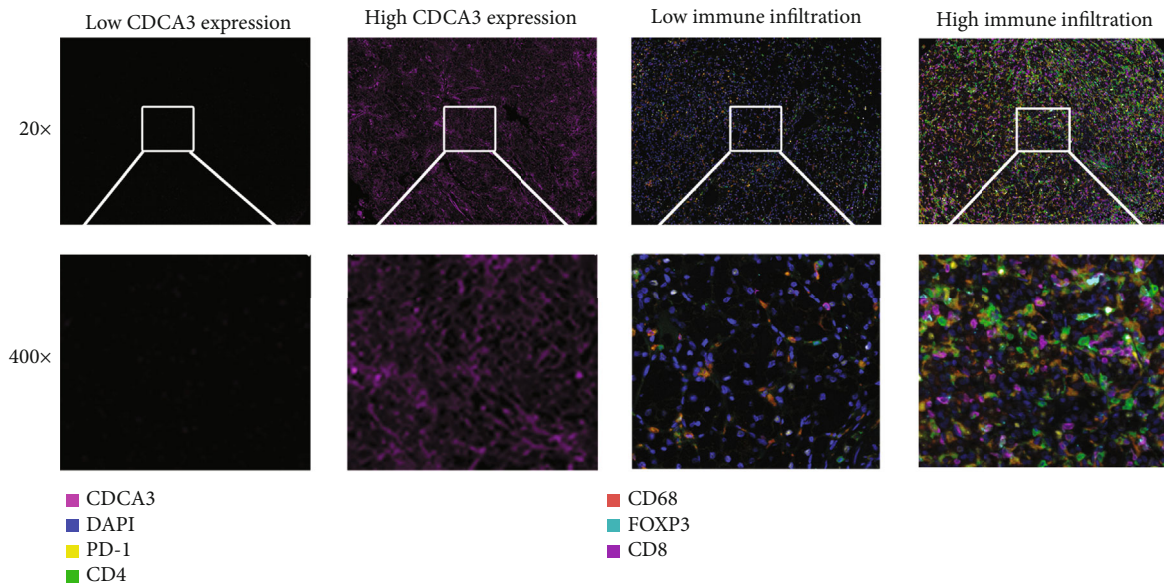
FIGURE 3: The relationship between CDCA3 and immune cell infiltration in tissue microarray. (a) Representative images of IF staining in tissues microarray. (b–f) Correlation between CDCA3 and CD8, CD4, FOXP3, CD68, FOXP3, and PD-1.

(a)

(b)

(c)

(d)
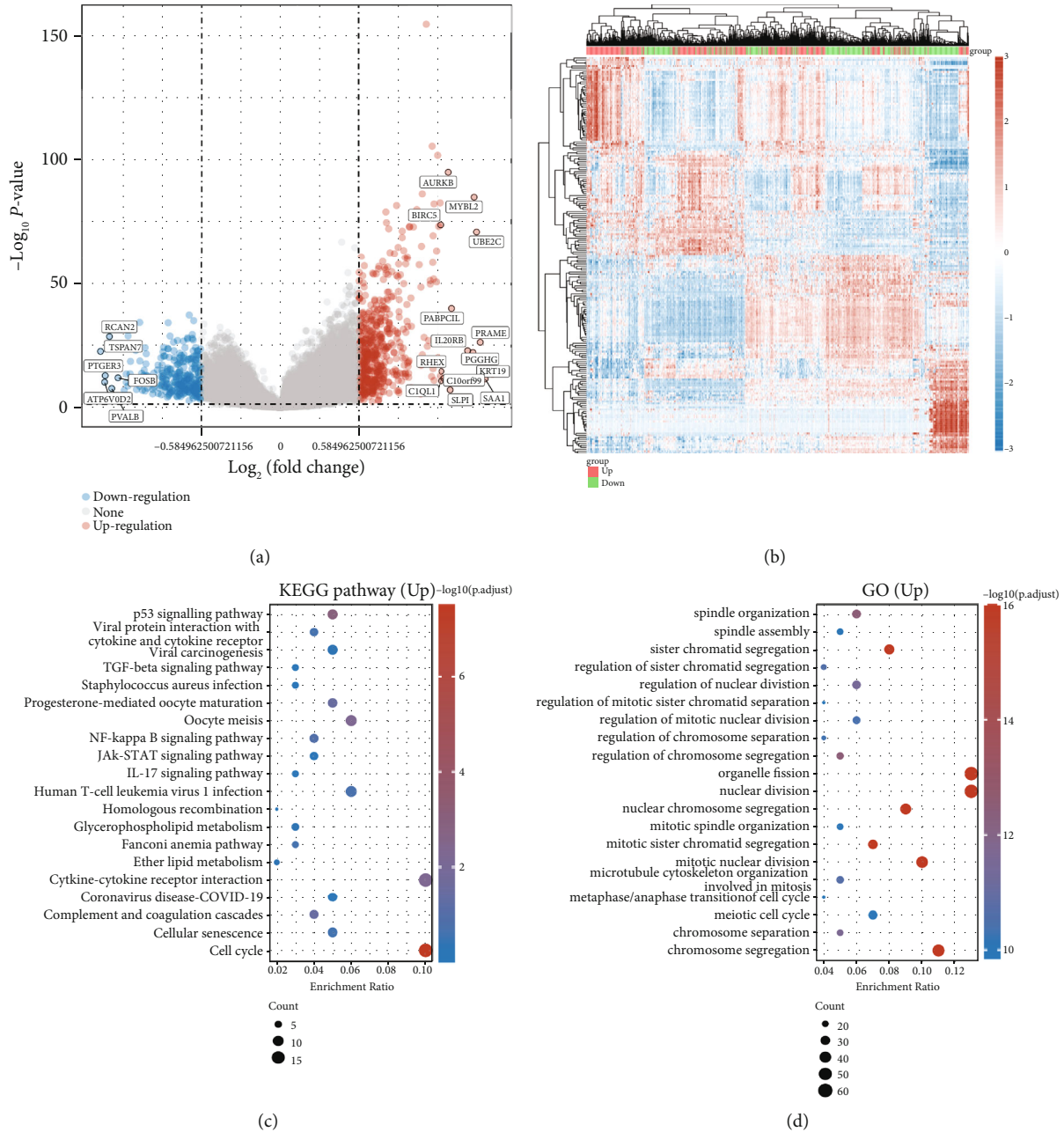
FIGURE 4: Enrichment analysis of CDCA3 positively correlated genes. (a) Distribution of differential genes with different CDCA3 expression levels. (b) The heat map of the differential genes expression in CDCA3 high and low expression groups. KEGG enrichment analysis (c) and GO enrichment analysis (d) of differential genes in CDCA3 high and low expression groups.

upregulated (Figure 2(e)). The distribution of immune cells in KIRC is shown in Figure 2(f). Figure 2(g) shows immune cells hardly express CDCA3. CDCA3 can regulate G2/M phase, so we analyzed the relationship between CDCA3 and immune cells G2/M checkpoint. Our results show a broad association of CDCA3 with immune cell G2/M checkpoints (Figure 2(h)).

Further, we conducted tissue microarray to try to prove the above results. Figure 3(a) shows that we performed IF staining in RCC tissue microarray. There was a significant positive correlation between CDCA3 and CD8

(Figure 3(b)). However, our study did not observe the correlation between CDCA3 and CD4, FOXP3, CD68, and PD-1 (Figures 3(c)–3(f)). In conclusion, CDCA3 was closely related to tumor immune cells infiltration and antitumor immunity. And CDCA3 may be important for RCC risk stratification and immunotherapy guidance.

3.3. Identification of Molecular Mechanism of CDCA3. The distribution of different genes among patients with different CDCA3 expression groups was shown in the volcano map (Figure 4(a)). The heat map showed the expression trend

(a)

(b)

(c)

(d)

Figure 5: Continued.

(e)
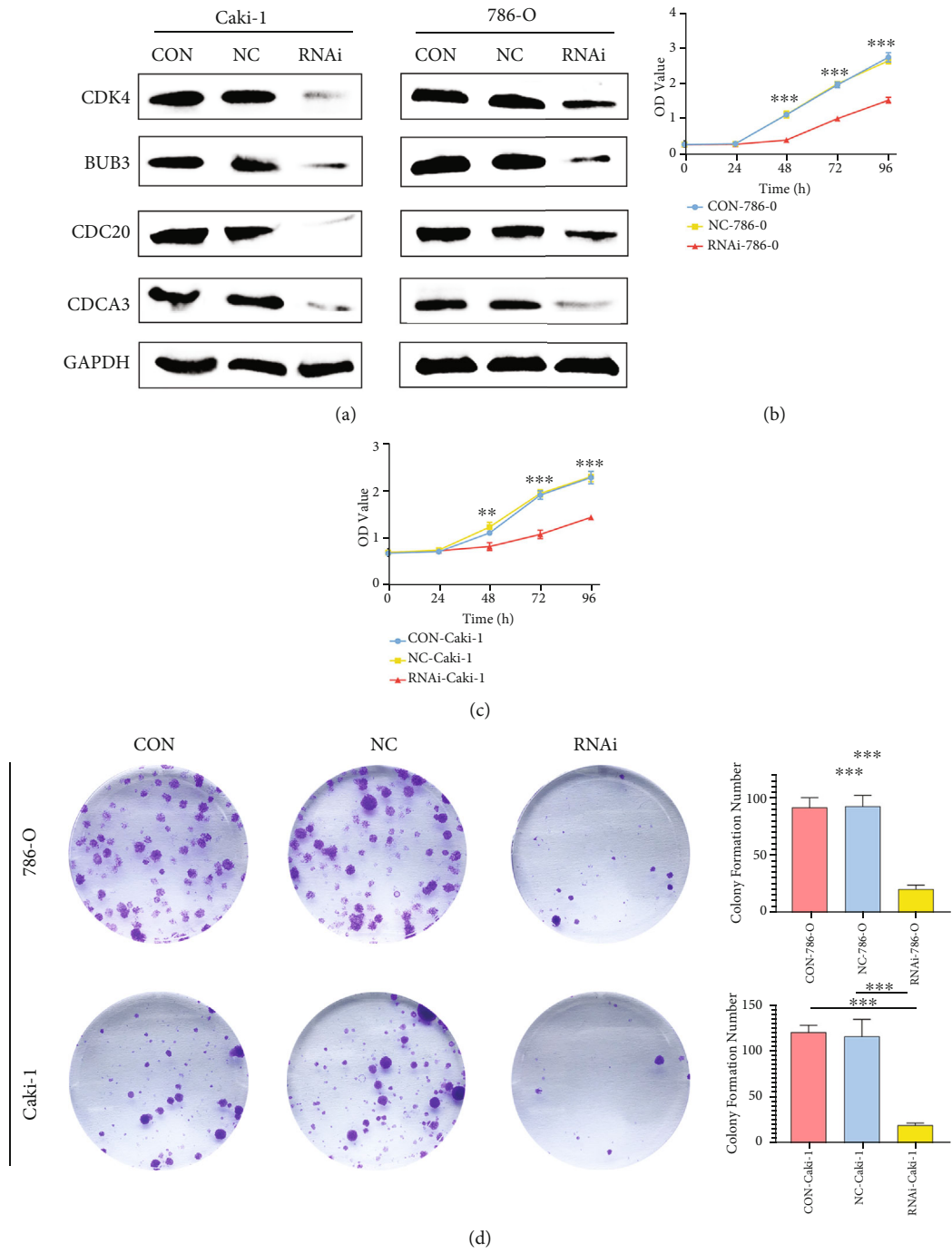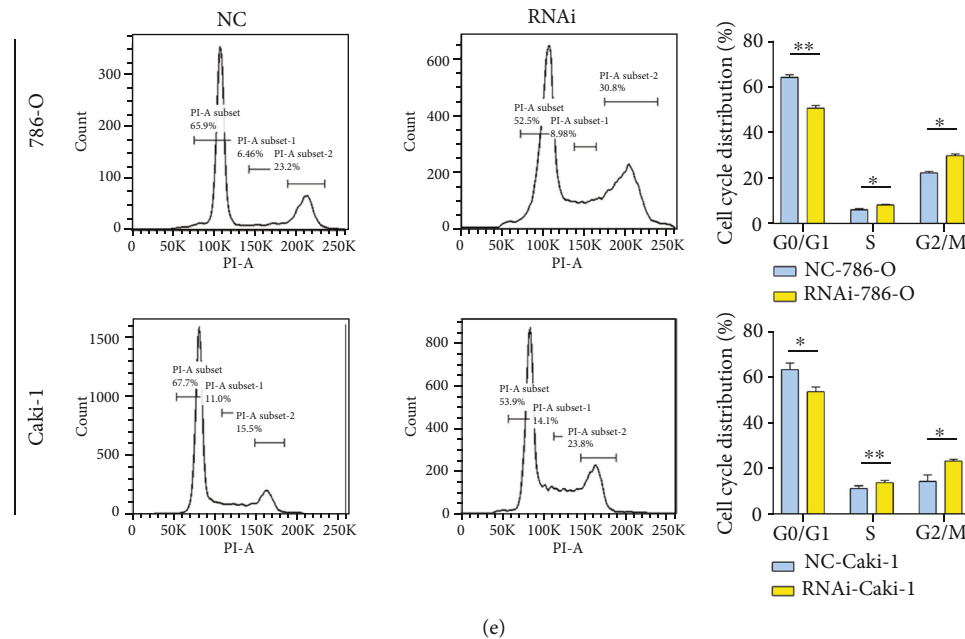
FIGURE 5: The function of CDCA3 was confirmed by in vitro experiments. (a) Western blot was used to detect the expression of CDCA3, CDK4, Bub3, and Cdc20 in different groups of cells. CCK-8 array to detect (b) 786-O and (c) Caki-1 proliferation. (d) Representative images of crystal violet stain on day 15. (e) Representative images of flow cytometry.($*p < 0.05$, $**p < 0.01$, $***p < 0.001$).

of 50 upregulated genes and 50 downregulated genes with the greatest difference (Figure 4(b)). KEGG enrichment analysis showed that the related pathways were mainly concentrated in p53 signal pathway, TGF-β signal pathway, NF-κB signal pathway, and JAK-STAT signal pathway. (Figure 4(c)). GO enrichment analysis showed that its biological function was mainly enriched in spindle organization, regulation of sister chromatid segregation, and nuclear division (Figure 4(d)). These results suggest that CDCA3 mainly affects cell cycle in RCC and may regulate antitumor immune response through NF-κB axis and other important immune-related pathways.

3.4. CDCA3 Knockdown Attenuated RCC Cell Proliferation and Arrested Cell Cycle. To further understand the effect of CDCA3 on the biological behavior of RCC, we constructed CDCA3-knockdown cell lines for functional experiments. Lentiviruses carrying CDCA3 shRNA were used to obtain CDCA3-knockdown Caki-1 and 786-O. The Western blot results showed that the expression of CDCA3 was significantly decreased in the RNAi group, indicating that the CDCA3-knockdown cell lines were successfully constructed (Figure 5(a)). Meanwhile, the expression of CDK4, BUB3, and Cdc20 was decreased (Figure 5(a)), which indicating cell cycle arrest. The CCK-8 assay showed that CDCA3 knockdown remarkably attenuated the cell proliferation (Figures 5(b) and 5(c)). The ability of colony formation was notably impaired after knockdown of CDCA3 gene (Figure 5(d)). The flow cytometric indicated that CDCA3 knockdown cause G1, S, and G2/M phase arrest (Figure 5(e)). In general, CDCA3 expression affects cell cycle operation and cell proliferation.

4. Discussion

Our study suggested that CDCA3 can independently predict prognosis and affect tumor progression in RCC. CDCA3 may also be involved in the regulation of immune-related pathways, and stimulated the infiltration of immune cells, such as CD8$^+$ T cells and Tregs. Importantly, we verified our results in vitro.

Scholars revealed that CDCA3 influence many tumor progression and treatment through a variety of pathways and is associated with poorer prognosis [8, 15]. Our results also showed consistency. Patients with high CDCA3 expression had significantly worse survival and clinical stage, which was confirmed by our results and public databases. One important reason is that dysregulation of cell cycle is the basis of abnormal proliferation of tumor cells. We also confirmed that downregulation of CDCA3 blocked the G2/M phase of cells and reduced cell proliferation ability. This directly proved that the functional localization of CDCA3 was a key regulatory protein in the cell cycle, and its abnormal expression can affect tumor progression and prognosis.

Infiltrating immune cells directly affect the occurrence, development, and treatment of tumors. It has been reported that CDCA3 is closely related to immune infiltration in hepatocellular carcinoma [16]. Our results showed that CDCA3 affected tumor infiltration of various immune cells, including CD8$^+$ T cells in endogenous and exogenous data. Previous studies have shown that CD8$^+$ T cells can recognize tumor-specific antigens and played a role in tumor control [17]. The high density of tumor infiltrating CD8$^+$ T cells has been proved to be associated with a good prognosis of most cancers [18], but the infiltration of CD8$^+$ T cells in

RCC was associated with a poor prognosis [19], this is consistent with our survival outcomes. Since immune cells hardly express CDCA3, antitumor therapy targeting CDCA3 may not cause damage to immune cells, which is a potential treatment. Our study was firstly proved that CDCA3 may be involved in the regulation of immune cell infiltration and tumorigenesis in RCC. But more importantly, the specific pathway through which CDCA3 affects immune infiltration needs further study.

As we know, immune checkpoint is a key molecule in tumor immune escape pathway. There were a lot of evidences showed that immune checkpoints were related to the benefit degree of ICIs treatment, which can be used as biomarkers for ICIs treatment [20–22]. Our results showed that patients with high expression of CDCA3 also expressed high levels of CTLA4 and PD-1. This initially showed that there was a close relationship between CDCA3 and immune checkpoints and further suggested that CDCA3 may participate in the immune pathway of RCC by regulating immune regulatory factors, which may be a potential target for immunotherapy. Moreover, findings suggested that TMB may predict clinical response to ICIs [23]. The neoantigen produced by TMB may be an important reason for stimulating antitumor response. In our study, we found that there was a positive correlation between CDCA3 and TMB, also suggesting that CDCA3 may predict the benefits of immunotherapy.

In summary, reactive TME is the key to immunotherapy, and CDCA3 helps to evaluate this phenomenon. Furthermore, enrichment analysis was performed to evaluate the actual molecular mechanism of CDCA3 in RCC. CDCA3 has been suggested to influence the NF-κB pathway to mediate tumor progression [12]. Our results supported this point. CDCA3 is also involved in P53 and TGF pathways. NF-κB is involved in the regulation of inflammation and innate immunity in tumor development. P53 also plays an important role in immune system. P53 mutation in cancer triggers B cell antibody response and CD8^{+} killing T cell response [24]. TGF-β can inhibit the proliferation, activation, and effector function of T cells. In addition, TGF-β further enhances immunosuppression in TME by promoting Tregs differentiation and destroying T cell immunity [25]. These evidences suggest that CDCA3 has a reasonable influence on TME, but more specific studies are needed to uncover the regulatory mechanisms.

TME is recognized as a complex dynamic ecosystem, which is composed of malignant tumor cells, various infiltration immune cells, fibroblasts, and a variety of cytokines. In this ecosystem, immune response plays an important role in tumorigenesis and development. RCC has always been regarded as an immunogenic malignant tumor [26–28], and it is usually insensitive to chemotherapy and radiotherapy. Immunotherapy is regarded as another therapeutic target in addition to chemotherapy and radiotherapy [29]. Clinicians are focusing on immunotherapy to create a new era of RCC treatment, trying to break through the traditional barrier [30]. The first thing to use immunotherapy is to evaluate the immune status, which is the premise of personalized treatment. Therefore, find a biomarker that can better indicate the immune status and curative effect of patients, which provides an important reference for immunotherapy of RCC. When we focus on CDCA3, the problem seems to become transparent. CDCA3 has the potential to evaluate prognosis and TME and helps to hierarchically label patients at high risk. Then apply medical intervention in advance, select appropriate treatment strategies, and improve the prognosis. However, our study has its limitations. First, the specific mechanism of CDCA3 on CD8^{+}T cells and its influence on immunotherapy of renal cell carcinoma need to be further explored; second, we have proved that CDCA3 can block the cell cycle, but there is no further study on the biological mechanism.

5. Conclusion

CDCA3 can be used as an oncogene to affect the prognosis of RCC patients. Downregulation of CDCA3 causes cell stagnation in G2/M phase, promotes cell apoptosis, and reduces proliferation ability. More importantly, the immunological implications of CDCA3 have also been preliminarily evaluated. CDCA3 may participate in the regulation of immune infiltration in tumor microenvironment by affecting the expression of many immune regulatory factors and TMB, which is expected to provide valuable reference for clinical ICIs treatment. Overall, CDCA3 can be used as a biomarker to evaluate prognosis and CD8^{+} T cell infiltration in RCC. Targeted therapy against CDCA3 is a promising new therapeutic modality, and focusing on it may help to improve the management of therapeutic resistance in the combination of ICI and TKI, but this needs further research to confirm.

Data Availability

All public data access addresses are visible in the manuscript. Data archiving will be made available on reasonable request and all of the authors are responsible to the data.

Conflicts of Interest

The authors declare no conflict of interest.

Authors' Contributions

All authors read and approved the final manuscript. Yuanyuan Bai and Yongyang Wu designed the experiments, performed the experiments, analyzed the data, and wrote the paper. Zhenjie Yin, Bingyong You, Yongmei Chen, and Daoxun Chen reviewed and revised the manuscript.

Acknowledgments

References

[1] A. Znaor, J. Lortet-Tieulent, M. Laversanne, A. Jemal, and F. Bray, "International variations and trends in renal cell carcinoma incidence and mortality," *European Urology*, vol. 67, no. 3, pp. 519–530, 2015.

[2] D. Y. Heng, W. Xie, M. M. Regan et al., "Prognostic factors for overall survival in patients with metastatic renal cell carcinoma treated with vascular endothelial growth factor-targeted agents: results from a large, multicenter study," *Journal of Clinical Oncology*, vol. 27, no. 34, pp. 5794–5799, 2009.

[3] F.-J. Hsueh and Y. Tsai, "Current and future aspect of immunotherapy for advanced renal cell carcinoma," *Urological Science*, vol. 31, no. 1, pp. 8–14, 2020.

[4] H. Raskov, A. Orhan, J. P. Christensen, and I. Gögenur, "Cytotoxic CD8$^+$ T cells in cancer and cancer immunotherapy," *British Journal of Cancer*, vol. 124, no. 2, pp. 359–367, 2021.

[5] J. I. Clark, M. K. K. Wong, H. L. Kaufman et al., "Impact of Sequencing Targeted Therapies With High-dose Interleukin-2 Immunotherapy: An Analysis of Outcome and Survival of Patients With Metastatic Renal Cell Carcinoma From an Ongoing Observational IL-2 Clinical Trial: PROCLAIM^{SM}," *Clinical Genitourinary Cancer*, vol. 15, no. 1, pp. 31–41.e4, 2017.

[6] D. Lavacchi, E. Pellegrini, V. E. Palmieri et al., "Immune checkpoint inhibitors in the treatment of renal cancer: current state and future perspective," *International Journal of Molecular Sciences*, vol. 21, no. 13, p. 4691, 2020.

[7] C. Kissling and S. Di Santo, "Tumor treating fields - behind and beyond inhibiting the cancer cell cycle," *CNS & Neurological Disorders Drug Targets*, vol. 19, no. 8, pp. 599–610, 2020.

[8] M. N. Adams, J. T. Burgess, Y. He et al., "Expression of CDCA3 is a prognostic biomarker and potential therapeutic target in non-small cell lung cancer," *Journal of Thoracic Oncology*, vol. 12, no. 7, pp. 1071–1084, 2017.

[9] Y. Zhang, W. Yin, W. Cao, P. Chen, L. Bian, and Q. Ni, "CDCA3 is a potential prognostic marker that promotes cell proliferation in gastric cancer," *Oncology Reports*, vol. 41, no. 4, pp. 2471–2481, 2019.

[10] H. Li, M. Li, C. Yang et al., "Prognostic value of CDCA3 in kidney renal papillary cell carcinoma," *Aging*, vol. 13, no. 23, pp. 25466–25483, 2021.

[11] Y. Liu, G. Cheng, Z. Huang et al., "Long noncoding RNA SNHG12 promotes tumour progression and sunitinib resistance by upregulating CDCA3 in renal cell carcinoma," *Cell Death & Disease*, vol. 11, no. 7, p. 515, 2020.

[12] P. Gu, M. Zhang, J. Zhu, X. He, and D. Yang, "Suppression of CDCA3 inhibits prostate cancer progression via NF-κB/cyclin D1 signaling inactivation and p21 accumulation," *Oncology Reports*, vol. 47, no. 2, 2021.

[13] K. B. Sahin, E. T. Shah, G. P. Ferguson et al., "Elevating CDCA3 Levels Enhances Tyrosine Kinase Inhibitor Sensitivity in TKI-Resistant EGFR Mutant Non-Small-Cell Lung Cancer," *Cancers*, vol. 13, no. 18, p. 4651, 2021.

[14] L. Bianchi, L. Rossi, F. Tomao, A. Papa, F. Zoratto, and S. Tomao, "Thyroid dysfunction and tyrosine kinase inhibitors in renal cell carcinoma," *Endocrine-Related Cancer*, vol. 20, no. 5, pp. R233–R245, 2013.

[15] Q. Chen, L. Zhou, X. Ye, M. Tao, and J. Wu, "miR-145-5p suppresses proliferation, metastasis and EMT of colorectal cancer by targeting CDCA3," *Pathology, Research and Practice*, vol. 216, no. 4, article 152872, 2020.

[16] Z. Wang, S. Chen, G. Wang, and S. Li, "CDCA3 is a novel prognostic biomarker associated with immune infiltration in hepatocellular carcinoma," *BioMed Research International*, vol. 2021, Article ID 6622437, 19 pages, 2021.

[17] D. S. Chen and I. Mellman, "Oncology meets immunology: the cancer-immunity cycle," *Immunity*, vol. 39, no. 1, pp. 1–10, 2013.

[18] W. H. Fridman, F. Pagès, C. Sautès-Fridman, and J. Galon, "The immune contexture in human tumours: impact on clinical outcome," *Nature Reviews. Cancer*, vol. 12, no. 4, pp. 298–306, 2012.

[19] Q. Pan, L. Wang, S. Chai, H. Zhang, and B. Li, "The immune infiltration in clear cell renal cell carcinoma and their clinical implications: a study based on TCGA and GEO databases," *Journal of Cancer*, vol. 11, no. 11, pp. 3207–3215, 2020.

[20] S. Bagchi, R. Yuan, and E. G. Engleman, "Immune checkpoint inhibitors for the treatment of cancer: clinical impact and mechanisms of response and resistance," *Annual Review of Pathology*, vol. 16, no. 1, pp. 223–249, 2021.

[21] G. Giannone, E. Ghisoni, S. Genta et al., "Immuno-metabolism and microenvironment in cancer: key players for immunotherapy," *International Journal of Molecular Sciences*, vol. 21, no. 12, p. 4414, 2020.

[22] Y. Lai, F. Tang, Y. Huang et al., "The tumour microenvironment and metabolism in renal cell carcinoma targeted or immune therapy," *Journal of Cellular Physiology*, vol. 236, no. 3, pp. 1616–1627, 2021.

[23] L. M. Sholl, F. R. Hirsch, D. Hwang et al., "The promises and challenges of tumor mutation burden as an immunotherapy biomarker: a perspective from the International Association for the Study of Lung Cancer pathology committee," *Journal of Thoracic Oncology*, vol. 15, no. 9, pp. 1409–1424, 2020.

[24] A. J. Levine, "P53 and the immune response: 40 years of exploration-a plan for the future," *International Journal of Molecular Sciences*, vol. 21, no. 2, p. 541, 2020.

[25] A. Dahmani and J. S. Delisle, "TGF-β in T cell biology: implications for cancer immunotherapy," *Cancers*, vol. 10, no. 6, p. 194, 2018.

[26] R. Raman and D. Vaena, "Immunotherapy in metastatic renal cell carcinoma: a comprehensive review," *BioMed Research International*, vol. 2015, Article ID 367354, 8 pages, 2015.

[27] C. Mazza, B. Escudier, and L. Albiges, "Nivolumab in renal cell carcinoma: latest evidence and clinical potential," *Therapeutic Advances in Medical Oncology*, vol. 9, no. 3, pp. 171–181, 2017.

[28] M. Itsumi and K. Tatsugami, "Immunotherapy for renal cell carcinoma," *Clinical & Developmental Immunology*, vol. 2010, article 284581, Article ID 284581, pp. 1–8, 2010.

[29] M. Binnewies, E. W. Roberts, K. Kersten et al., "Understanding the tumor immune microenvironment (TIME) for effective therapy," *Nature Medicine*, vol. 24, no. 5, pp. 541–550, 2018.

[30] S. Biswas and T. Eisen, "Immunotherapeutic strategies in kidney cancer–when TKIs are not enough," *Nature Reviews Clinical Oncology*, vol. 6, no. 8, pp. 478–487, 2009.

Research Article

APOBEC3B and CD274 as Combined Biomarkers for Predicting Response to Immunotherapy in Urothelial Carcinoma of the Bladder

Chuanhao Zhang [1,2,3] **Zhichao Cheng** [4] **Zhe Wang** [2,3] **Genghao Zhao** [1,2,3] **Yonghui Yuan** [5] **and Ruoyu Wang** [2,3]

[1]*Graduate School of Dalian Medical University, Dalian, China*
[2]*Departement of Medical Oncology, Affiliated Zhongshan Hospital of Dalian University, Dalian, China*
[3]*The Key Laboratory of Biomarker High Throughput Screening and Target Translation of Breast and Gastrointestinal Tumor, Dalian University, Dalian, China*
[4]*Graduate School of Xuzhou Medical University, Xuzhou, China*
[5]*Cancer Hospital of China Medical University Liaoning Cancer Hospital & Institute, Shenyang, China*

Correspondence should be addressed to Zhe Wang; wangzhe@dlu.edu.cn, Yonghui Yuan; yyxhdh@126.com, and Ruoyu Wang; wangruoyu@dlu.edu.cn

Immunotherapy has become a promising form of treatment for cancers. There is a need to predict response to immunotherapy accurately. In the UCSC Xena, pan-cancer analysis revealed a positive relationship between APOBEC3B (A3B) and tumor mutational burden ($R = 0.28$, $P < 0.001$) and microsatellite instability ($R = 0.12$, $P < 0.05$). Naturally, the A3B high expression group had higher tumor mutational burden and microsatellite instability than the low expression group. The bladder cancer (BLCA) cohort in The Cancer Genome Atlas (TCGA) revealed tumor mutational signatures of A3B high and low expression groups. Compared to the low expression group, the high expression group had a higher number of SNPs and mutations. Subsequently, A3B was profiled for immune cell infiltration and immune checkpoints in bladder cancer. The results showed that A3B was positively correlated with most immune cells. Compared with the A3B low expression group, the A3B high expression group had higher expression of immune checkpoints. A3B was positively correlated with CD274 ($R = 0.12$, $P = 0.016$). This indicated that the high expression of A3B may have a better response to immunotherapy. Furthermore, data from the IMvigor210 immunotherapy clinical trial was used to confirm the findings of this study. The combined survival analysis of A3B and CD274 showed that the group of patients with high expression of CD274 and A3B was found to have a significantly higher survival rate than the rest of the patient group ($P < 0.047$). The results demonstrated that A3B has a significant role in immunotherapy. Moreover, the combined biomarkers of A3B and CD274 were more effective in predicting response to immunotherapy in bladder urothelial carcinoma. The findings of this study provide valuable insights for precision medicine.

1. Introduction

Bladder cancer is the 11th most common cause of cancer-related deaths worldwide [1]. In recent years, immunotherapy has emerged as a promising cancer treatment modality.

It is essential to have a thorough understanding of the heterogeneity of the tumor microenviroment [2]. Tumor mutational burden (TMB), microsatellite instability (MSI), and programmed death-ligand 1 (PD-L1) could be used as predictive markers to identify patients likely to benefit from
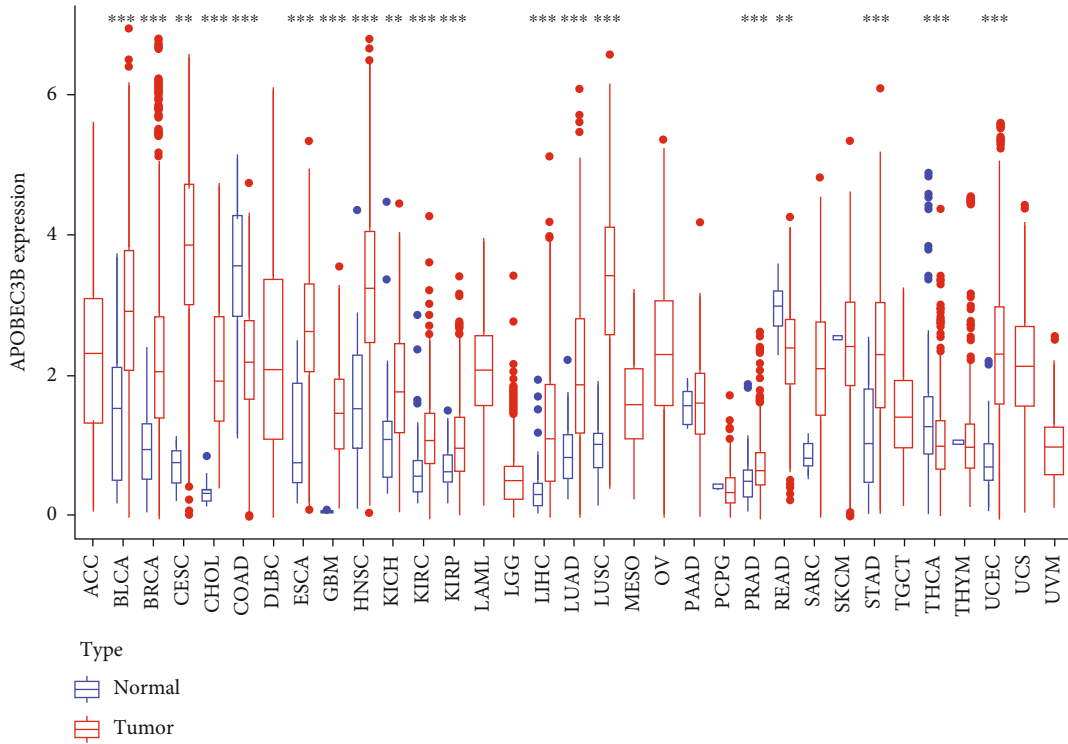
(a)
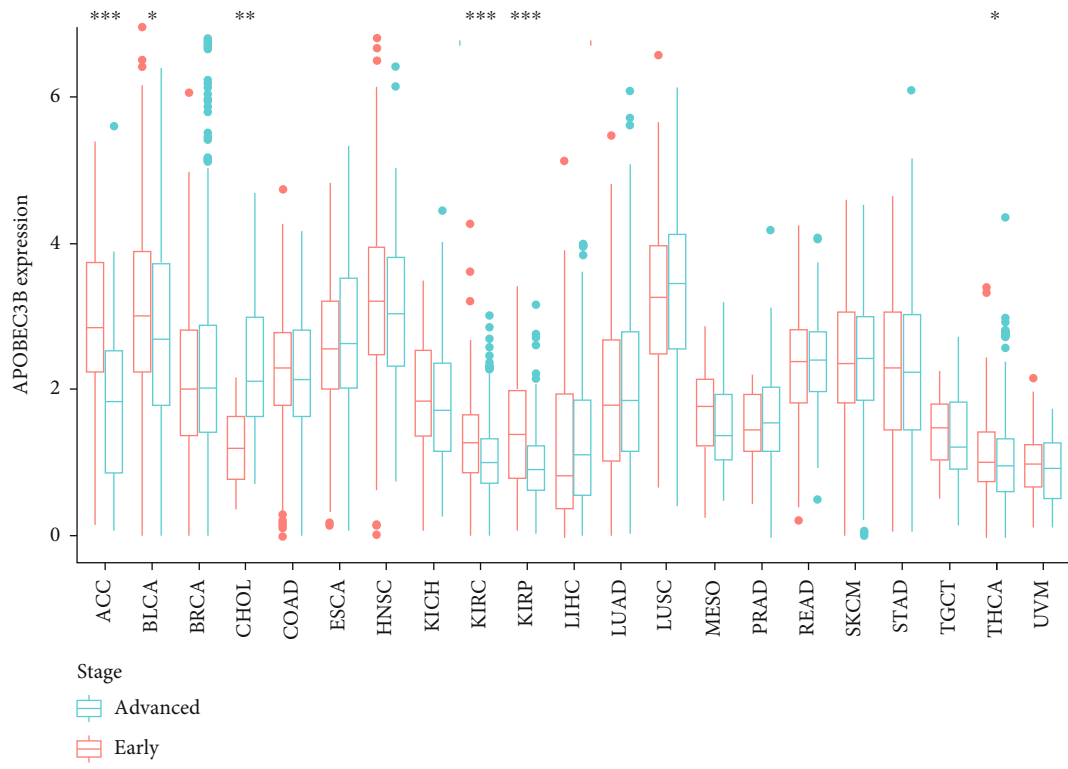
(b)

Figure 1: Differential expression of A3B in pan-cancer. (a) Boxplots showing the differential expression of A3B in normal and tumor tissues in pan-cancer. (b) Boxplots showing the differential expression of A3B in the early and late stages of pan-cancer. $^*P < 0.05$, $^{**}P < 0.01$, $^{***}P < 0.001$.

(a)

(b)

Figure 2: Continued.

(c)
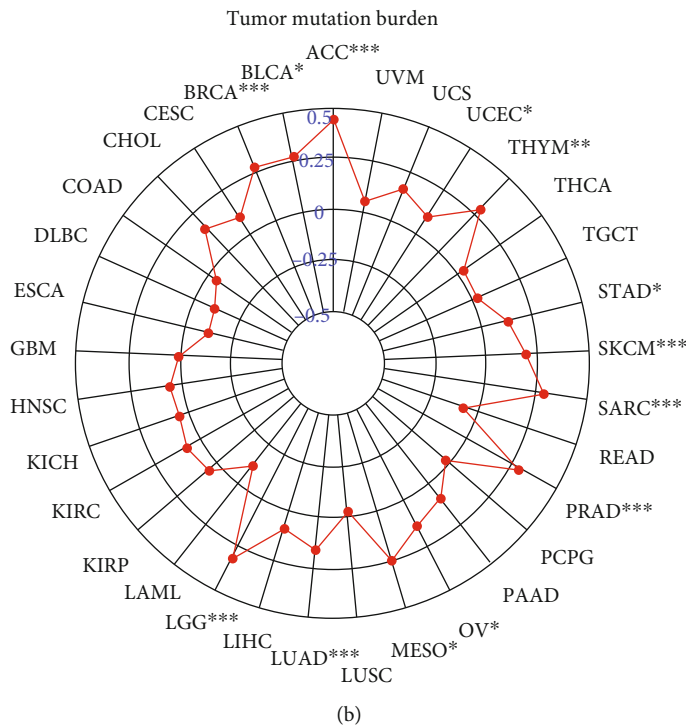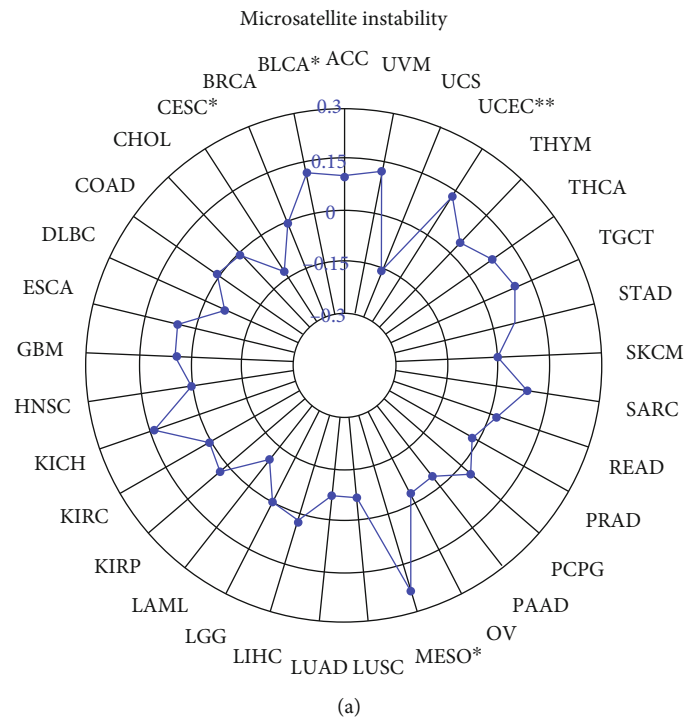
(d)
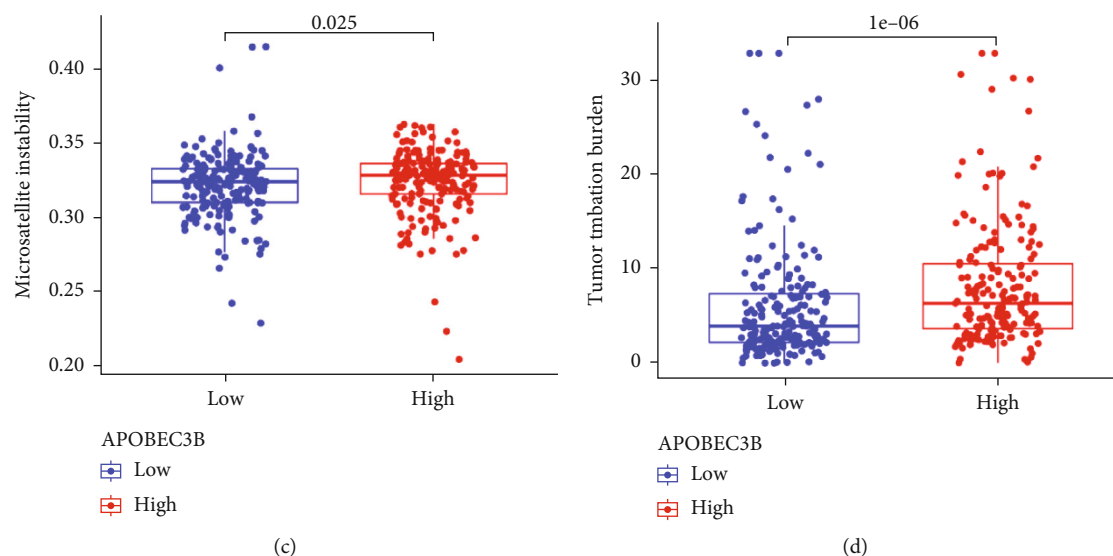
FIGURE 2: Correlation between A3B, TMB, and MSI. (a) Correlation between A3B and MSI in pan-cancer. (b) Differences in the expression of MSI between the high and low A3B expression groups in the TCGA-BLCA dataset. (c) Correlation between A3B and TMB in pan-cancer. (d) Differences in the expression of TMB between the high and low A3B expression groups in the TCGA-BLCA dataset. $^{*}P < 0.05$, $^{**}P < 0.01$, $^{***}P < 0.001$.

immunotherapy [3–6]. Immunotherapy targeting single biomarkers have been demonstrated to be less effective than that targeting composite biomarkers. Therefore, there is a need to explore combined biomarkers that could be targeted to improve the effectiveness of immunotherapy.

Human apolipoprotein B mRNA editing catalytic polypeptide-like 3B (APOBEC3B), one of the seven members of the cytidine deaminase family, is upregulated in multiple cancer types [7, 8]. Furthermore, the APOBEC3B (A3B) mutational signature is enriched in various cancer types, including the bladder, breast, cervical, and thyroid cancers [9, 10]. A high tumor mutation burden is used as a predictive biomarker to identify patients who may benefit from immune checkpoint inhibitors (ICIs). According to a previous study, A3B was positively correlated with PD-L1 expression and T-cell infiltration [11]. Therefore, we hypothesized that A3B could be a potential biomarker for predicting response to immunotherapy.

Using bioinformatics tools, we explored the correlation between A3B and response to immunotherapy. Further, we explored the significance of combined biomarkers of A3B and PD-L1 (CD274) against CD274 alone in predicting response to immunotherapy.

2. Materials and Methods

2.1. Data Collection. Pan-cancer RNA sequencing and clinical data from 33 types of cancers were downloaded from the UCSC Xena database (http://xena. ucsc.edu/). In addition, mutation data were obtained from the GDC website (https://portal.gdc.cancer.gov/). Data from the IMvigor210 clinical trial were downloaded through the "IMvigor210-CoreBiology" R package (http://research-pub.gene.com/ IMvigor210CoreBiologies/).

2.2. Differential Expression of A3B. Differential expression of APOBEC3B genes between tumor and paracancerous tissues was conducted using the "ggpubr" R package. The results were presented in boxplots. The tumors were staged as stage 0, stage I, stage II, stage III, and stage IV. Stages 0, I, and II were defined as early stages, while stages III and IV were defined as late stages. Boxplots were used to show differences between the early and late stages of tumors.

2.3. Tumor Mutation Signature of A3B. The association between A3B and MSI or TMB in pan-cancer was drawn using the "fmsb" R package. The results were presented in radar charts. Data in the TCGA-BLCA dataset were divided into high and low expression groups based on the median A3B expression value. The expression of MSI and TMB between the A3B high- and low-expression groups were compared using the "limma" R package [12]. The "maftools" R package [13] was used to visualize and draw waterfall plots showing mutational signatures between the high and low expression groups of A3B.

2.4. Immune Correlation Analysis. Immunophenotyping data were downloaded from the UCSC Xena website (Supplementary Table 1). C1 means wound healing, C2 means IFN-gamma dominant, C3 means inflammatory, C4 means lymphocyte depleted, C5 means immunologically quiet, and C6 means TGF-beta dominant. After that, boxplots showing the different immunophenotypes were drawn. Data on immune cell infiltration were obtained from the TIMER2.0 online website (http://timer.comp-genomics.org/) [14–16]. The correlation between A3B and immune cells was visualized using the "tidyverse" R package. Further, differences in immune checkpoints between the high and low expression groups were compared by the Wilcoxon test.

(a)
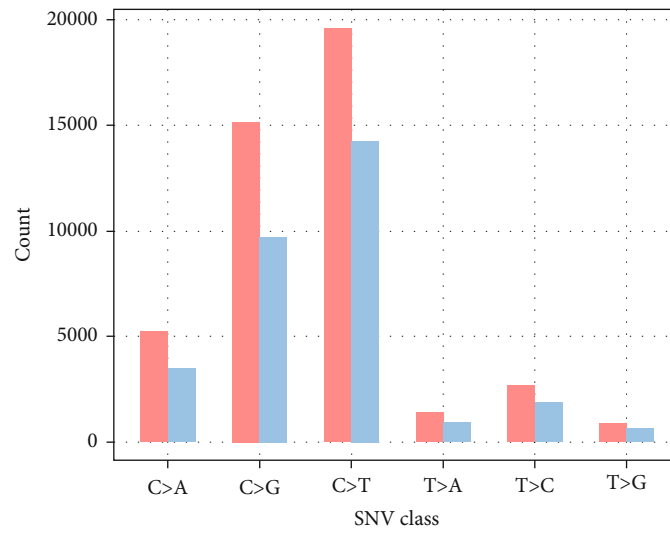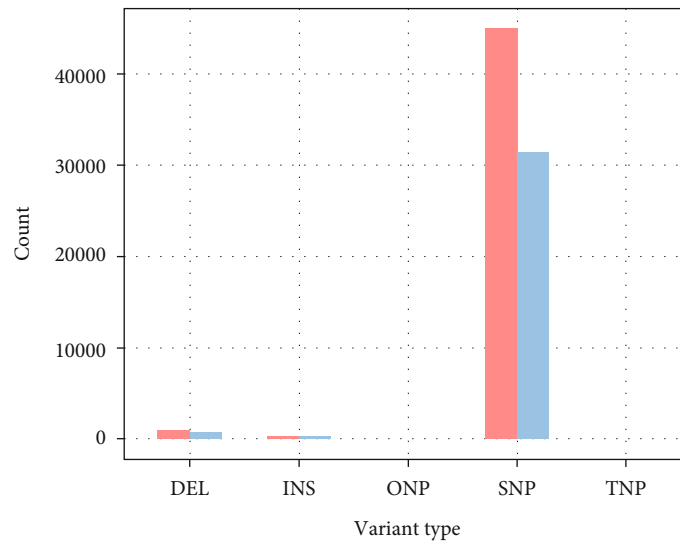
(b)

FIGURE 3: Continued.
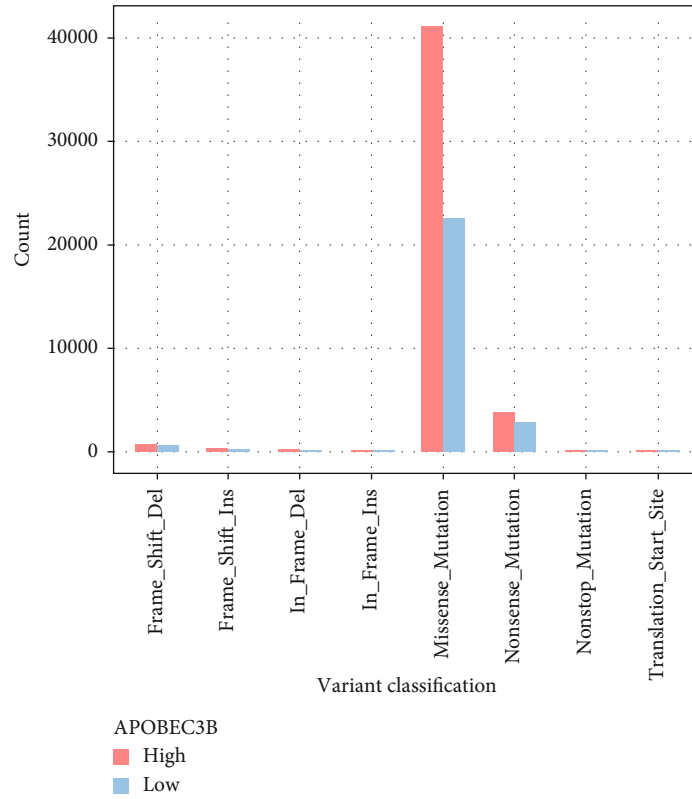
(c)

High-APOBEC3B group

Altered in 194 (97.98%) of 198 samples

(d)

Figure 3: Continued.

Low-APOBEC3B group
Altered in 182 (92.86%) of 196 samples

Nonsense_Mutation   In_Frame_Del
Missense_Mutation   In_Frame_Ins
Frame_Shift_Del   Multi_Hit
Frame_Shift_Ins

(e)
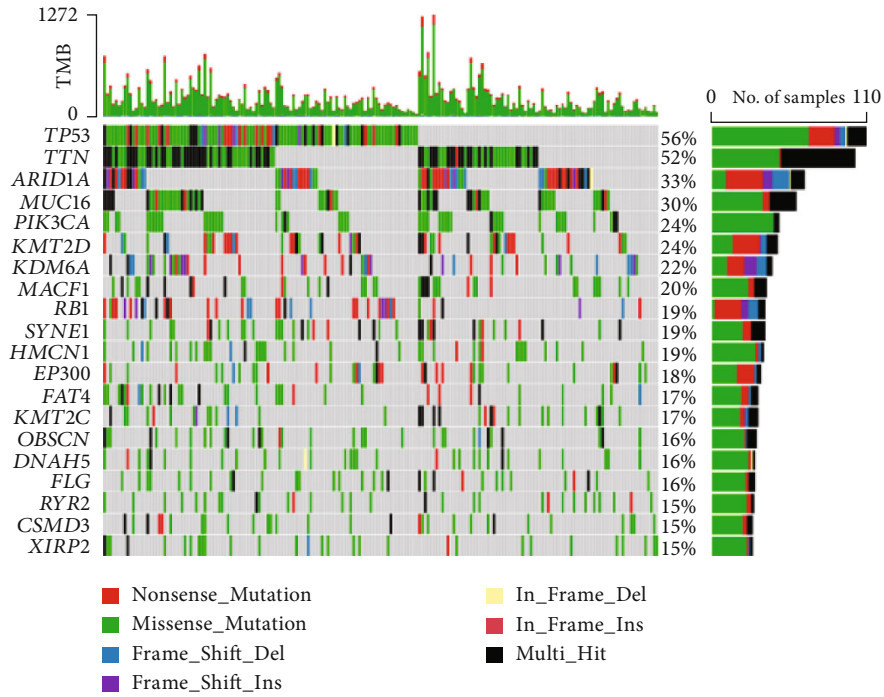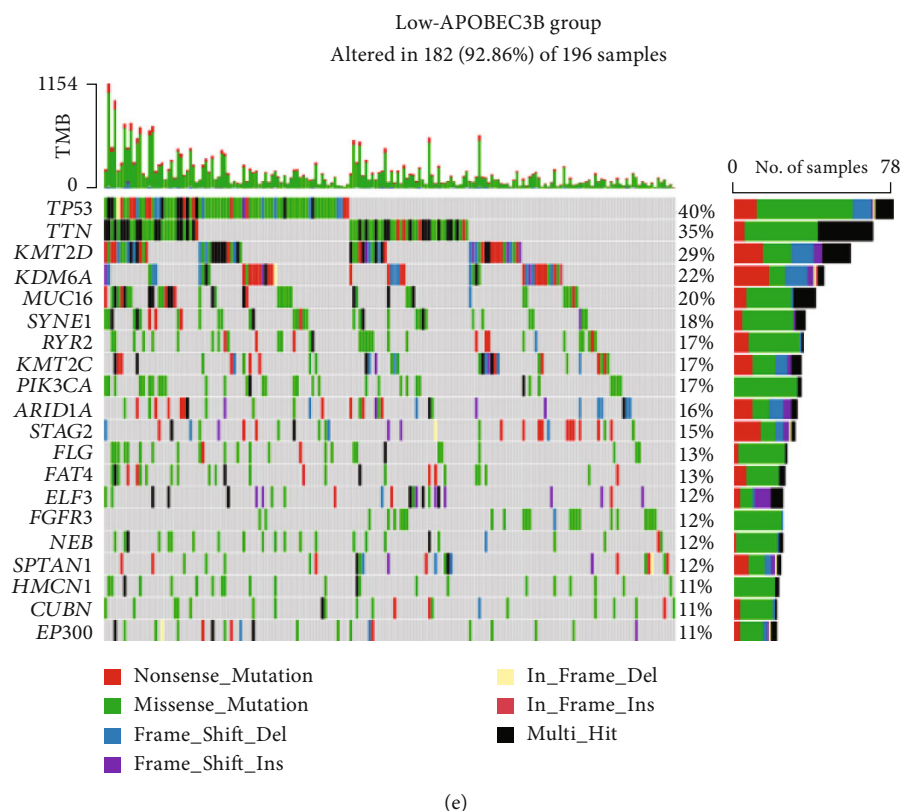
FIGURE 3: Mutations in the high and low A3B expression groups in the TCGA-BLCA. (a) Mutations in the A3B high expression group. (b) Mutations in the A3B low expression group. (c) Waterfall plot showing the top 20 mutated genes in the A3B high expression group. (d) Waterfall plot showing the top 20 mutated genes in the A3B low expression group.

2.5. Immunotherapy Response. Data from the IMvigor210 immunotherapy cohort, including 195 patients with bladder urothelial carcinoma with complete information on survival, were analyzed. Spearman's correlation was used to show the correlation between A3B and CD274. Further, patients were stratified into four groups based on the expression of A3B and CD274, including A3B high CD274 high expression group, A3B high CD274 low expression group, A3B low CD274 low expression group, and A3B low CD274 high expression group. Survival analysis was done using the "survival" R package.

2.6. Statistical Analysis. All statistical analyses were performed using R statistical software (version 4.0.3). The Kruskal-Wallis test was used to analyze differences in the distribution of the immune cell types. Spearman's correlation was used for the correlation between A3B and CD274. Kaplan-Meier survival analysis was used to analyze survival between groups. The P values <0.05 (*), 0.01 (**), and 0.001 (***) were considered statistically significant.

3. Results

3.1. Differential Expression of A3B in Pan-Cancer. The differential expression analysis of A3B among the 33 types of cancers showed significant differences in the expression of A3B in bladder cancer (BLCA), breast cancer (BRCA), cervical squamous cell carcinoma and endocervical adenocarcinoma

(CESC), colon adenocarcinoma (COAD), esophageal cancer (ESCA), glioblastoma multiforme (GBM), head and neck squamous cell carcinoma (HNSC), kidney chromophobe (KICH), kidney renal clear cell carcinoma (KIRC), kidney renal papillary cell carcinoma (KIRP), liver hepatocellular carcinoma (LIHC), lung adenocarcinoma (LUAD), lung squamous cell carcinoma (LUSC), prostate cancer (PRAD), rectal adenocarcinoma (READ), stomach adenocarcinoma (STAD), thyroid carcinoma (THCA), and uterine corpus endometrial carcinoma (UCEC) (Figure 1(a)). Similarly, the differential expression analysis of A3B in the different pathological stages (early stages: stages 0, I, and II; and advanced stages: stages III and IV) revealed significant differences in adrenal cortex carcinoma (ACC), bladder cancer (BLCA), cholangiocarcinoma (CHOL), kidney renal clear cell carcinoma (KIRC), kidney renal papillary cell carcinoma (KIRP), and thyroid carcinoma (THCA) (Figure 1(b)).

3.2. MSI and Tumor Mutational Signatures of A3B. TMB and MSI are predictive markers for immunotherapy response. The correlation between MSI and pan-cancer was shown on a radar chart. A3B and MSI were shown to be correlated in several cancer types, including BLCA ($R = 0.12$, $P < 0.05$), CESC ($R = -0.13$, $P < 0.05$), MESO ($R = 0.24$, $P < 0.05$), and UCEC ($R = 0.13$, $P < 0.01$) (Figure 2(a)). In addition, as shown in Figure 2(b), A3B was significantly correlated with TMB in ACC ($R = 0.44$, $P < 0.001$), BLCA ($R = 0.28$, $P < 0.001$), BRCA ($R = 0.28$,
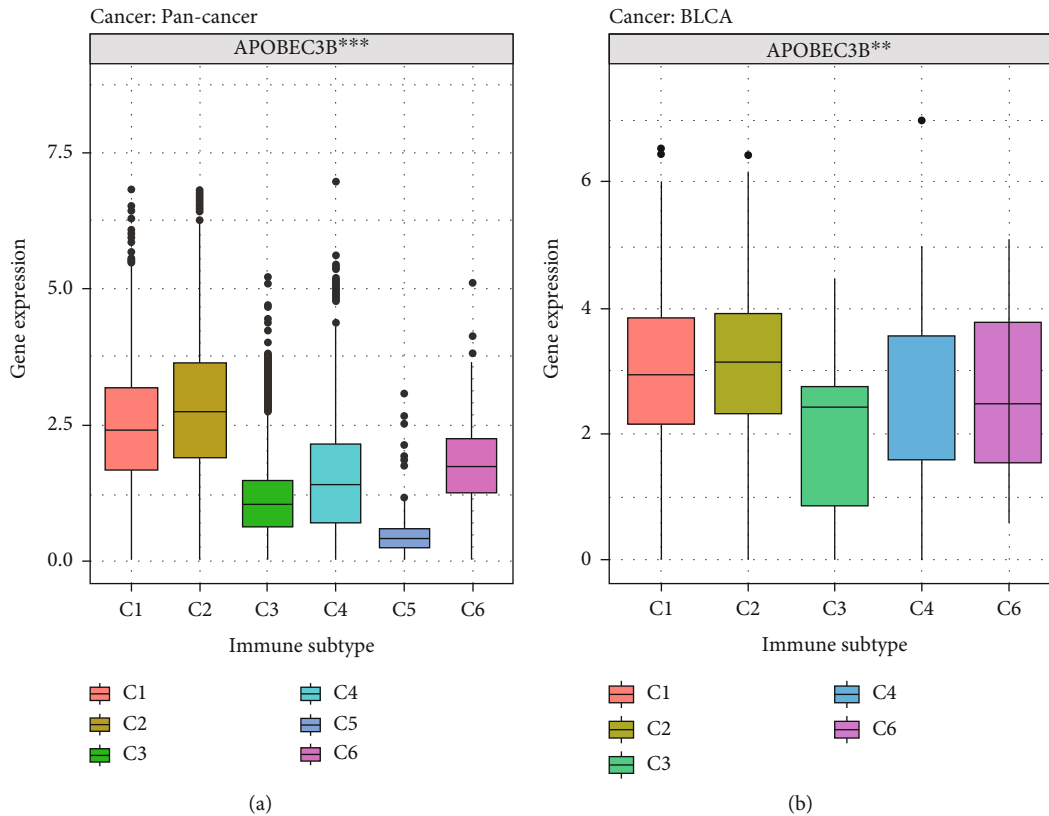
Figure 4: Immunophenotyping in pan-cancer and the TCGA-BLCA. (a) Immunophenotyping of A3B in pan-cancer. (b) Immunophenotyping of A3B in bladder cancer. C1: wound healing; C2: IFN-gamma dominant; C3: inflammatory; C4: lymphocyte depleted; C5: immunologically quiet; C6: TGF-beta dominant. $^{**}P < 0.01$, $^{***}P < 0.001$.

$P < 0.001$), LGG ($R = 0.32$, $P < 0.001$), LUAD ($R = 0.16$, $P < 0.001$), MESO ($R = 0.25$, $P < 0.05$), OV ($R = 0.14$, P < 0.05), PRAD ($R = 0.29$, $P < 0.001$), SARC ($R = 0.29$, $P < 0.001$), SKCM ($R = 0.19$, $P < 0.001$), STAD ($R = 0.13$, $P < 0.05$), THYM ($R = 0.29$, $P < 0.01$), and UCEC ($R = 0.10$, $P < 0.05$). A3B was associated with TMB and MSI in BLCA, MESO, and UCEC. The only in-depth analysis we performed was on bladder cancer to facilitate the study of immunotherapy. Therefore, we analyzed the differential expression of MSI between the high and low A3B expression groups in the TCGA-BLCA dataset. As shown in Figure 2(a), A3B was positively correlated with MSI. Furthermore, the A3B high expression group had a higher expression of MSI (Figure 2(c)). Similarly, the A3B high expression group had a higher expression of TMB (Figure 2(d)). Data were divided into A3B high and low expression groups based on the median cutoff value. The single nucleotide polymorphism and C > T were the most prevalent type in the TCGA-BLCA dataset (Figures 3(a) and 3(b)). Furthermore, missense mutations were shown to be the primary mutations in the A3B high expression group (Figure 3(c)). However, the above indicators of the A3B low expression group were lower than those of the A3B high expression group (Figures 3(a)–3(c)). The waterfall plot revealed that mutations are more prevalent in the high-expression A3B group compared to the low-expression A3B group (Figures 3(d) and 3(e)).

3.3. Immune Correlation Analysis of Pan-Cancer and Bladder Cancer. In recent years, immunotherapy has become a promising treatment modality for cancer patients. The expression of A3B in each immunophenotype was analyzed based on pan-cancer immunophenotypic data (Figure 4(a)). Notably, A3B was significantly higher in C1 (wound healing) and C2 (IFN-gamma dominant) than the other immunotypes. However, the expression of A3B was significantly low in C5 (immunologically quiet). Similarly, analysis of A3B expression among the different immune cell types in the TCGA-BLCA dataset revealed a significantly high expression of A3B in C1 and C2 cell types and a significantly low expression of A3B in C5 (Figure 4(b)). These results revealed an association between A3B and cellular immunity. There was no data available on C5 typing in the TCGA-BLCA dataset.

Further, we explored the relationship between A3B and immune cell infiltration, immune checkpoints, and CD274. The relationship between immune cells and A3B was shown on a bubble chart. The majority of immune cells were positively correlated with A3B, including CD8+ T cells, B cells, macrophages, and NK cells, while a few were negatively correlated. Overall, the A3B high expression group usually had a large amount of immune cell infiltration. Immunotherapy is undoubtedly more effective in an environment with high immune cell infiltration (Figure 5(a)). In addition, several immune checkpoints, including CD274, HAVCR2,
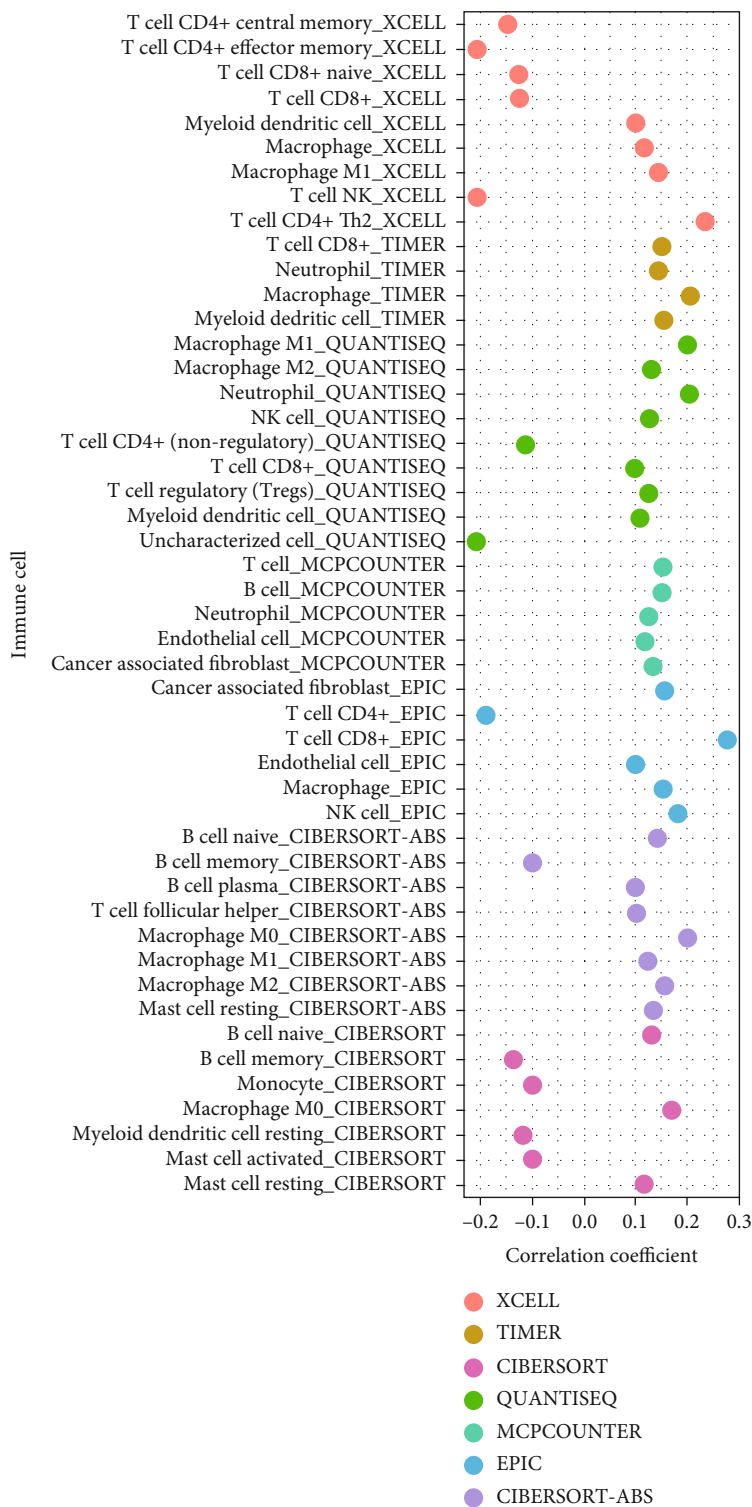
(a)

Figure 5: Continued.

(b)

(c)
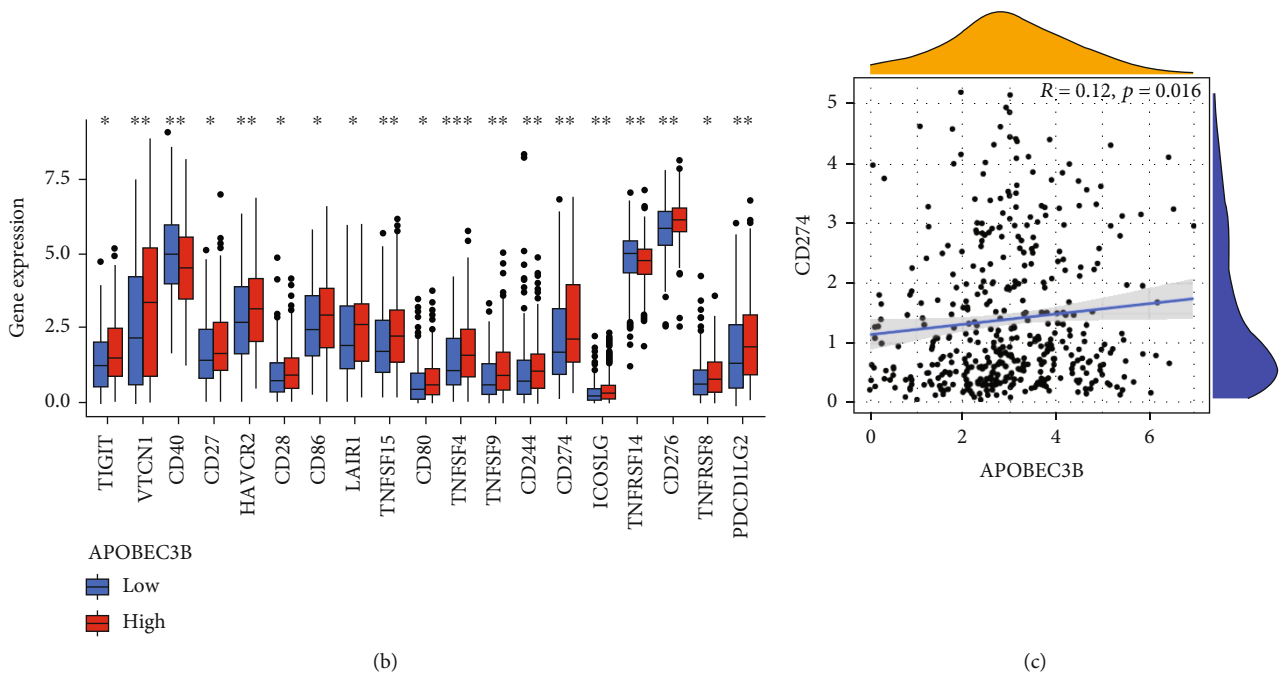
FIGURE 5: Immune correlation analysis of A3B in the TCGA-BLCA cohort. (a) Scatter plot showing the correlation between A3B and immune cells. (b) Boxplots showing differences in immune checkpoints between the high and low A3B expression groups. (c) Correlation between A3B and CD274. $^*P < 0.05$, $^{**}P < 0.01$, $^{***}P < 0.001$.

and TIGIT were highly expressed in the A3B high expression group (Figure 5(b); Supplementary Table 2). Finally, there was a significant correlation between A3B and CD274 (Figure 5(c)) ($R = 0.12$, $P = 0.016$). These results reveal that A3B plays an essential role in immunotherapy. Since A3B is closely related to immunotherapy response markers such as MSI, TMB, and CD274, we hypothesized that A3B could be exploited as marker for immunotherapy response.

3.4. Validation of A3B in an Immunotherapy Cohort. Next, we analyzed the publicly available data from the IMvigor210 immunotherapy cohort, which included 195 patients with bladder urothelial carcinoma. The results revealed that A3B was associated with CD274 in the immunotherapy cohort ($R = 0.22$, $P = 0.038$) (Figure 6(a)). In addition, the survival analysis revealed that the patient group with a high expression of CD274 and A3B had significantly higher survival rate than the patient group with low expression of CD274 and A3B (Figure 6(b)). In addition, the patient group with a high expression of CD274 and A3B had better survival rate than the patient group with a high expression of CD274 and a low expression of A3B. These results suggested that immunotherapy targeting both CD274 and A3B could be more effective than immunotherapy targeted against a single biomarker. Moreover, the overall survival analysis revealed that the CD274 and A3B low expression group had significantly lower survival than the CD274 low expression and A3B high expression group. Furthermore, the overall survival of the CD274 high expression and A3B high expression group was significantly higher than that of the CD274 low expression group and A3B high expression

group. Taken together, these results revealed that immunotherapeutic agents targeting A3B and CD274 would be more effective than those targeting only one biomarker.

4. Discussion

Accumulating evidence has shown that A3B plays significant role in immunity, including tumor mutational signatures, immune cell infiltration, immune checkpoints, and immunotherapy. Therefore, to determine the role of A3B as a predictive biomarker for immunotherapy response in individual cancers, we conducted a preliminary exploration of A3B in pan-cancer. Notably, A3B was shown to be a predictive biomarker for immunotherapy response in bladder cancer. Furthermore, immunotherapy targeting composite biomarkers is more effective than targeting a single biomarker.

According to a previous study, APOBEC-mediated mutagenesis had a significant correlation with APOBEC mRNA levels, particularly A3B [9]. This study revealed that the single nucleotide polymorphism, $C \rightarrow T$ transitions in cervical, bladder, lung, head and neck, and breast cancers was positively correlated with A3B overexpression, consistent with other previous studies [9, 10, 17]. Moreover, we demonstrated a positive correlation between A3B and MSI. A3B has been shown to induce mutations. Furthermore, microsatellite instability is due to mutations in some mismatch repair genes, such as hMLH1, hPMS2, hMSH2, and hMSH6 [18].

Previous studies have shown that APOBEC enzymes play a role in the innate immune response, mainly in host defense against exogenous viruses and endogenous retrofactors [19, 20]. Surprisingly, APOBEC enzymes have been

(a)

(b)
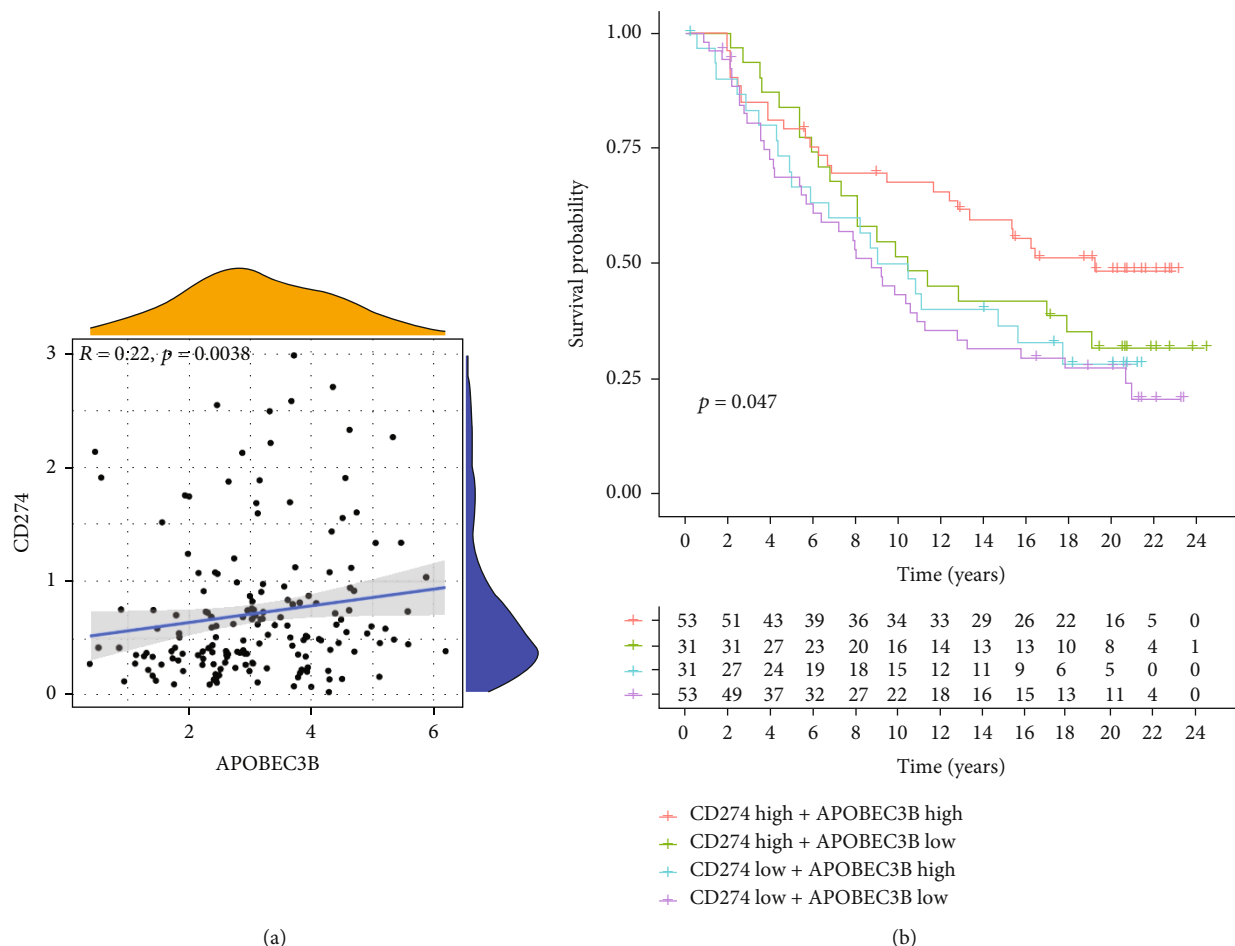
FIGURE 6: Validation of A3B in the IMvigor210 immunotherapy cohort. (a) Spearman correlation of A3B and CD274. (b) Survival analysis of the A3B combined with CD274 group. A3B and CD274 were divided into high and low expression groups based on the median value.

discovered in immune responses. According to Xia et al., APOBEC3B is a potential biomarker for predicting response to immunotherapy and survival in gastric cancer patients. In particular, APOBEC3B ^{high} CD8+ T cell ^{high} gastric cancer patients were more likely to benefit from adjuvant chemotherapy (ACT) and PD-1 blockade [21]. Hot tumors tend to have a higher immune cell infiltration and immune checkpoint expression [22]. Hot tumors show a reliable response to immunotherapy. Conversely, treatment of cold tumors with immunotherapy remains challenging. According to the present study, the A3B high expression group had a large amount of immune cell infiltration, including CD8+ T cells, B cells, macrophages, and NK cells. Furthermore, immune cells showed a high expression of immune checkpoints such as CD274, HAVCR2, and TIGIT. These results demonstrate a significant association between A3B and immunotherapy.

Several studies have investigated composite biomarkers. According to Yan et al., the composite biomarkers, NKG2A and PD-L1 in muscle-invasive bladder cancer were effective in predicting response to PD-L1 inhibitors and cisplatin-based ACT chemotherapy regimen [23]. Furthermore, the IMvigor210 immunotherapy clinical trial revealed that targeted therapy against the combined biomarkers of A3B

and CD274 was more effective than that targeting CD274 alone.

This study did not validate the findings of the IMvigor210 immunotherapy clinical trial. Therefore, further studies should be conducted to validate the findings of this study. In our view, APOBEC3B is a promising target for cancer therapy, just like Zou et al.'s study [24].

5. Conclusion

This study demonstrated that the combined biomarker of APOBEC3B and CD274 was more effective in predicting the response to PD-1/PD-L1 inhibitors than a single biomarker of CD274 in bladder urothelial carcinoma. In addition, the study revealed that APOBEC3B was positively correlated with TMB and MSI.

Data Availability

The original contributions presented in the study are included in the article/supplementary materials. Further inquiries can be directed to the corresponding authors.

Conflicts of Interest

The authors declare that the research was conducted in the absence of any commercial or financial relationships that could be construed as a potential conflict of interest.

Authors' Contributions

CZ and ZC made the same contribution to this research. CZ, ZW, and RW contributed to conception and design of the study. CZ and ZC organized the database. ZW performed the statistical analysis. CZ, GZ, and ZC wrote the first draft of the manuscript. YY improved the manuscript. All authors contributed to manuscript and read and approved the submitted version.

Acknowledgments

Supplementary Materials

Supplementary 1. Table S1. Immunophenotyping data in pan-cancer.

Supplementary 2. Table S2 Immune checkpoint related genes.

References

[1] J. Ferlay, I. Soerjomataram, R. Dikshit et al., "Cancer incidence and mortality worldwide: sources, methods and major patterns in GLOBOCAN 2012," *International Journal of Cancer*, vol. 136, no. 5, pp. E359–E386, 2015.

[2] M. A. Podolsky, J. T. Bailey, A. J. Gunderson, C. J. Oakes, K. Breech, and A. B. Glick, "Differentiated state of initiating tumor cells is key to distinctive immune responses seen in H-RasG12V–induced squamous tumors," *Cancer Immunology Research*, vol. 5, no. 3, pp. 198–210, 2017.

[3] M. D. Hellmann, M. K. Callahan, M. M. Awad et al., "Tumor mutational burden and efficacy of nivolumab monotherapy and in combination with Ipilimumab in small-cell lung cancer," *Cancer Cell*, vol. 33, no. 5, pp. 853–861.e4, 2018.

[4] T. Powles, J. P. Eder, G. D. Fine et al., "MPDL3280A (anti-PD-L1) treatment leads to clinical activity in metastatic bladder cancer," *Nature*, vol. 515, no. 7528, pp. 558–562, 2014.

[5] Y. Xiao and G. J. Freeman, "The microsatellite instable subset of colorectal cancer is a particularly good candidate for checkpoint blockade immunotherapy," *Cancer Discovery*, vol. 5, no. 1, pp. 16–18, 2015.

[6] M. Yarchoan, A. Hopkins, and E. M. Jaffee, "Tumor mutational burden and response rate to PD-1 inhibition," *The New England Journal of Medicine*, vol. 377, no. 25, pp. 2500-2501, 2017.

[7] C. Swanton, N. McGranahan, G. J. Starrett, and R. S. Harris, "APOBEC enzymes: mutagenic fuel for cancer evolution and heterogeneity," *Cancer Discovery*, vol. 5, no. 7, pp. 704–712, 2015.

[8] J. D. Salter, R. P. Bennett, and H. C. Smith, "The APOBEC protein family: united by structure, divergent in function," *Trends in Biochemical Sciences*, vol. 41, no. 7, pp. 578–594, 2016.

[9] S. A. Roberts, M. S. Lawrence, L. J. Klimczak et al., "An APOBEC cytidine deaminase mutagenesis pattern is widespread in human cancers," *Nature Genetics*, vol. 45, no. 9, pp. 970–976, 2013.

[10] M. B. Burns, N. A. Temiz, and R. S. Harris, "Evidence for APOBEC3B mutagenesis in multiple human cancers," *Nature Genetics*, vol. 45, no. 9, pp. 977–983, 2013.

[11] S. Wang, M. Jia, Z. He, and X. S. Liu, "APOBEC3B and APOBEC mutational signature as potential predictive markers for immunotherapy response in non-small cell lung cancer," *Oncogene*, vol. 37, no. 29, pp. 3924–3936, 2018.

[12] M. E. Ritchie, B. Phipson, D. Wu et al., "Limma powers differential expression analyses for RNA-sequencing and microarray studies," *Nucleic Acids Research*, vol. 43, no. 7, article e47, 2015.

[13] A. Mayakonda, D. C. Lin, Y. Assenov, C. Plass, and H. P. Koeffler, "Maftools: efficient and comprehensive analysis of somatic variants in cancer," *Genome Research*, vol. 28, no. 11, pp. 1747–1756, 2018.

[14] T. Li, J. Fu, Z. Zeng et al., "TIMER2.0 for analysis of tumor-infiltrating immune cells," *Nucleic Acids Research*, vol. 48, no. W1, pp. W509–W514, 2020.

[15] T. Li, J. Fan, B. Wang et al., "TIMER: a web server for comprehensive analysis of tumor-infiltrating immune cells," *Cancer Research*, vol. 77, no. 21, pp. e108–e110, 2017.

[16] B. Li, E. Severson, J. C. Pignon et al., "Comprehensive analyses of tumor immunity: implications for cancer immunotherapy," *Genome Biology*, vol. 17, no. 1, p. 174, 2016.

[17] M. B. Burns, L. Lackey, M. A. Carpenter et al., "APOBEC3B is an enzymatic source of mutation in breast cancer," *Nature*, vol. 494, no. 7437, pp. 366–370, 2013.

[18] J. R. Eshleman and S. D. Markowitz, "Mismatch repair defects in human carcinogenesis," *Human Molecular Genetics*, vol. 5, no. 1, pp. 1489–1494, 1996.

[19] V. C. Vieira and M. A. Soares, "The role of cytidine deaminases on innate immune responses against human viral infections," *BioMed Research International*, vol. 2013, Article ID 683095, 18 pages, 2013.

[20] K. J. Kuong and L. A. Loeb, "APOBEC3B mutagenesis in cancer," *Nature Genetics*, vol. 45, no. 9, pp. 964-965, 2013.

[21] S. Xia, Y. Gu, H. Zhang et al., "Immune inactivation by APOBEC3B enrichment predicts response to chemotherapy and survival in gastric cancer," *Oncoimmunology*, vol. 10, no. 1, article 1975386, 2021.

[22] D. S. Chen and I. Mellman, "Elements of cancer immunity and the cancer-immune set point," *Nature*, vol. 541, no. 7637, pp. 321–330, 2017.

[23] S. Yan, H. Zeng, K. Jin et al., "NKG2A and PD-L1 expression panel predicts clinical benefits from adjuvant chemotherapy and PD-L1 blockade in muscle-invasive bladder cancer," *Journal for Immunotherapy of Cancer*, vol. 10, no. 5, article e004569, 2022.

[24] J. Zou, C. Wang, X. Ma, E. Wang, and G. Peng, "APOBEC3B, a molecular driver of mutagenesis in human cancers," *Cell & Bioscience*, vol. 7, no. 1, p. 29, 2017.

Review Article

The Roles of Tumor-Associated Macrophages in Prostate Cancer

Chenglin Han, Yuxuan Deng, Wenchao Xu, Zhuo Liu, Tao Wang ⓘ, Shaogang Wang ⓘ, Jihong Liu ⓘ, and Xiaming Liu ⓘ

Department of Urology, Tongji Hospital, Tongji Medical College, Huazhong University of Science and Technology, Wuhan, China

Correspondence should be addressed to Jihong Liu; jhliu@tjh.tjmu.edu.cn and Xiaming Liu; xmliu77@hust.edu.cn

The morbidity of prostate cancer (PCa) is rising year by year, and it has become the primary cause of tumor-related mortality in males. It is widely accepted that macrophages account for 50% of the tumor mass in solid tumors and have emerged as a crucial participator in multiple stages of PCa, with the huge potential for further treatment. Oftentimes, tumor-associated macrophages (TAMs) in the tumor microenvironment (TME) behave like M2-like phenotypes that modulate malignant hallmarks of tumor lesions, ranging from tumorigenesis to metastasis. Several clinical studies indicated that mean TAM density was higher in human PCa cores versus benign prostatic hyperplasia (BPH), and increased biopsy TAM density potentially predicts worse clinico-pathological characteristics as well. Therefore, TAM represents a promising target for therapeutic intervention either alone or in combination with other strategies to halt the "vicious cycle," thus improving oncological outcomes. Herein, we mainly focus on the fundamental aspects of TAMs in prostate adenocarcinoma, while reviewing the mechanisms responsible for macrophage recruitment and polarization, which has clinical translational implications for the exploitation of potentially effective therapies against TAMs.

1. Introduction

Statistics demonstrated that the morbidity rates of prostate cancer (PCa) have shown a remarkable increase worldwide, which seriously threatens public health and survival [1, 2]. Surgery and radiation are the standard primary treatment against early patients with localized prostate malignancies, followed by androgen deprivation therapy (ADT), like surgical or chemical castration if this disease recurs. Currently, sipuleucel-T, enzalutamide, abiraterone, and radium-223 have been approved by the Food and Drug Administration (FDA) for clinical application. Unfortunately, the response is only transient in initial treatments due to the intrinsic or acquired resistance, and thus has different effects on earlier endpoints and overall survival (OS) [3]. In addition, most patients will stop responding to ADT over a while and progress towards a lethal outcome known as castration-resistant prostate cancer (CRPC), which has not been adequately addressed [4]. Thus, prostate carcinoma remains a refractory malignancy, which wistfully calls for an original therapeutic strategy to lower the cost burden. There

is also an unmet clinical need to further explore pathological mechanisms underlying carcinogenesis and progression.

It has been proved that tumorigenesis is a complicated and gradual process in which multiple mutations and progressive stages accumulate. Oncogenic mutation, like PTEN loss, is implicated in an early stage of prostate tumor development. Beyond tumor-intrinsic alteration, recent evidence points to the critical role of the tumor microenvironment (TME) in tumor progression and therapeutic response. TME, as a host of a sophisticated signal network, provides a fertile ground conducive to tumor survival [5]. Except for the subject of neoplastic cells, TME contains multiple nonmalignant stromal cells, like macrophages, endothelial cells, and fibroblasts [6, 7]. Among these cells, tumor-associated macrophages (TAMs) act as the central regulators of the interplay between tumor and surroundings [8]. In general, TAMs are divided into two dichotomous subsets: classically activated (M1) and alternatively activated (M2) macrophages [9], and their status depends spatially and temporally on integrated cues provided by TME [10]. Thus, this classification paradigm is an acknowledged

oversimplification and could not accurately recapitulate native PCa-associated macrophages, since multiple macrophage subpopulations have been observed in vivo [10, 11].

Several researchers believe that aberrance in macrophage fate brings about a reverse clinical outcome, as in autoimmune disease and cancer. In metastatic-CRPC (mCRPC) samples, abiraterone or enzalutamide-sensitive patients exhibited increased pro-inflammatory mediators, including interferon-γ (IFN-γ), interleukin-5 (IL-5), and tumor necrosis factor-α (TNF-α), which were generally identified as M1 markers [12]. Macrophages have intrinsic tumoricidal properties, yet most TAMs predominantly displayed functional characteristics of M2-like macrophages in tumor sites [13]. Recently, we have come to appreciate that the M2-TAMs increased stepwise from normal prostate to mCRPC. A higher density of TAMs increases the risk of tumor recurrence after transurethral resection of the prostate [14]. The Gleason score (GS), a predictive index for disease progression, derives from a pathologist's evaluation of prostate cancer tissue microarrays. Basically, five different prognostic groups were classified according to the final score, when ≤6 points usually mean better prognostic results [15]. The abundance of M2-like macrophages is also strongly associated with a higher GS and indicates worse specific survival and recurrence-free survival after hormone therapy [16, 17]. In a large PCa cohort, patients with higher M2-TAM influx exhibited enhanced resistance to immunotherapy and had a nearly twofold increase in mortality [18].

The direct or indirect contact detail is the hotspot regarding cell-cell interaction. In this review, we first discussed the intrinsic mechanism responsible for TAM reprogramming and the effects of TAMs on PCa development in multiple aspects. Cancer immunotherapy strategies targeting TAMs are then presented.

2. Macrophage Origin

In addition to mediating the first line of defense against pathogenic insult, macrophages, as a crucial part of innate immunity, can repair damaged tissue to support tissue homeostasis [19]. The heterogeneity is a significant character of macrophages. Given that macrophages assume supportive functions specialized to their resident tissue compartments, they are endowed with different names, such as Kupffer cells (liver), Langerhans cells (skin), and osteoclasts (bone) [20]. Bone marrow–derived monocytes enter the bloodstream and reach the majority of the tissues in vivo, where they are further differentiated into tissue-resident macrophages. However, the histological macrophages also arise from an embryonic precursor (yolk sac and/or fetal liver). These macrophages appear to have stem cell–like abilities and persist throughout life by local self-renewal [19, 21]. Therefore, as in other tissues, macrophages in the prostate consist of both blood-derived and embryonic-derived populations, where it is still unclear whether macrophage lineages with distinct origins exert diverse functions.

Macrophages constitute the dominant population within the TME and can be identified and quantified by using CD68 staining as a marker [22]. The emerging evidence indicated it is a dual origin that TAMs derive from. In prostate tumors, the TME is preferentially enriched with myeloid cells in both human and murine models. Firstly, a variety of chemokines, like colony stimulating factor-1 (CSF-1), granulocyte colony stimulating factor (G-CSF), and C-C motif chemokine ligand 2 (CCL-2), whether secreted from tumor cells, or stromal host cells, are associated with the recruitment and formation of tumor-related immune cells. On the other hand, TAMs could originate from myeloid progenitors that exist in the yolk, as in glioma and pancreatic cancer [23, 24].

TAMs can be continuously replenished in vivo. A human PCa specimen reveals that a milieu containing abundant factors and vesicles derived from tumor cells drives TAMs to aggregate on the surface [25]. PTEN deficiency correlated with the CXCL8 upregulation and subsequent macrophage infiltration. RNA-sequencing showed that overproduction of chemokines is induced in macrophages, which may contribute to higher levels of myeloid cells in advanced prostate tumors. CCL2-CCR2 axis has been shown to modulate macrophage number and phenotype for TME remodeling, which is consistent with increased tumor volumes observed here. There is no difference in the proliferation of PC-3$^{\text{lucCCL2}}$ and PC-3$^{\text{lucMock}}$ in vitro. Nevertheless, the PC-3$^{\text{lucCCL2}}$ tumor growth was significantly faster than the control in vivo. These data showed that CCL2 mediated the recruitment and retention of vast monocytic precursors in neoplastic tissues to enhance tumor burden, yet neutralizing antibodies targeting CCL-2 reduced macrophage mobilization [26, 27]. Also, spondin-2 (SPON2) overexpression has been observed in the serum or tissue samples of patients diagnosed as PCa [28]. Functionally, SPON2 activates PYK2 and increases its downstream RhoA and cortactin expression through interacting with $\alpha4\beta1$ integrin, thereby promoting cytoskeletal remodeling of monocytes for transendothelial migration [29]. Colony-stimulating factor-1 receptor (CSF-1R), a primary regulator of macrophage development, correlates with normal prostate growth and prostate cancer progression. Human prostatectomy samples showed intense staining of CSF-1R in areas of carcinoma and TAMs.

A large number of myeloid cells infiltrated into irradiated tumor sites in a murine PCa model. Mechanistic studies have suggested that local irradiation induces ABL1-dependent CSF-1 production, followed by activation of CSF1/CSF1R signaling for systemic macrophage recruitment [30]. Strikingly, recent studies point to the intricate interaction of TAMs with stromal cells. CAVIN1 is abundantly expressed in the normal prostate stroma, while its level is downregulated in the PCa stroma. This decrease in stromal CAVIN1 contributes to the upregulation of inflammatory signatures, like increased matrix metalloproteinase-3 (MMP3), dickkopf-1 (DKK1), and CSF-1 secretion, thus attracting macrophages for a tumor-supportive microenvironment [31]. The urokinase-type plasminogen activator/urokinase-type plasminogen activator receptor (uPA/uPAR) axis may play a central role in the aggressive prostate disease through direct and indirect interactions with integrins, growth factors, and endocytosis receptors. To our knowledge, a study that demonstrated

a direct link between activation of the uPA/uPAR axis and macrophage infiltration in PCa development has also been reported, in which stromal-derived uPA was regarded as a possibly predominant source within the TME [32, 33].

3. Macrophage Polarization

Except for their heterogeneity, macrophages are known to exhibit remarkable plasticity. The differentiated macrophages adopt appropriate phenotypes to regulate the diverse biological process. The functional evolution of macrophages is a highly dynamic process that is finely determined by signal transduction and metabolism [34]. The dichotomous classification of macrophages is currently generalized as the classically activated M1 and alternatively activated M2 phenotypes, which are described as extremes of functional states [35]. M1 and M2 macrophages represent distinct functions and transcriptional profiles in vivo, such as antigen expression, secreted factors, and metabolic pathways. The bi-directional activated potency of macrophages highly requires a key "switch" to respond to distinct peripheral stimuli. Macrophage destiny is not fixed, and two polarized states can be reversibly converted via reprogramming under a particular microenvironment. Indeed, macrophages exist across a dynamic spectrum, and even share mixed M1 and M2 characters.

In brief, M1 macrophages with phagocytosis property drive Th1 response and participate in the early inflammatory process. Lipopolysaccharide (LPS), an essential bacterial component, engages directly the Toll-like receptor 4 (TLR-4) on the membrane surface, thus enabling monocyte differentiation into an M1-like subtype that is characterized by higher levels of reactive oxygen species (ROS), inducible nitric oxide synthase 2 (iNOS), and MHC II molecules [36, 37]. Classical M1 macrophages execute pathogen clearance by secreting various pro-inflammatory factors, like IL-1β, IL-12, and TNF-α. Conversely, alternatively activated M2 macrophages mediate wound healing and fibrosis, thus leading to the resolution of inflammation. In the context of cancer, monocytes are quickly differentiated towards M2-like TAMs characterized by higher arginase-1 (Arg1) activity and the surface marker F4/80^{high} CD163$^+$CD206$^+$, suggesting a transition from L-arginine catabolism into depletion [38]. Supporting this notion, TAMs also highly express autocrine factors, like transforming growth factor-β (TGF-β) and IL-10, to promote their own maturation [39].

Generally, the most specific antibody recognizing CD163 could distinguish M2 from M1 macrophages. In the xenograft section of nude mice with seven common human PCa cell lines, more than 94% of all TAMs display an M2-like phenotype, and few M1-polarized macrophages are distributed in the periphery [17]. Recently, a study reports that prostate stereotactic body radiotherapy (SBRT), a neoadjuvant method to radical prostatectomy, amazedly alters the immune microenvironment within PCa. Multiplex immune-fluorescence (mIF) determines the increase of CD163$^+$ macrophage subsets in densities and reaches a 5.61-fold change 2 weeks after SBRT [40]. M1-type polarization is experimentally induced in vitro using exogenous toll-like receptor agonist, IFN-γ or combined with LPS, whereas the most potent M2-type is attained upon Th2 cytokine (like IL-4 and IL-13) stimuli [41]. THP-1 monocyte from human peripheral blood is frequently used to study the impact of TAMs in carcinogenesis due to its reproducible nature. More importantly, molecular profiles of M1-/M2-subtype derived from THP-1 in vitro are similar to that in intracorporal macrophages that have undergone polarization [42].

In view of the intricate signaling network in TME, the regulators of macrophage differentiation are not wholly revealed; thus, an enhanced understanding of their activation is helpful to identify effective molecular targets for pharmacological intervention. In this section, we emphatically illustrated the mechanism of macrophage polarization (Figure 1).

3.1. Microenvironment-Regulated Macrophage State. A variety of cytokines in the TME dictate the macrophage state. Macrophage colony-stimulating factor (M-CSF) appears competent to increase the number of TAMs through modulating GTPase Rac2, but M-CSFR blockers attenuate the polarization of Ly6C^{hi} monocytes to M2-like MHC-II^{lo} TAM [43]. Meanwhile, the extent of IL-6 expression in the stromal TME was positively associated with the abundance of F4/80$^+$ TAMs in PCa specimens [44–46]. One study provides experimental evidence that IL-6 acts through the IL-6R/Janus kinase 2 (JAK2)/signal transducer and activator of transcription-3 (STAT3) pathway to skew THP-1 monocyte toward an M2-like phenotype, without affecting its migration [47]. In addition, IL-6 enhances IL-4-dependent M2 polarization by boosting IL-4Rα expression under chronic inflammatory conditions [48]. An earlier study reported that the cross communication between cancer-associated fibroblasts (CAFs) and TAMs may further fuel PCa progression [49]. CAFs could induce inflammation and angiogenesis by stimulating macrophage infiltration via secretion of various cytokines, like monocyte chemotactic protein-1 (MCP-1), stromal-derived growth factor-1 (SDF-1), and CXCL14 [50]. In another study, CCR-2 dependent recruitment of macrophages by resident CAFs was reported to support tumor growth [51]. Recent data show that adenosine generated by CAFs can mediate the expansion and/or differentiation of M2-like macrophages [52]. Raised levels of G protein-coupled receptor 30 (GPR30) in prostate CAFs contribute to recruitment of monocytes and M2 differentiation of macrophage-like cells, which is partially associated with CXCL12 expression [53]. However, the staining of estrogen receptor alpha (ERα) in CAFs is relatively weak compared with the adjacent nonmalignant tissue, leading to a short time to hormonal relapse [54, 55]. Compelling evidence suggests that CAF.ERα (+) has a lower capability to attract macrophages into tumor sites and suppresses M2-type macrophages in the PCa microenvironment. After co-culture with the CAF.ERα (+), macrophages expressed less M2 macrophage-related markers, including IL-10, YM1 and Fuzz1, but not Arg-1. Further mechanism dissection indicated that CCL5 and IL-6 derived
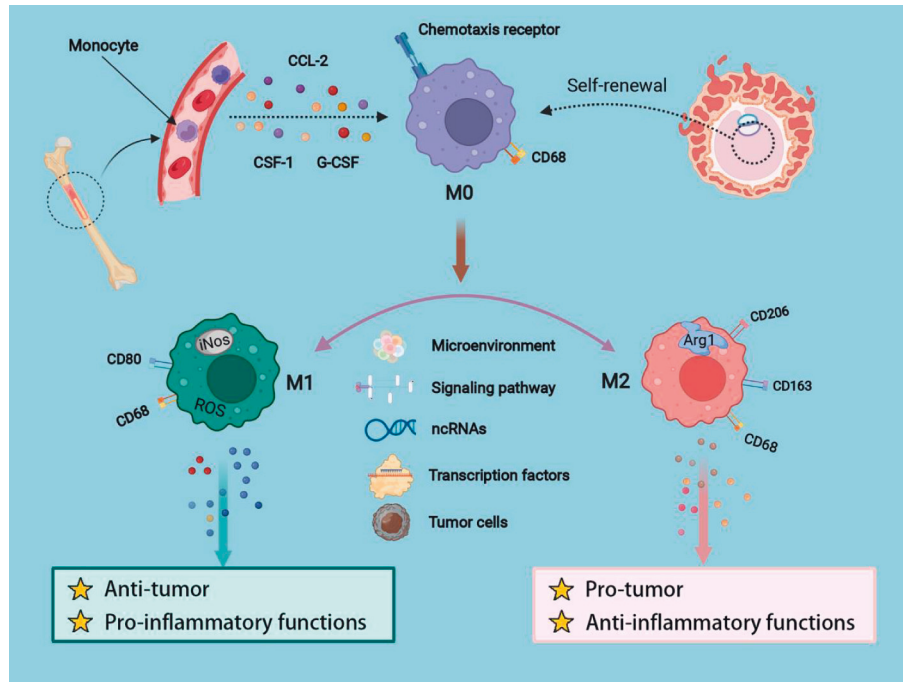
Figure 1: Representative images of the regulation of macrophage recruitment and polarization.

from CAF.ERα (−) may be implicated in macrophage recruitment and TAM generation [56]. Also, higher IL-4 and IL-13 levels in CAF.ERα (−) cells further support this conclusion.

Hypoxia-responsive macrophages favor fast tumor growth [57]. Hypoxia is a prominent characteristic of the TME, and an increase in M2-TAM infiltration is observed in prostate tumor tissues due to their tropism to hypoxia. Both 5-LOX and hypoxia inducible factor-1(HIF-1) in hypoxic areas boost macrophage mobility, partially by inducing MMP-7 expression [39]. Moreover, infiltrated macrophages tend to adopt M2-like features in the aged, oxidative, or mionectic milieu. One hallmark of the aging prostate is more significant infiltration of inflammatory cells, with a large release of growth factors. Compared with young mice, RM-9 prostate tumor cells orthotopically transplanted into the prostate grew at a faster rate in old mice. Further investigation showed that increased intra-tumoral leukocytes in the aged prostatic environment, especially F4/80$^+$macrophage, could possibly be attributed to upregulation of unique cytokines profiles, including IL-6 and IL-9 [58]. Furthermore, hypoxia-mediated lower expression of intra-tumoral pigment epithelium-derived factor (PEDF) facilitates the transformation of monocytes into prostatic TAMs. Serving as an immune-modulatory factor, PEDF raises the levels of M1-specific markers, such as iNOS, IL-12, and TNF-α, whereas restraining IL-10 and Arg-1 expression in macrophages [59].

One critical metabolic nature of malignant cells is the enhanced activity of glycolysis, even in aerobic conditions, which is known as the "Warburg Effect" [60]. Lactate, metabolic by-products of glycolysis, forms a heterogeneous acidification niche that could direct the functional roles of

macrophages. Lactic acids generated by glycolytic tumor cells were reported earlier to drive the pro-tumoral polarization of macrophages via the ERK/STAT3 signaling activation [61]. In line with these findings, recent studies show that lactate either mediates HIF-1 expression or increases Nrf2/heme oxygenase-1(HO-1) activation by elevating the intracellular ROS to elicit M2-like functional polarization [62]. Particularly in the late stage of PCa, elevated MCT4 expression is beneficial for preserving intracellular pH via assisting lactate outflow across the plasma membrane [63]. Current research proposes a scenario in which acidity, independent of lactate, can alter the activation state of TAMs. The zwitterionic buffer-based medium was used to simulate extracellular acidosis. Acidic condition (pH 6.8) did not affect the viability of activated macrophages, yet increased the expression of Arg1 and CD206 in IL-4-polarized macrophages. In addition, M2-like macrophage aggregation was usually accompanied by intra-tumoral lipid deposition. The fatty acid-enriched TME induces mitochondrial respiration of infiltrating monocytes via modulating the mTOR pathway, thus regulating their pro-tumoral phenotype [64].

3.2. Signaling Pathway-Associated with Macrophage Education. Like the cyclic AMP (cAMP)-protein kinase A (PKA) pathway, intracellular signaling cascades are responsible for M1/M2 polarization. Early research observed that both total PKA and phosphorylated PKA were decreased in the M1 subpopulation, whereas were upregulated in M2 subtypes. Mechanically, PKA regulatory IIα subunit (PRKAR2A) can occupy the transmembrane domain of the IFN-γ receptor to inhibit the downstream Jak2-STAT1 pathway. On the other side, PKA provokes the activation of

cAMP response element-binding protein (CREB) for IL-10, Arg-1, and VEGFa generation, and amplifies the regulation of IL-4 on M2-type polarization [65]. Significantly, prostaglandin E2 (PGE$_2$) promoted the activity of the EP4 receptor, thereby increasing anti-inflammatory signatures via a cAMP/PKA/CREB-dependent pathway [66]. Paradoxically, though increasing PKA levels through interacting with EP4 receptor, PGE$_3$ inhibits CD206 expression in THP-1 cells and reduces the proportion of CD68$^+$ and CD206$^+$ cells in tumor tissue. According to a recent study, there is only a slight but stable increase of PKA in the M2-like phenotype, yet PKA inhibitor H-89 can suppress a shift towards the M2 state. It is plausible to speculate that M2-TAM polarization depends on PKA activation that is reversely insufficient for M2 skewing, which warrants further investigation into the significance of PKA in macrophage differentiation [67].

LAMP2a (lysosome-associated membrane protein type 2A), located in the lysosomal membrane, acts as a novel intracellular switch to re-educate macrophages towards M2 phenotype through selectively targeting and degrading substrates of CRTC1 and PRDX1. At tumor sites of LAMP2a KO mice, an increase in pro-inflammatory M1-like subtype was observed. LAMP2a is manifested to be activated by various external stressors in TME, such as hypoxia and androgen deprivation [68]. The RON receptor (MST1R), a Met tyrosine kinase receptor family member, exists preferentially in prostate epithelial cells and macrophages [69, 70]. Prior work demonstrated macrophage-intrinsic RON as a negative regulator of macrophage activation. Specific loss of RON signaling in macrophages increased intra-tumoral iNOS staining in the transgenic adenocarcinoma of mouse prostate (TRAMP) model. Notably, prostate epithelial RON heightens MST1R activity of macrophages in a paracrine manner and promotes IL-6 and IL-33 generation, which indirectly accelerates prostate tumor growth through driving M2-like macrophage polarization [71]. However, macrophage scavenger receptor (MSR) is only expressed in macrophages, and MSR-positive inflammatory cells are broadly considered as M2-subtype in several types of malignancies, like glioma and ovarian epithelial tumors. In contrast, a sequence deficiency of MSR was initially found in one metastatic PCa sample, and the decreased expression of MSR was a predictor of poor prognosis [72, 73]. Immunohistochemistry analysis suggests that MSR labels most M2-macrophages in the PCa biopsy. IL-6/TGF-β restricts the MSR-transcriptional levels of THP-1 cells, thus modifying the gene expression of M2 markers. It probably ascribes to the comprehensive outcome of multi-factors in vivo, like distinct lineages, surrounding stromal cells, and the local environment, and the role of MSR in macrophage polarization remains to be further elaborated [74].

TGF-β, as a pleiotropic cytokine, exerts dual functions in cancer. Flow-cytometric analysis shows that recombinant TGF-β upregulates the expression of M2 markers in THP-1 cells, which points to the involvement of the TGF-β-mediated pathway in the regulation of macrophage phenotypes [75]. TGF-β induces M2-like polarization through Snail mediation, where downstream SMAD2/3 and PI3K/AKT signaling activation is indispensable [76]. TGF-β also synergizes with IL-10 to enhance the activation of M2 macrophages [77]. One novel finding that the activated Akt/FoxO1 pathway induced by TGF-β is responsible for the transformation of LPS-stimulated macrophages toward M2-subtypes improves our understanding of the roles of TGF-β in M2 polarization [78]. The bone morphogenetic protein (BMP) is a pivotal member of the TGF-β super-family, and specific deficiency of myeloid BMPR1 leads to an increase in the number of TNFα^+ M1 macrophages, thus impairing mouse prostate cancer growth [79]. Various BMP ligands, like BMP4, BMP6, and BMP7, can support M2 macrophages, whereas the BMP inhibitor DMH1 impedes M2-like polarization of macrophages isolated from tumors, with lower IL-10 and Cox2 levels. These findings supported our hypothesis that BMP signaling is noteworthily required for M2 macrophage activation [80].

3.3. Noncoding RNAs (ncRNAs)-Mediated Epigenetic Regulations.

Noncoding RNAs are a unique subclass of regulatory RNAs that cannot be translated into proteins. MicroRNA (miRNA) and long noncoding RNAs (lncRNA), as master epigenetic molecules, could regulate about 90% of human genes, which has attracted more attention. Among them, lncRNAs with a length greater than 200 nucleotides can be either cis or trans acting element to regulate gene expression in all respects: epigenetic, transcriptional, and posttranscriptional. lncRNAs, as molecular signals, decoy, guide, or scaffold, interact with DNAs, mRNA, other ncRNAs, or protein to exert their functions [81]. miRNAs are characterized by a length of about 22 nucleotides and control cellular biological processes by pairing to specific sequences of diverse mRNAs 3$'$untranslated region (3$'$UTR) at the same time [82]. Several ncRNAs and proteins have long been believed to play pivotal roles in determining the direction of macrophage polarization [83]. Lnc-M2 binds to PKA protein to activate its downstream CREB, thereby facilitating the process of M2 macrophage polarization [84]. Previously, a study indicated that M1 macrophages had higher levels of lncRNA-CCAT1 than that in M0 and M2 macrophages. Knock-down of CCAT1 increased the M2-phenotypic transformation and subsequent pro-tumorigenic functions by regulating miR-148a/PKCζ [85]. However, LINC00467 favors the higher expression of M2-characteristic genes via the miR-494-3p/STAT3 axis in prostate cancer [86]. Similarly, lncRNA-SNHG1 promotes M2-like macrophage polarization via increased STAT6 phosphorylation [87]. In macrophages, lncRNA-EPS is defined as a transcriptional brake that inhibits pro-inflammatory gene expression. Mechanistic studies indicate that lncRNA-EPS interacts with heterogeneous nuclear ribonucleoprotein L (hnRNPL) via a CANACA motif located in its 3$'$ end to change nucleosome position and repress transcription of immune response genes (IRGs) [88]. LncRNA CDKN2B-AS1 is principally expressed in the nucleus of THP-1 macrophages and restrains M2 polarization by forming RNA-DNA triplex with CDKN2B promoter [89]. miR-101-3p drives a pro-inflammatory phenotype in unpolarized monocyte-derived macrophages

(MDMs), at least in part by targeting TRIB1. qRT-PCR results demonstrated that miR-101-3p dramatically elevated the mRNA levels of TNF-α, IL-8, and CD80, whereas having no effects on the expression of M2-associated genes [90]. As an inhibitory regulator of JAK/STAT signaling, suppressor of cytokine signaling (SOCS) negatively regulates the state of macrophages and dendritic cells [91]. miRNA let-7b-5p overexpression domesticates macrophages towards M2-subtypes through regulating the SOCS1/STAT pathway, followed by prostate cancer progression [92].

Circular RNAs (circRNAs) are single-stranded RNAs characterized by having covalently closed loops and specific tertiary structure. Current studies support that circRNAs function as miRNAs sponges, alternative splicing mediators, and protein templates [93]. A high throughput circRNA microarray assay was conducted to evaluate circRNA signature of M1 and M2 macrophages. Compared with M2 macrophages, the expression of circRNA-010056, circRNA-003780, and circRNA-010231 is upregulated in M1-type macrophages, whereas the levels of circRNA-013630, circRNA-003424, circRNA-018127, and circRNA-001489 are downregulated [94]. circPPM1F is involved in LPS-induced M1-like activation through forming circPPM1F–HUr–PPM1F–NF-κB axis [95]. circCdy can also mediate M1 polarization by curbing the transportation of IRF4 into the nucleus [96]. However, circSAFB2, as a sponge for miR-620, promotes the polarization of M2 macrophages through modulating JAK1/STAT3 axis [97].

3.4. Transcription Factors. Directed by extracellular signals, several transcription factors, including interferon regulatory factors (IRFs), NF-κB, c-Myc, STAT3/6, Klf4, and C/EBPβ, participate in cellular transformation. TLR-4-mediated activation of downstream IRFs and NF-κB regulators facilitates iNOS expression and NO generation, yet deletion of c-Myc or C/EBPβ in macrophages impairs M2-like programs [98]. c-Myc is not implicated in macrophage proliferation and survival, but it is pivotal in alternative macrophage activation. c-Myc controls 45% of M2-related genes by either directly interacting with their promoters (e.g., MRC1 and ALOX15) or indirectly influencing other transcription factors (e.g., STAT6 and PPARγ) [99]. In c-Myc-KO mice, isolated TAMs exhibit attenuated abilities of tissue remodeling [100]. Furthermore, myeloid cells undergo M2-phenotypic alteration under FBXW7 knockout conditions. Mechanistically, FBXW7 deficiency attenuates the K48-linked polyubiquitination and resultant degradation of c-Myc, followed by higher levels of Arg1, Ym1, and Fizz1 [101].

STAT3 positively affects the phenotypic transition from M1 into M2 mediated by prostate tumor cell-culture supernatant. JAK2/STAT3 signaling activation is implicated in IL-6-mediated M2-like polarization. In addition, p-STAT3 encourages M2 activation through inhibiting negative regulators, such as NF-κB and p-STAT1 [102]. Cooperation between STAT6 and PPARγ is responsible for IL-4-orientated M2-polarization, whereas STAT6 acetylation is a negative regulatory mechanism underlying M2 polarization. The E3 ligase Trim24 catalyzes CREB-binding protein (CREBBP) ubiquitination and subsequent STAT6 acetylation to restrict M2 macrophage activation [103]. Notch signaling, a highly conserved pathway, is recognized as the determinant in the orientation of macrophage polarization. When the Notch transduction is blocked, macrophages exhibit functional characteristics of an M2-like phenotype. However, in the absence of myeloid Klf4, bone marrow–derived macrophages (BMDMs) express fewer M2-like indicators, like Arg-1, mannose receptor (MR), and display a pro-inflammatory gene expression signature supporting M1 differentiation [104].

Androgen receptor (AR), as a member of the nuclear receptor super-family, is involved in regulating cellular events. A study illustrates that activation of AR signaling is not exclusively limited to prostate epithelial cells but lies in TAMs. AR translocates into the nuclei and binds DNA at enhancer regions via the AP-1 complex in macrophages, which is incompatible with epithelial tumor cells where AR acts on the DNA by transcription motifs. ChiP-seq analysis indicated AR-binding proximal to M2-symbolic genes of tissue-resident macrophages, including IL-10, CD163, and CD206. Androgens have broad immune-regulatory effects, and androgen/AR may exert an unexpected role in macrophage polarization. These genes were elevated upon R1881 stimulation, whereas RD162, an AR signaling blocker, partially restored the initial expression. The reconstitution of androgen (DHT, dihydrotestosterone) also significantly increased the relative percentage of CD163$^+$CD206$^+$ double-positive in MDMs. The M2-promoting effect of DHT was just specific for macrophages via AR-binding sites that were most prominently found in intronic and distal intergenic regions. Interestingly, bicalutamide and flutamide reduced CD163$^+$ macrophage infiltration, while promoting the expression of pro-inflammatory cytokines (IFN-γ, TNF-α) in PCa samples; however, later studies reported contradicting results [105, 106].

Furthermore, a trend towards fewer TAM markers was observed in alveolar macrophages lacking AR compared to AR-proficient macrophages [107]. Some investigators found that IL-4 initiates AR signaling for M2 differentiation, supporting AR as an enhancer of TAM differentiation [108]. Indeed, AR expression in macrophages from endogenous sources is deficient, less than 100 times than in PCa cell lines. Given that ADT is a systemic treatment, the simple inhibition of AR signaling by ADT may be insufficient for transformation from M2 toward M1 phenotype. Generally, ADT domesticates the M2-like polarization in a paracrine pattern by modulating other host cells, including tumor cells, which are not only limited by blocking the androgen/AR axis in macrophage-like cells.

3.5. Tumor Cells. A study indicates that human macrophages undergo certain alterations in the presence of PCa cells, which is not easily surmounted. Prostate TAMs could be

reprogrammed through direct contact with PCa cells. Till date, multiple lines of evidence consistently indicate that there is a paracrine effect between cancer-derived factors and recipient macrophages. Yet, these immunomodulatory mediators certainly warrant investigation into their specific contributions to macrophage activation.

The supernatant of PC-3 cells effectively leads to a change in macrophage profile from M1 into M2 in vitro, and that shift is mainly associated with IL-10-mediated STAT3 phosphorylation. Similarly, milk fat globule-EGF factor 8 (MFG-E8) contained in exosomes from PCa cells drives an M2-like state by activating the STAT3/SOCS3 pathway [109]. A basic research yields interesting discoveries that PCa-derived CRAMP firstly chemoattracts immature myeloid progenitors (IMPs) into the TME and then modulates their differentiation into the M2-like macrophages. Molecular mechanisms indicate that CRAMP upregulated formyl peptide receptor 2 (FPR2) in an autocrine pattern, thereby inducing STAT3-dependent M-CSF and MCP-1 generation for M2 skewing in CRAMP-enriched TME [110]. Protein kinase C zeta (PKCζ), a tumor suppressor, negatively correlates with the abundance of CD206$^+$ macrophages. A co-culture model is used to simulate the physiological interaction between PCa cells and macrophages herein. Silencing of PKCζ in PC-3 and DU145 cell lines indirectly initiates M2 polarization by mediating the secretion of critical cytokines, including IL-4 and IL-13 [111]. In addition, the generation of TNF-α/β and M2 macrophages was attenuated in the PC3-shKPNA4 primary tumor tissues. Comprehensive analysis suggested that TNF activated by KPNA4 increases TAM gene markers in primary mouse monocytes, altering the microenvironment for immune escape [112]. However, another study demonstrated the positive correlation of TRIB1 with the frequent presence of CD163$^+$ macrophages in clinical PCa specimens [113]. Mechanistic dissection revealed that TRIB1 contributed to the secretion of CXCL2 and IL-8 via IKB-zeta mediation in tumor cells, followed by an increase in the M2-like population. Furthermore, enhanced AIRE regulated by transcription factor Elk-1 in androgen-independent PCa cells is equipped to polarize peripheral monocytes towards an M2-like phenotype by modulating IL-6 and PGE secretion [114].

Tumor cells also control the macrophage-activated state by indirectly influencing/activating peripheral stroma cells within TME. Macrophage inhibitory cytokine-1 (MIC-1) production is augmented in prostate cancer cells by adipocytes-mediated lipolysis and fatty acid release, which enforces the secretion of IL-6 and IL-8 from periprostatic CAFs for M2-polarization [115]. Macrophages can undergo phenotypic transformation via metabolic reprogramming. Alternatively activated macrophages have been shown to prefer fatty acid oxidation [116]. Notably, KRAS^{G12D} is generated in tumor cells via autophagy-dependent ferroptosis in the oxidative microenvironment and is subsequently packaged into exosomes for release. Extracellular KRAS^{G12D} is taken in by macrophages via AGER/RAGE, followed by M2 activation via STAT3-dependent fatty acid oxidation [117].

4. The Roles of Macrophages in Tumorigenesis

The transition from premalignant lesions to adenocarcinoma is a multistep process. It is commonly accepted that TAMs, as highly active immune effectors, exhibit either antitumor or protumor activity, which hinges on tissue-specific regulation and tumor-developed stage. Chronic inflammation is an epidemiologic factor for prostate cancer. In nascent tumors, circulating precursors are recruited to gather around the inflammatory milieu, and are subsequently differentiated into M1-like macrophages. They secrete stimulatory cytokines activating T effector cells to eradicate mutant neoplastic cells. Conditional medium (CM) of M1-polarized macrophages promotes apoptosis of PC-3 cells and suppresses tumor parameters, including metastasis and angiogenesis [118]. Nevertheless, a large number of M1 macrophages can also aggravate inflammatory damage in various pathological processes. Massive M1 activation causes severe cytokine storms and corresponding mutation accumulation in prostate epithelial cells via repeated injury, ultimately initiating the carcinogenic process. Complex and dynamic communication occurs between cancer cells and immune cells. As tumors grow and spread, the macrophage statue is subverted towards an antiphlogistic phenotype, representing alternation of the immune compartments. Advances in cancer research coincidentally suggest that M2-macrophages make up the majority of TAMs, especially in advanced stages of PCa, which usually correlates with an increased lethal risk [10, 119, 120]. The biological roles of TAMs in tumor formation and progression are multifactorial, which will be reviewed below (Figure 2).

4.1. Therapeutic Resistance. Endocrine therapy is the primary treatment for patients with advanced PCa. Nearly all patients still inevitably progress to advanced CRPC after about two years, which remains a major clinical challenge, despite primary symptomatic relief. Our initial efforts focused on exploring cell-autonomous alteration in CRPC populations. lncRNA HOXD-AS1 regulates chemoresistance of CRPC via WDR5 recruitment [121]. Activation of MAPK signaling by CXCR7 contributes to enzalutamide resistance [122].

Multiple studies emphasized that TAMs influence the clinical response to hormone therapy in vivo. Patients with TAMs <22/high power field (HPF) assume a better response to ADT than those with higher numbers of TAMs ($P < 0.001$). Currently, we notice that a decrease of M2-like macrophages mediated initially by androgen deprivation is transient and appears to reverse with long-term ADT employment [123]. Castrating tumor-bearing mice triggers an influx of leukocytes into prostate tumors. The increased stained intensity of CD68 and CD163 has been described in castrated TRAMP mice and radical prostatectomy samples from ADT-treated patients. SEMA3A was co-expressed with TAMs and correlated with the progression of CRPC. Interestingly, the SEMA3A transcription levels are upregulated after ADT, which elicits recruitment and M2-like
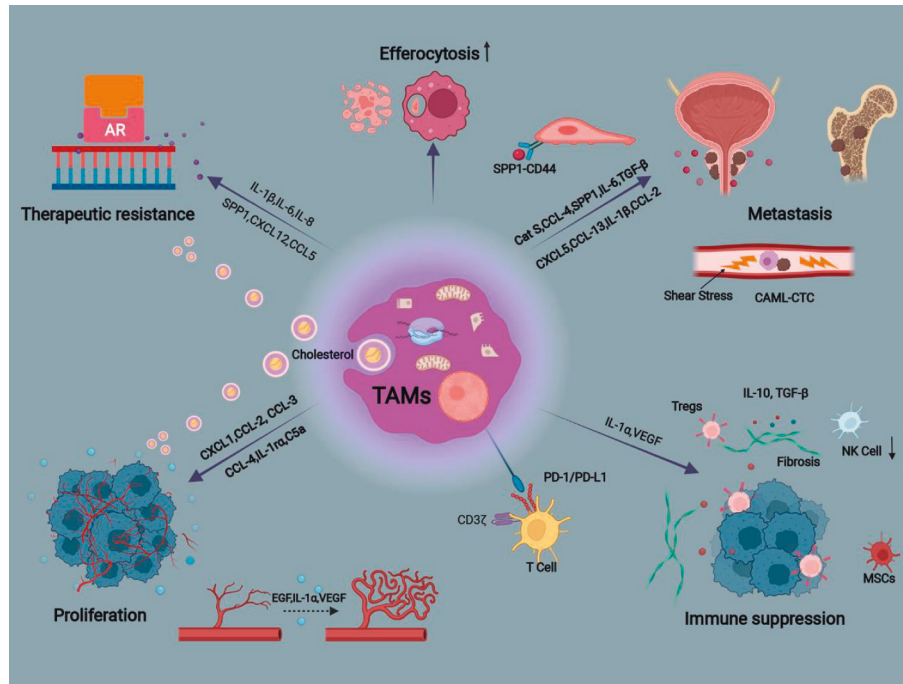
FIGURE 2: Tumor-associated macrophages mediate therapeutic resistance, proliferation, metastasis and immune suppression in prostate cancer. TAMs, tumor-associated macrophages; cat (S) cathepsin; CAML, cancer-associated macrophage-like cell; CTC, circulating tumor cell; tregs, regulatory T cells; NK, nature killer; MSCs, mesenchymal stem cells.

polarization of monocytes via NRP1 receptor and promotes ADT resistance [124].

Critically, results from in vivo and in vitro models confirm that the emergence of CRPC partially depends on the production of compensatory growth factors by TAMs. Macrophages were also demonstrated to stimulate AR translocation into the nucleus in PCa cells in co-cultures. IL-1β, primarily generated in the M2-subtype, either mediates MEKK1 activation or causes TAB2-dependent nuclear receptor corepressors (N-CoR) dismissal from AR, which contributes to therapeutic resistance via conversion of AR antagonists to agonists [125]. Persistent AR activation remains a critical driver in castration resistance. Despite castrated levels of serum androgens, there is a higher degree of intra-tumoral androgens in CRPC, nearly the same as those of eugenic men [126]. Prostate cancer cells express most steroidogenic enzymes and are therefore capable of converting cholesterol to androgens. Single-cell RNA sequencing analysis shows that this subset of TAMs is characterized by an accumulation of lipids. Clear evidence points to an appreciable increase in the transcriptional levels of steroid and bile acid in M2-like TAMs.

BMDMs can express various genes associated with cholesterol influx/efflux more than the PCa cell lines, including Abcg1, CD36, and Scarb1 [127]. They could absorb cholesterol in the form of low-density lipoprotein (LDL) and transfer particles containing rich cholesterol into neighboring prostate tumor cells, where it acts as a precursor to enhance androgen biosynthesis for nuclear translocation of AR [128]. The BMP-6 secreted by PCa cells induced IL-6 generation in recipient macrophages, and reciprocally, the

AR-transcriptional activity was elicited to avail castration resistance in CaP cells [129].

Alternatively, PCa progression may arise in the deficiency of a functional AR. As the strategies targeting AR have become widespread, the incidence of neuroendocrine prostate cancer (NEPC) has risen substantially, which manifests with lower AR signaling activity and grows independently of the androgen. Neuroendocrine differentiation (NED) is an emerging mechanism of resistance to cancer therapies [130]. NEPC cells themselves acquire the characteristics of stem cells, while conducing to resistance acquisition by surrounding tumor cells [19]. IL-6, a pleiotropic cytokine, activates the TGF-β/SMAD2 axis and its downstream p38MAPK to drive NED of PCa cells under androgen depletion conditions [131]. IL-6 derived from TAMs also appears competent to upregulate the expression of parathyroid hormone-related peptide (PTHrP) that is an indicator of NED, which forms a positive loop and leads to enhanced NEPC tumorigenesis in vivo [132]. Noteworthily, sterol regulatory element-binding protein−2 (SREBP-2) increased tumor-synthetic cholesterol, which can be assimilated by TAMs via scavenger receptor (SR)-mediated endocytosis for IL-8 generation [133]. Increasing evidence suggests that IL-8 can promote the NED of prostate cancer through activating MAPK/ERK signaling. It is also verified to attenuate TRAIL-induced apoptosis of PCa cells by regulating c-FLIP transcription [134].

SPP1 has great significance to M2 polarization and phenotype maintenance [102]. Single-cell data identifies SPP1 as a luxuriant TAM-secretary factor under the hypoxic microenvironment. SPP1 either expands the glycolysis

program or increases the expression of p-glycoprotein for multidrug resistance in PCa cells [135]. Since the reciprocal crosstalk formed by TAMs with tumors, the second-line treatment like docetaxel combined with prednisone may also fail to restrict the aggressiveness of advanced CRPC. With exposure to docetaxel, the levels of several cytokines secreted by PCa cells were increased, like CSF-1 and IL-10, thus counteracting its anti-cancer efficacy [136]. Especially, CSF-1 stimulates polarization of neighboring macrophages towards an M2-like phenotype that reciprocally releases CXCL12 to sustain tumor survival via CXCR4 [137]. Meanwhile, TAM-derived CCL5 activates β-catenin/STAT3 signaling and upregulates the transcription factor Nanog, thus resulting in increased chemoresistance of PCa [138, 139].

4.2. Proliferation. TAMs can modulate early prostate tumorigenesis by promoting genetic instability, independently of any other carcinogenesis [140]. AR activator CCL-4 generated by M2-polarized macrophages mediates downregulation of P53/PTEN in RWPE-1 cells and augments the production of EMT markers. All prostate disorders are initially attributed to excessive proliferation of normal prostate epithelial cells. A 3-D co-culture model reveals that an elevated proliferative rate of normal prostate PZ-HPV-7 epithelial cells is achieved via activation of ERK and AKT induced by TAMs-secreted cytokines, like CCL-3, IL-1ra, and GDNF [25]. In another experiment, immortalized RWPE-1 cells alone formed well-organized spheroids after 24 days, whereas aggregated into a disorganized structure when cultured with macrophage-CM. Prostate intraepithelial neoplasia (PIN), a precursor lesion, is always the first step for prostate tumor construction [141]. TAMs are capable of increasing the percentage of nuclear cyclin D1-positive PIN cells. Later tests demonstrated that CXCL1, C5a, and CCL-2 derived by TAMs mainly potentiate PIN-cell proliferation through activating ERK without impacting cell apoptosis [142]. High-fat diet (HFD)-accelerated tumor growth was correlated with the increased M2/M1 ratio and IL-6 expression in the model mice. In human prostate cancer, IL-6 secretion was restricted to the prostatic stromal component, whereas IL-6 was derived mainly by local macrophages upon HFD stimulation. Higher IL-6 levels result in prostate cancer progression via STAT3 phosphorylation in tumor cells [143]. TAM-released IL-8 was demonstrated to sufficiently drive prostate tumor formation by modulating the STAT3/MALAT1 axis [144].

Given that tumor growth requires nutrition, the pro-angiogenic properties of TAMs are considered as the culprits of malignant transformation. To support this, a histopathologic study shows that the number of CD163^{+} macrophages is positively associated with the micro-vessel density (MVD) and proliferative Ki67-stained intensity [145]. TIE-2^{+} TAMs exhibit a unique angiopoietin receptor with neovascular capacity. Furthermore, M2-like TAMs secreted epidermal growth factor (EGF) to actuate neovascularization and carcinogenesis. The Smad1-induced IL-1α production of macrophages is an important mechanism whereby BMP-6

accelerates prostate tumor growth in vivo [146]. IL-1α, known as pro-angiogenic chemokines, enhances PCa-associated angiogenesis via IL-1R/CXCL8 [147]. Similarly, CCN3-mediated M2 phenotype increased VEGF expression and subsequently triggered endothelial tube formation. A pre-clinical study observed the elevation of ERα in prostate tumor mass and cells. It simultaneously demonstrated that ERα activation initiates downstream oncogenic signaling by interacting with HIF-1α in the hypoxic milieu [148]. Cholesterol from TAMs also acts as an endogenous ERα agonist to favor adaptive growth of prostate cancer. Recently, TAM is also identified as a crucial cellular link in paracrine tumor-tumor interplay. Consistent with animal experimental results, high-grade tumors encouraged the rapid growth of adjacent less-malignant tumors in patients with multifocal prostate cancer [149]. However, high-metastatic MLL did not affect low-metastatic AT1 viability in a co-culture system, suggesting that direct interactions between tumor cells were minor. Further analysis shows that soluble factors derived from an aggressive prostate tumor circulate into the milieu of distant indolent tumors, where neovascularization for blood supply markedly increases due to the massive accumulation of M2-like TAMs.

4.3. Metastasis. In prostate cancer, an increased proportion of iNOS^{+} macrophages is observed in organ-confined foci. In contrast, higher infiltration of CD163^{+} macrophages is conducive to extracapsular extension, suggesting M2-type macrophages can increase PCa-metastatic potential [50, 119]. IL-4 is responsible for the generation of macrophage-supplied cathepsin S (Cat S) protease that heightens the risk of pelvic metastasis in TRAMP mice and patients with prostate malignancy [150, 151]. Perivascular Cat S pro-form is activated in an acidic condition, allowing further E-cadherin degradation during metastatic colonization of distant organs. Secreted SPP1 remodel extracellular matrix for prostate cancer invasion [28]. The interaction of SPP1-CD44, a cell-surface receptor, is an important paracrine pattern to regulate tumor metastasis. Single-cell analysis also suggests that EMT is the biological process in tumor cells most relevant to SPP1^{+}TAMs [152]. It was previously established that AR activation directly controlled the transcription of Triggering Receptor Expressed on Myeloid cells-1 (TREM-1) and upregulated its downstream chemokines, such as CCL-3, CCL-4, and CCL-13, which nonspecifically bind to chemokine receptors to promote the exfoliation of PCa cells. Immunohistochemical staining showed that CCR2, CCR3, and CCR4 staining were observed in primary and metastatic PCa cells on tissue microarrays, while CCR3 and CCR4 were absent in normal prostate cells [105]. Also, the elevation of CCL-4 is associated with Snail upregulation in high-grade PIN and prostate carcinoma [140].

Paradoxically, ADT increases the probability of distant metastasis in some PCa patients, although accompanied by tumor decrease and reduced PSA levels [104]. A clinical trial shows that 52% of PCa patients develop new bone lesions after abiraterone treatment for four months, which may be at

least partially explained by increased TAM-secretory cytokines. Inquiringly, targeting AR with siRNA in macrophages promoted the migration of LNCaP cells in a co-culture system. Further analysis found that AR silencing induced CCL-2 elevation and resultant EMT process of PCa cells via CCL2/CCR2/STAT3 signaling [153]. Bone metastasis commonly occurs in men with recurrent CRPC, leading to a 5-year survival rate of 25%. M2-like TAMs constitute one-sixth of the total cells in PCa-resident bone lesions. Flow cytometry demonstrated that a vast majority of CD163-positive cells exist in mCRPC tissue obtained from the first right rib. Double-staining showed that HO-1 is broadly produced in CD163$^+$ cells, and its expression is higher in aggressive prostate tumors. HO-1 is found to facilitate iron delivery and Fe^{3+} accumulation in tumor cells, whereas inhibition of HO-1 significantly retards bone-metastases in other PCa experimental models [154]. Ca2+/calmodulin (CaM)-dependent protein kinase kinase 2 (CaMKK2) is selectively expressed in macrophages. It regulates metabolic responses and manipulates the niche of bone microenvironment to benefit PCa cells by releasing inflammatory cytokines [155]. Both CCL-2 and IL-6 secreted from TAMs are also demonstrated to add a risk of bone metastasis, thus determining the advanced stage of metastatic prostate tumors [26, 107]. Instead, cancer cell death could lead to tumor growth and bone destruction, which partially ascribes to macrophage-efferocytotic capacity. During tumor progression, chronic inflammation inevitably causes tissue damage and cell death. Apoptotic/necrotic tumor cells are cleared and phagocytosed by macrophages, known as efferocytosis. Efferocytosis is crucial to preserve tissue integrity but may also have deleterious effects. Compared to M1-like macrophages, M2-like macrophages were displayed to be ~4-fold more capable of efferocytosis. A study reported that efferocytosis of TAMs induces CXCL5 secretion by activating NF-κB and STAT3 signaling in vitro, thus accelerating colonization of disseminated PCa cells and osseous progression [156]. In the context of cancer, the efferocytotic function of TAMs could be further enhanced by chemotherapies or other targeted therapies. This amplificatory effect triggers the secretion of extensive pro-inflammatory cytokines, like TGF-β and CCL-2, which perpetuates M2 polarization and forms feed-forward loops to exacerbate skeletal metastasis [56].

The metastatic process of prostate tumors is accompanied by prominent alteration in the basement membrane and extracellular matrix (ECM). Much evidence depicts that intense MMP-9 and IL-1β staining were observed in M2-like macrophages and tumor cells at the invasive prostate zone. MMP-9, as a cancer biomarker, participates in ECM degradation and facilitates tumor aggressiveness. Emerging roles of IL-1β in PCa development have been revealed. IL-1β activates AR function for enhanced tumor mobility [157]. Besides, a raised level of MIC-1 mediated by IL-1β in serum contributes to actin reorganization of tumor cells through activating FAK-RhoA signaling, thus reducing adhesion at an early stage [158]. PCa cell-derived IL-1β promoted Marco-dependent lipid accumulation, and reciprocally, the migratory capacity of tumors was enhanced by CCL6

released by lipid-loaded TAMs [159]. Nowadays, several studies emphasize that TAM-derived uPA mediates uPAR-dependent cleavage of the $\alpha6\beta1$ integrin ($\alpha6\beta1$), which means pericellular laminin proteolysis [33].

Aggressive tumor cells intravasate into the blood vessel, thus becoming circulating tumor cells (CTCs). Homing to target organs is only possible when PCa cells survive in the circulation. Recently, a study reported that TAMs leave primary sites and attach CTCs in the peripheral blood of PCa patients, which is called circulating cancer-associated macrophage-like cells (CAMLs) [160]. Further investigation shows that contacts with CAMLs induced epithelial-mesenchymal plasticity and endow CTCs with an aggressive nanomechanical phenotype that can resist the shear stress of the bloodstream and advance seed-distant metastases [161].

4.4. Immune Suppression. The M1/M2 imbalance skews the immune response to opposite directions, which weakens immunological monitoring and helps tumor cells avoid the lethal attack. Macrophages of M2-like subtype themselves have poor antigen-presenting nature and allow desensitization of PCa cells to cytotoxicity mediated by nature killer (NK) cells. Several indirect and direct actions of TAMs on autologous T lymphocyte number and activation have been suggested. The depletion of L-arginine, an essential nutrient for T cells, is a vital contributor to the immuno-suppressive TME in patients with cancer. Increased Arg1 expression in M2 macrophages could induce metabolic starvation of effector T-cell by clearing L-arginine, which favors the lower frequencies of circulating cytotoxic T cells. mCRPC lesions, known as "cold" tumors, exhibit poor T-cell infiltration and functionally inactive T cells. A recent study illustrated that TAMs either exclude CD8$^+$ T cells from tumor mass via granulin-induced fibrosis or impair T-cell activities by inhibiting its-receptor CD3ζchain, thus aggravating the immune evasion to support unchecked neoplastic growth [10, 162]. PD-L1 expressed on TAMs also binds to PD-1 of T cells, and subsequently transmits inhibitory signaling into T cells [163]. More significantly, TAMs phagocytose T cell-superficial anti-PD-1 antibodies and lower therefore the benefit from immunotherapy [164]. Regulatory T cells (Tregs) control cellular responses to death-associated stimuli by affecting both innate and adaptive immunity in the context of cancer. They can inhibit the activation of CD4$^+$, CD8+ T cells, and NK cells via cytokine generation (IL-10 and TGF-β) or direct cell-cell contact, thus operating immunosuppressive functions. High Treg numbers have been described in the peripheral blood and tumor mass of PCa patients, which is why the vaccine has a weak antitumor effect [165]. Bioinformatics analysis points to a positive association of TAMs and Tregs in number in high-risk score PCa patients [119]. TAMs may induce Tregs production and cooperate with them to form a unique niche that elicits tumor progression. Elevated expression of Axl, MerTK, and Tyro3 receptor kinases acquired in M2 macrophages stimulate the influx of lymphocytes and its succedent differentiation into Tregs

[12, 166]. Strikingly, TAMs assist mesenchymal stem cells (MSCs) in displaying enhanced immunosuppressive activity in PCa. IL-1α derived from TAMs induces excessive expression of TGF-β in MSCs [167]. Likewise, TAMs-released VEGF restrains the maturation of dendritic cells and increases the proportion of MSCs, thereby influencing the overall organization of the immune response [168].

5. Promising Strategies for PCa Treatment via Targeting TAMs

Given the dual roles of TAMs in orchestrating PCa progression, significant attention has been drawn to tumor immunotherapy targeting TAMs to disrupt immune tolerance. Broadly, current TAM therapeutic strategies pertain to the following three groups: (1) depleting total TAM count; (2) reprogramming M2-like macrophages to the tumoricidal M1-like phenotype; (3) inhibiting the crosstalk between TAMs and tumor cells (Figure 3).

5.1. Depleting Total TAM Count. Lower macrophage count is considered a better prognostic indicator in PCa biopsy specimens. A study reported that the incidence of lymph node and bone metastasis in mice containing PC-3MM2 cells declined after macrophage abrogation induced by clodronate liposome. Consistent with these findings, macrophage depletion extended survival during ADT [127]. However, this attempt may be unsuccessful in clinical trials, largely because of severe, off-target side effects. Since its distinct marks or peripheral atmosphere, selective growth suppression of M2-subsets aids in prostate tumor regression and reduces metastatic potential in pre-clinical models.

As mentioned above, AR activation is responsible for M2-like differentiation. Compared with PTEN$^{+/-}$ mice, prostate size remarkably decreased in genetic background mice with macrophage AR knockout (MARKO) and PTEN$^{+/-}$, suggesting that AR-deficient macrophages can attenuate PTEN deficiency–induced prostate carcinogenesis. A study demonstrates that a selective AR degradation enhancer, ASC-J9® negates the pro-survival activity of TAMs and re-models TME towards an antitumoral immunity, providing a potential drug target for restraining early PIN development. Once a neoplasm has started, several approaches to androgen deprivation, like surgical castration, reversely modulate the accumulation of M2-polarized TAMs, which can be undermined by metformin through inducing COX2/PGE2 downregulation. Against this backdrop, a rational combination of metformin with ADT was proposed to augment the durable response in cancer patients.

Due to the tumor-homing ability of TAMs, chemokine-chemokine receptor blockers may display potential for therapeutics in the future. As described previously, RON overexpression in PCa cells enhances CCL2 production for macrophage recruitment and RON-overexpressing tumors alter macrophage state to drive growth under androgen-deprived conditions. It is therefore plausible that combining RON inhibition with macrophage depletion promotes CRPC sensitization to ADT [169]. Coincidentally, anti CCR2 antagonist could reduce the side effects induced by ADT, although single antibody targeting CCL2 failed in a phase II clinical trial [170]. Preclinical evidence suggests that blocking the CSF1/CSF1R axis effectively prevents the influx of TAMs and weakens their pro-tumorigenic influence. Despite having negligible effects on prostate tumor growth in vitro, the selective CSF1-R inhibitor, PLX3397, can alone cause a significant reduction of myeloid-derived suppressor cells (MDSCs) and F4/80$^+$ macrophages in primary tumor sites. With this concern in mind, PLX3397 may helpfully improve prognosis when combined with other regimens like docetaxel and irradiation [171]. At the molecular level, CSF1-R blockade impedes radiotherapy-induced Arg1, CSF-1, and MMP expression, thus preventing the acquired resistance mediated by M2-polarized macrophages [30].

Knock-down of TR4 nuclear receptors suppresses the macrophage infiltration and consequent malignant invasion and metastasis by altering the TIMP-1/MMP2/MMP9 signals, which indicates that developing small molecule inhibitors targeting TR4 represents a feasible strategy against PCa. Notably, the difference between M1 and M2 macrophages may be utilized to achieve differentiated strike. Due to higher expression of CD115 in M2 phenotype than M1 population, trabectedin preferentially reduces the amount of M2-like macrophages by targeting CD115$^+$ cells to rehabilitate the bone microenvironment, eventually leading to lessened tumor burden in the skeleton [172]. Intra-tumoral invariant natural killer T (iNKT) cells also remodel the antitumor microenvironment. After iNKT cells are transferred into PCa-bearing mice, selective killing of M2 macrophages and M1-subtype survival would happen via cooperative CD1d, CD40, and Fas engagement [173]. Acidic TME is expected to be exploited for tumor-specific imaging and therapy. The increased intra-tumoral pH had no significant difference in myeloid cell infiltration, but it cut off M2-like TAM activation caused by prostate tumors. More prominently, pH-responsive peptides or pH-sensitive nanosystems can target-specific acidic milieu rich in macrophages to improve the total efficacy. Delivery of STAT6 inhibitor decorated into a nanocarrier with a pH-sensitive PEG outer layer that only sheds in the acidic TME diminishes the number of TAMs in tumor tissues, whereas avoiding regulation of M2-subpopulation in healthy organs with neutral pH [174].

5.2. Reprogramming M2-Like Macrophages to the Tumoricidal M1-Like Phenotype. Recently, the potential of reprogrammed macrophage subsets has been explored. Injection of M1-derived exosome-mimetic nanovesicles that skews M2 towards an immunocompetent profile resulted in smaller tumor size in vivo, and potentiated antitumor efficacy of immune checkpoint inhibitor, like anti-PD-L1 antibody [175]. Macrophage polarization is not fixed, and domesticating TAMs to reverse their pro-tumoral properties provides a therapeutic window. Hyperbaric oxygen therapy is greatly anticipated. It either modifies the hypoxic
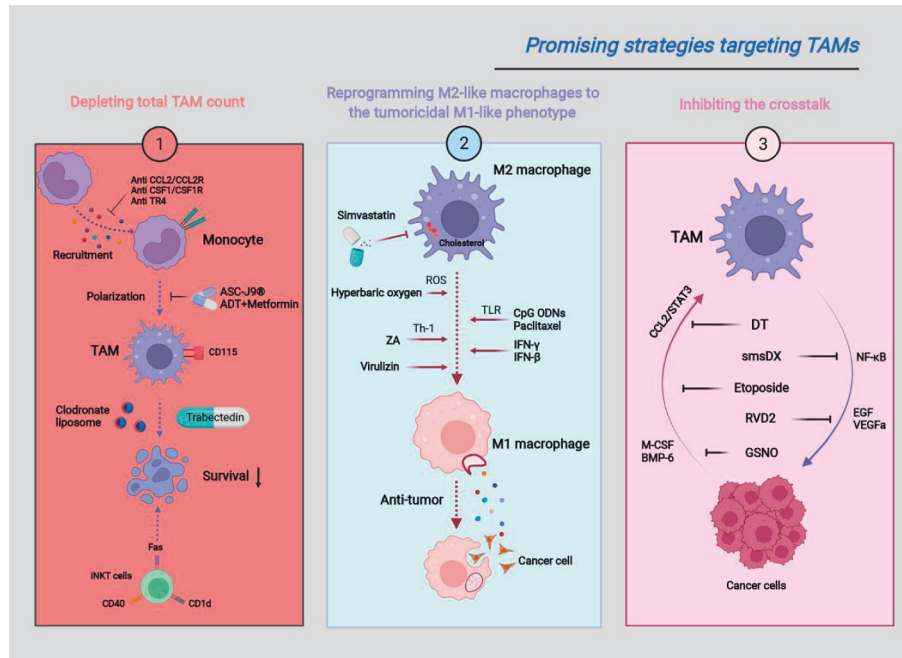
FIGURE 3: Promising strategies targeting TAMs for prostate cancer therapy. DT, dihydroisotanshinone I; ZA, zoledronic acid; smsDX, somatostatin derivate; RVD2, resolvin D2.

microenvironment via an increased supply of oxygen or induces ROS over-production, which reduces the number and activity of M2 macrophages [176]. The administration of zoledronic acid (ZA) boosts the production of Th-1 cytokines (IL-12 and poly: C) that re-educated TAMs towards M1-type to suppress primary tumor growth and spontaneous lung metastasis, which has been applied for treating symptomatic skeletal lesion [177]. TLR agonists, like CpG ODNs, enhance cellular phagocytosis by repolarizing M2-M1 macrophages [66]. Likewise, paclitaxel alters the signature of TAMs into an M1-like profile in a TLR4-dependent manner, thus disrupting tumor promotion [178]. Exosomes have recently emerged as attractive natural nano-sized vesicles for drug delivery, due to their excellent biocompatibility and potential capacity to express targeting ligands [179]. The IFN-γ fusion protein was anchored in the PCa cell–derived exosome to prepare the IFN-γ-exosomal vaccine. Notably, it increases the quantity of M1 macrophages and enhances their ability to engulf RM-1 cell-derived exosomes, thereby clearing the regulatory effects of the latter. Pharmacological inhibition of cholesterol metabolism is also beneficial to M2 reprogramming. In the cellular study, Simvastatin adjusts the M2-M1 phenotypic transition of murine BMDMs via inhibition of LXR/ABCA1 responsible for cholesterol homeostasis, with TNF-α increase and TGF-β decrease, ultimately overcoming EMT-induced chemoresistance [180].

However, several successful immunotherapies for PCa are highly dependent on the preexistence of macrophages in tumor sites. The principal effect of an adenoviral vector-encoding murine IFN-β on PC-3MM2 growth inhibition is indirectly influencing other host cells of the microenvironment. At present, repolarization of M2-like TAMs is

regarded as a requirement for carcinostatic activities of IFN-β. It could induce a detectable increase in iNOS-positive cells and reduce levels of M2-associated molecules responsible for angiogenesis and tumor invasion [181]. Virulizin also had a favorable toxicity profile in various human tumor xenograft models including PCa, whereas whole-body loss of macrophages compromised its anti-cancer effects. Further analysis suggested that Virulizin formed a niche in the TME that attenuated tumor progression by reversing TAMs into a pro-inflammatory subtype with higher TNF-α levels. More significantly, Virulizin increases IL-12β production in M1-like macrophages, thus enhancing NK cells–mediated cytotoxicity against PCa [182].

Furthermore, researchers observed that when PCa cells were present, M1 phenotype could not be fully restored even with M1-like cytokine stimulation, usually accompanied by diminished cytotoxicity. This finding implies that attempts to repolarize prostate TAMs will be sufficiently effective with concomitantly destroying adjacent tumor cells [183].

5.3. Inhibiting the Crosstalk between TAMs and Tumor Cells. Malignant cells readily cooperate with TAMs to aggravate tumor evolvement by forming a vicious cycle. The protective effects of dihydroisotanshinone I (DT) against PCa are just achieved by targeting their crosstalk via inhibition of the CCL2/STAT3 axis [184]. The majority of TAMs infiltrating PTEN-null PCa usually expressed the CXCR2 receptor; therefore, pharmacological blockade of the CXCR2 re-educated TAMs toward a TNFα-releasing pro-inflammatory phenotype to induce senescence and tumor inhibition. Meanwhile, it should be noted that the employment of CXCR2 antagonist needs to take into account

the level of PTEN in the tumors, as these tumor cells with Pten deletion upregulate TNFR1 [185]. TAMs secrete IL-6, whereas the inhibition of the IL-6/STAT3 axis re-sensitizes PCa cells to paclitaxel. NF-κB signaling also plays a crucial role in the action of this paracrine loop. Within the TME, cytokines derived from TAMs increase the activity of NF-κB in the neoplastic population, which in turn stimulates macrophage infiltration via increased CSF-1 to promote prostate tumorigenesis. However, somatostatin derivate (smsDX) dramatically counteracts these effects by inhibiting the NF-κB pathway. In addition, smsDX could dampen PCa-metastatic potential provoked by M2-like macrophages by binding with its somatostatin receptor 1/2 (SSRT1/2) [186]. Enjoyably enough, the polarization of THP-1 cells co-cultured with PC-3 cells is skewed to M1-like macrophages upon etoposide treatment, followed by an increase in etoposide-induced apoptosis of tumor cells [187]. Resolvin D2 (RVD2) alone has no effects on the proliferation of PCa cells, whereas attenuating their growth rate in a Transwell model. Further analysis shows that it diminished excretive growth factors (VEGFa and EGF) in THP-1 cells, suggesting that RVD2 exerts cytotoxic functions through intervening by cell-to-cell wireless communication [67]. S-nitrosoglutathione (GSNO), an NO donor, impedes CRPC growth in the murine model. Studies report that the inhibitive action of GSNO on CRPC is targeting the TME but is not cell-autonomous. Compared to PBS-treated mice, GSNO suppressed the generation of various cytokines, especially M-CSF and BMP-6. As a result, the M1/M2 ratio was increased. On the other hand, p-ERK-mediated VEGF in macrophages was inhibited following therapy with GSNO, indicating a disruptive effect of NO on TAM activity [188].

The subcellular mechanism underlying the cholesterol exchange between tumor cells and macrophages has yet to be identified. However, the potent agonist of liver X receptor β (LXRβ), RGX-104 limits their communication by preventing cholesterol metabolism. Therefore its application is expected to extend survival after ADT. A recent report shows statins, known to decrease systemic cholesterol levels, significantly improve the benefits of ADT in patients [189]. These agents reduced the availability of circulating cholesterol for ingestion by TAMs and its transfer towards neighboring tumor cells during ADT, possibly delaying the onset of CRPC. Similarly, treatment with PBP10, an inhibitor of lipid molecule lipoxin A4 (LXA4), abolished the role of PCa cell-derived LXA4 in M2 phenotype transformation by inhibiting METTL3/STAT6 [190].

6. Conclusions and Future Perspectives

In response to certain surrounding stimuli, macrophages are recruited into the TME and convert into TAMs. It is increasingly clear that such TME preferentially drives macrophages to undergo M2-like polarization, and the altered macrophages play a vital role in influencing the process of prostate tumor growth, metastasis, and therapeutic resistance. Since TAMs occupy the large number of intratumorally infiltrating immune cells, more attention would be paid to develop novel immunotherapies directly targeting TAMs or their functional mediators for improved treatment efficacy.

To expedite clinical translation, we need to clarify several questions in future directions. Which histological types of patients are suitable for TAM-directed therapy? More evidence indicated that relative contributions of TAM-subtypes in these populations need to be considered for precision medicine. Could the patients achieve benefits from long-term M2-M1 repolarization treatment? More importantly, which transcription factors are involved in phenotypic reversibility? How do epigenetic factors modulate gene profiles of TAMs, and are they firmly inherited? Unfortunately, the detailed connection between TAMs and tumor cells has not been fully determined, which remains informative to pursue. Furthermore, enhancing our knowledge on the origin and functions of TAM subsets in the tumor milieu will contribute to tapping TAMs-targeted therapeutic potential to the full as adjuvant antitumor strategies.

Data Availability

The data used to support the findings of this study can be obtained from Chenglin Han and Xiaming Liu upon request.

Conflicts of Interest

All authors declare that they have no conflicts of interest related to this paper.

Authors' Contributions

Chenglin Han wrote the original draft; Yuxuan Deng, Wenchao Xu, and Zhuo Liu performed the article revision. Tao Wang and Shaogang Wang performed the supervision. Jihong Liu and Xiaming Liu revised the manuscript critically. Xiaming Liu obtained funding and approved the final manuscript.

Acknowledgments

References

[1] S. Wang, G. Xu, F. Chao, C. Zhang, D. Han, and G. Chen, "HNRNPC promotes proliferation, metastasis and predicts prognosis in prostate cancer," *Cancer Management and Research*, vol. 13, pp. 7263–7276, 2021.

[2] Y. Chen, F. Sun, L. Zhang, J. Zhou, and J. Hou, "miR-499a inhibits the proliferation and apoptosis of prostate cancer via targeting UBE2V2," *World Journal of Surgical Oncology*, vol. 19, p. 250, 2021.

[3] A. Davies, V. Conteduca, A. Zoubeidi, and H. Beltran, "Biological evolution of castration-resistant prostate cancer," *European Urology Focus*, vol. 5, pp. 147–154, 2019.

[4] A. Calcinotto, C. Spataro, E. Zagato et al., "IL-23 secreted by myeloid cells drives castration-resistant prostate cancer," *Nature*, vol. 559, pp. 363–369, 2018.

[5] N. B. Hao, M. H. Lu, Y. H. Fan, Y. L. Cao, Z. R. Zhang, and S. M. Yang, "Macrophages in tumor microenvironments and the progression of tumors," *Clin Dev Immunol*, vol. 2012, Article ID 948098, 2012.

[6] S. J. Turley, V. Cremasco, and J. L. Astarita, "Immunological hallmarks of stromal cells in the tumour microenvironment," *Nature Reviews Immunology*, vol. 15, pp. 669–682, 2015.

[7] H. Takahashi, K. Sakakura, T. Kudo et al., "Cancer-associated fibroblasts promote an immunosuppressive microenvironment through the induction and accumulation of protumoral macrophages," *Oncotarget*, vol. 8, pp. 8633–8647, 2017.

[8] A. M. Malfitano, S. Pisanti, F. Napolitano, S. Di Somma, R. Martinelli, and G. Portella, "Tumor-associated macrophage status in cancer treatment," *Cancers*, vol. 12, no. 7, p. 1987, 2020.

[9] P. Ruytinx, P. Proost, J. Van Damme, and S. Struyf, "Chemokine-induced macrophage polarization in inflammatory conditions," *Frontiers in Immunology*, vol. 9, p. 1930, 2018.

[10] E. J. Hoffmann and S. M. Ponik, "Biomechanical contributions to macrophage activation in the tumor microenvironment," *Frontiers in Oncology*, vol. 10, p. 787, 2020.

[11] P. J. Murray and T. A. Wynn, "Protective and pathogenic functions of macrophage subsets," *Nature Reviews Immunology*, vol. 11, pp. 723–737, 2011.

[12] S. K. Pal, D. Moreira, H. Won et al., "Reduced T-cell numbers and elevated levels of immunomodulatory cytokines in metastatic prostate cancer patients de novo resistant to abiraterone and/or enzalutamide therapy," *International Journal of Molecular Sciences*, vol. 20, no. 8, p. 1831, 2019.

[13] A. Mantovani, S. Sozzani, M. Locati, P. Allavena, and A. Sica, "Macrophage polarization: tumor-associated macrophages as a paradigm for polarized M2 mononuclear phagocytes," *Trends in Immunology*, vol. 23, pp. 549–555, 2002.

[14] I. F. Lissbrant, P. Stattin, P. Wikstrom, J. E. Damber, L. Egevad, and A. Bergh, "Tumor associated macrophages in human prostate cancer: relation to clinicopathological variables and survival,," *Int J Oncol*, vol. 17, no. 3, pp. 445–451, 2000.

[15] S. Tyagi, N. Tyagi, A. Choudhury, G. Gupta, M. M. A. Zahra, and S. A. Rahin, "Identification and classification of prostate cancer identification and classification based on improved convolution neural network," *Biomed Res Int*, vol. 2022, Article ID 9112587, 2022.

[16] N. Nonomura, H. Takayama, M. Nakayama et al., "Infiltration of tumour-associated macrophages in prostate biopsy specimens is predictive of disease progression after hormonal therapy for prostate cancer," *BJU International*, vol. 107, pp. 1918–1922, 2011.

[17] B. T. Copeland, H. Shallal, C. Shen, K. J. Pienta, C. A. Foss, and M. G. Pomper, "Imaging and characterization of macrophage distribution in mouse models of human prostate cancer," *Molecular Imaging and Biology*, vol. 21, pp. 1054–1063, 2019.

[18] J. C. Zarif, J. A. Baena-Del Valle, J. L. Hicks et al., "Mannose receptor-positive macrophage infiltration correlates with prostate cancer onset and metastatic castration-resistant disease," *eur urol oncol*, vol. 291, no. 4, pp. 429–436, 2019.

[19] M. Laviron and A. Boissonnas, "Ontogeny of tumor-associated macrophages," *Frontiers in Immunology*, vol. 10, p. 1799, 2019.

[20] S. Gordon, A. Pluddemann, and F. Martinez Estrada, "Macrophage heterogeneity in tissues: phenotypic diversity and functions," *Immunological Reviews*, vol. 262, pp. 36–55, 2014.

[21] L. C. Davies, S. J. Jenkins, J. E. Allen, and P. R. Taylor, "Tissue-resident macrophages," *Nature Immunology*, vol. 14, pp. 986–995, 2013.

[22] A. T. Kumar, A. Knops, B. Swendseid et al., "Prognostic significance of tumor-associated macrophage content in head and neck squamous cell carcinoma: a meta-analysis," *Frontiers in Oncology*, vol. 9, p. 656, 2019.

[23] Y. Zhu, J. M. Herndon, D. K. Sojka et al., "Tissue-resident macrophages in pancreatic ductal adenocarcinoma originate from embryonic hematopoiesis and promote tumor progression," *Immunity*, vol. 47, pp. 323–338.e6, 2017.

[24] Z. Chen, X. Feng, C. J. Herting et al., "Cellular and molecular identity of tumor-associated macrophages in glioblastoma," *Cancer Research*, vol. 77, pp. 2266–2278, 2017.

[25] P. C. Chen, H. C. Cheng, J. Wang et al., "Prostate cancer-derived CCN3 induces M2 macrophage infiltration and contributes to angiogenesis in prostate cancer microenvironment," *Oncotarget*, vol. 5, pp. 1595–1608, 2014.

[26] K. Mizutani, S. Sud, N. A. McGregor et al., "The chemokine CCL2 increases prostate tumor growth and bone metastasis through macrophage and osteoclast recruitment," *Neoplasia*, vol. 11, pp. 1235–1242, 2009.

[27] R. D. Loberg, C. Ying, M. Craig et al., "Targeting CCL2 with systemic delivery of neutralizing antibodies induces prostate cancer tumor regression *In vivo*," *Cancer Research*, vol. 67, pp. 9417–9424, 2007.

[28] G. Lucarelli, M. Rutigliano, C. Bettocchi et al., "Spondin-2, a secreted extracellular matrix protein, is a novel diagnostic biomarker for prostate cancer," *The Journal of Urology*, vol. 190, pp. 2271–2277, 2013.

[29] C. Huang, R. Ou, X. Chen et al., "Tumor cell-derived SPON2 promotes M2-polarized tumor-associated macrophage infiltration and cancer progression by activating PYK2 in CRC," *Journal of Experimental & Clinical Cancer Research*, vol. 40, p. 304, 2021.

[30] J. Xu, J. Escamilla, S. Mok et al., "CSF1R signaling blockade stanches tumor-infiltrating myeloid cells and improves the efficacy of radiotherapy in prostate cancer," *Cancer Research*, vol. 73, pp. 2782–2794, 2013.

[31] J. Y. Low, W. N. Brennen, A. K. Meeker, E. Ikonen, B. W. Simons, and M. Laiho, "Stromal CAVIN1 controls prostate cancer microenvironment and metastasis by modulating lipid distribution and inflammatory signaling," *Molecular Cancer Research*, vol. 18, pp. 1414–1426, 2020.

[32] J. Zhang, S. Sud, K. Mizutani, M. R. Gyetko, and K. J. Pienta, "Activation of urokinase plasminogen activator and its receptor Axis is essential for macrophage infiltration in a prostate cancer mouse model," *Neoplasia*, vol. 13, pp. 23–30, 2011.

[33] I. C. Sroka, C. P. Sandoval, H. Chopra, J. M. C. Gard, S. C. Pawar, and A. E. Cress, "Macrophage-dependent cleavage of the laminin receptor $\alpha6\beta1$ in prostate cancer," *Molecular Cancer Research*, vol. 9, pp. 1319–1328, 2011.

[34] A. J. Covarrubias, H. I. Aksoylar, and T. Horng, "Control of macrophage metabolism and activation by mTOR and Akt signaling," *Seminars in Immunology*, vol. 27, pp. 286–296, 2015.

[35] P. Italiani and D. Boraschi, "From monocytes to M1/M2 macrophages: phenotypical vs. Functional differentiation," *Frontiers in Immunology*, vol. 5, p. 514, 2014.

[36] C. Han, Z. Wang, Y. Xu et al., "Roles of reactive oxygen species in biological behaviors of prostate cancer," *Biomed Res Int*, vol. 2020, Article ID 1269624, 2020.

[37] A. Sica and A. Mantovani, "Macrophage plasticity and polarization: in vivo veritas," *Journal of Clinical Investigation*, vol. 122, pp. 787–795, 2012.

[38] Y. L. Zhang, Q. Li, X. M. Yang et al., "SPON2 promotes M1-like macrophage recruitment and inhibits hepatocellular carcinoma metastasis by distinct integrin–rho GTPase–hippo pathways," *Cancer Research*, vol. 78, pp. 2305–2317, 2018.

[39] K. Rabold, M. G. Netea, G. J. Adema, and R. T. Netea-Maier, "Cellular metabolism of tumor-associated macrophages - functional impact and consequences," *FEBS Letters*, vol. 591, pp. 3022–3041, 2017.

[40] N. Kane, T. Romero, S. Diaz-Perez et al., "Significant changes in macrophage and CD8 T cell densities in primary prostate tumors 2 weeks after SBRT," *Prostate Cancer Prostatic Dis*, 2022.

[41] A. Mantovani, A. Sica, S. Sozzani, P. Allavena, A. Vecchi, and M. Locati, "The chemokine system in diverse forms of macrophage activation and polarization," *Trends in Immunology*, vol. 25, pp. 677–686, 2004.

[42] M. Genin, F. Clement, A. Fattaccioli, M. Raes, and C. Michiels, "M1 and M2 macrophages derived from THP-1 cells differentially modulate the response of cancer cells to etoposide," *BMC Cancer*, vol. 15, no. 1, p. 577, 2015.

[43] V. Mendoza-Reinoso, D. Y. Baek, A. Kurutz et al., "Unique pro-inflammatory response of macrophages during apoptotic cancer cell clearance," *Cells*, vol. 9, no. 2, 2020.

[44] S. W. Kim, J. S. Kim, J. Papadopoulos et al., "Consistent interactions between tumor cell IL-6 and macrophage TNF-α enhance the growth of human prostate cancer cells in the bone of nude mouse," *International Immunopharmacology*, vol. 11, pp. 862–872, 2011.

[45] J. Mauer, B. Chaurasia, J. Goldau et al., "Signaling by IL-6 promotes alternative activation of macrophages to limit endotoxemia and obesity-associated resistance to insulin," *Nature Immunology*, vol. 15, pp. 423–430, 2014.

[46] Z. Culig and M. Puhr, "Interleukin-6 and prostate cancer: current developments and unsolved questions," *Molecular and Cellular Endocrinology*, vol. 462, pp. 25–30, 2018, part.

[47] I. H. Han, H. O. Song, and J. S. Ryu, "IL-6 produced by prostate epithelial cells stimulated with Trichomonas vaginalis promotes proliferation of prostate cancer cells by inducing M2 polarization of THP-1-derived macrophages," *PLoS Neglected Tropical Diseases*, vol. 14, no. 3, pp. e0008126, Article ID e0008126, 2020.

[48] H. Y. Chung, J. H. Kim, I. H. Han, and J. S. Ryu, "Polarization of M2 macrophages by interaction between prostate cancer cells treated with trichomonas vaginalis and adipocytes," *Korean Journal of Parasitology*, vol. 58, pp. 217–227, 2020.

[49] R. Kalluri, "Basement membranes: structure, assembly and role in tumour angiogenesis," *Nature Reviews Cancer*, vol. 3, pp. 422–433, 2003.

[50] G. Comito, E. Giannoni, C. P. Segura et al., "Cancer-associated fibroblasts and M2-polarized macrophages synergize during prostate carcinoma progression," *Oncogene*, vol. 33, pp. 2423–2431, 2014.

[51] G. Ren, X. Zhao, Y. Wang et al., "CCR2-Dependent recruitment of macrophages by tumor-educated mesenchymal stromal cells promotes tumor development and is mimicked by TNFα," *Cell Stem Cell*, vol. 11, pp. 812–824, 2012.

[52] G. Gunaydin, "CAFs interacting with TAMs in tumor microenvironment to enhance tumorigenesis and immune evasion," *Frontiers in Oncology*, vol. 11, Article ID 668349, 2021.

[53] R. Zhang, J. Zong, Y. Peng et al., "GPR30 knockdown weakens the capacity of CAF in promoting prostate cancer cell invasion via reducing macrophage infiltration and M2 polarization," *J Cell Biochem*, 2021.

[54] G. Daniels, L. L. Gellert, J. Melamed et al., "Decreased expression of stromal estrogen receptor alpha and beta in prostate cancer," *Am J Transl Res*, vol. 6, no. 2, pp. 140–146, 2014.

[55] O. Celhay, M. Yacoub, J. Irani, B. Dore, O. Cussenot, and G. Fromont, "Expression of estrogen related proteins in hormone refractory prostate cancer: association with tumor progression," *The Journal of Urology*, vol. 184, pp. 2172–2178, 2010.

[56] C. R. Yeh, S. Slavin, J. Da et al., "Estrogen receptor α in cancer associated fibroblasts suppresses prostate cancer invasion via reducing CCL5, IL6 and macrophage infiltration in the tumor microenvironment," *Molecular Cancer*, vol. 15, no. 1, p. 7, 2016.

[57] C. Carmona-Fontaine, M. Deforet, L. Akkari, C. B. Thompson, J. A. Joyce, and J. B. Xavier, "Metabolic origins of spatial organization in the tumor microenvironment," *Proc Natl Acad Sci U S A*, vol. 114, no. 11, pp. 2934–2939, 2017.

[58] D. L. Bellinger, M. S. Dulcich, C. Molinaro et al., "Psychosocial stress and age influence depression and anxiety-related behavior, drive tumor inflammatory cytokines and accelerate prostate cancer growth in mice," *Frontiers in Oncology*, vol. 11, Article ID 703848, 2021.

[59] T. Nelius, C. Samathanam, D. Martinez-Marin et al., "Positive correlation between PEDF expression levels and macrophage density in the human prostate," *Prostate*, vol. 73, no. 5, pp. 549–561, 2013.

[60] R. A. Gatenby and R. J. Gillies, "Why do cancers have high aerobic glycolysis?" *Nature Reviews Cancer*, vol. 4, pp. 891–899, 2004.

[61] X. Mu, W. Shi, Y. Xu et al., "Tumor-derived lactate induces M2 macrophage polarization via the activation of the ERK/STAT3 signaling pathway in breast cancer," *Cell Cycle*, vol. 17, pp. 428–438, 2018.

[62] R. Feng, Y. Morine, T. Ikemoto et al., "Nrf2 activation drive macrophages polarization and cancer cell epithelial-mesenchymal transition during interaction," *Cell Communication and Signaling*, vol. 16, p. 54, 2018.

[63] A. Pereira-Nunes, S. Simoes-Sousa, C. Pinheiro, V. Miranda-Goncalves, S. Granja, and F. Baltazar, "Targeting lactate production and efflux in prostate cancer," *Biochim Biophys Acta Mol Basis Dis*, vol. 1866, no. 11, Article ID 165894, 2020.

[64] H. Wu, Y. Han, Y. Rodriguez Sillke et al., "Lipid droplet-dependent fatty acid metabolism controls the immune suppressive phenotype of tumor-associated macrophages," *EMBO Molecular Medicine*, vol. 11, no. 11, Article ID e10698, 2019.

[65] H. Y. Wu, X. Q. Tang, H. Liu, X. F. Mao, and Y. X. Wang, "Both classic Gs-cAMP/PKA/CREB and alternative Gs-cAMP/PKA/p38β/CREB signal pathways mediate exenatide-stimulated expression of M2 microglial markers," *Journal of Neuroimmunology*, vol. 316, pp. 17–22, 2018.

[66] S. Xia, J. Ma, X. Bai et al., "Prostaglandin E2 promotes the cell growth and invasive ability of hepatocellular carcinoma cells by upregulating c-Myc expression via EP4 receptor and the

PKA signaling pathway," *Oncology Reports*, vol. 32, pp. 1521–1530, 2014.

[67] K. Shan, N. Feng, J. Cui et al., "Resolvin D1 and D2 inhibit tumour growth and inflammation via modulating macrophage polarization," *Journal of Cellular and Molecular Medicine*, vol. 24, pp. 8045–8056, 2020.

[68] R. Wang, Y. Liu, L. Liu et al., "Tumor cells induce LAMP2a expression in tumor-associated macrophage for cancer progression," *EBioMedicine*, vol. 40, pp. 118–134, 2019.

[69] P. K. Wagh, B. E. Peace, and S. E. Waltz, "Met-related receptor tyrosine kinase Ron in tumor growth and metastasis," *Adv Cancer Res*, vol. 100, pp. 1–33, 2008.

[70] M. A. Leonis, M. N. Thobe, and S. E. Waltz, "Ron-receptor tyrosine kinase in tumorigenesis and metastasis," *Future Oncology*, vol. 3, pp. 441–448, 2007.

[71] C. Sullivan, N. E. Brown, J. Vasiliauskas, P. Pathrose, S. L. Starnes, and S. E. Waltz, "Prostate epithelial RON signaling promotes M2 macrophage activation to drive prostate tumor growth and progression," *Molecular Cancer Research*, vol. 18, pp. 1244–1254, 2020.

[72] Z. H. Arbieva, K. Banerjee, S. Y. Kim et al., "High-resolution physical map and transcript identification of a prostate cancer deletion interval on 8p22," *Genome Research*, vol. 10, pp. 244–257, 2000.

[73] N. Nonomura, H. Takayama, A. Kawashima et al., "Decreased infiltration of macrophage scavenger receptor-positive cells in initial negative biopsy specimens is correlated with positive repeat biopsies of the prostate," *Cancer Science*, vol. 101, pp. 1570–1573, 2010.

[74] N. Nishimura, M. Harada-Shiba, S. Tajima et al., "Acquisition of secretion of transforming growth factor-beta 1 leads to autonomous suppression of scavenger receptor activity in a monocyte-macrophage cell line, THP-1," *J Biol Chem*, vol. 273, no. 3, pp. 1562–1567, 1998.

[75] L. C. Cheng, Y. J. Chao, C. Y. Wang et al., "Cancer-derived transforming growth factor-β modulates tumor-associated macrophages in ampullary cancer," *OncoTargets and Therapy*, vol. 13, pp. 7503–7516, 2020.

[76] F. Zhang, H. Wang, X. Wang et al., "TGF-β induces M2-like macrophage polarization via SNAIL-mediated suppression of a pro-inflammatory phenotype," *Oncotarget*, vol. 7, Article ID 52294, 2016.

[77] A. S. Lagana, F. M. Salmeri, H. Ban Frangez, F. Ghezzi, E. Vrtacnik-Bokal, and R. Granese, "Evaluation of M1 and M2 macrophages in ovarian endometriomas from women affected by endometriosis at different stages of the disease," *Gynecological Endocrinology*, vol. 36, pp. 441–444, 2020.

[78] F. Liu, H. Qiu, M. Xue et al., "MSC-secreted TGF-β regulates lipopolysaccharide-stimulated macrophage M2-like polarization via the Akt/FoxO1 pathway," *Stem Cell Research & Therapy*, vol. 10, p. 345, 2019.

[79] P. Jiramongkolchai, P. Owens, and C. C. Hong, "Emerging roles of the bone morphogenetic protein pathway in cancer: potential therapeutic target for kinase inhibition," *Biochemical Society Transactions*, vol. 44, pp. 1117–1134, 2016.

[80] C. L. Ihle, D. M. Straign, M. D. Provera, S. V. Novitskiy, and P. Owens, "Loss of myeloid BMPR1a alters differentiation and reduces mouse prostate cancer growth," *Frontiers in Oncology*, vol. 10, p. 357, 2020.

[81] L. Wang, M. Shang, Q. Dai, and P. A. He, "Prediction of lncRNA-disease association based on a Laplace normalized random walk with restart algorithm on heterogeneous networks," *BMC Bioinformatics*, vol. 23, p. 5, 2022.

[82] S. Wang, A. Talukder, M. Cha, X. Li, and H. Hu, "Computational annotation of miRNA transcription start sites," *Briefings in Bioinformatics*, vol. 22, pp. 380–392, 2021.

[83] P. Zhang, W. Wu, Q. Chen, and M. Chen, "Non-coding RNAs and their integrated networks," *Journal of Integrative Bioinformatics*, vol. 16, no. 3, 2019.

[84] Y. Chen, H. Li, T. Ding et al., "Lnc-M2 controls M2 macrophage differentiation via the PKA/CREB pathway," *Molecular Immunology*, vol. 124, pp. 142–152, 2020.

[85] J. Liu, D. Ding, Z. Jiang, T. Du, J. Liu, and Z. Kong, "Long non-coding RNA CCAT1/miR-148a/PKCζ prevents cell migration of prostate cancer by altering macrophage polarization," *The Prostate*, vol. 79, pp. 105–112, 2019.

[86] H. Jiang, W. Deng, K. Zhu et al., "LINC00467 promotes prostate cancer progression via M2 macrophage polarization and the miR-494-3p/STAT3 Axis," *Frontiers in Oncology*, vol. 11, Article ID 661431, 2021.

[87] S. Zong, W. Dai, X. Guo, and K. Wang, "LncRNA-SNHG1 promotes macrophage M2-like polarization and contributes to breast cancer growth and metastasis," *Aging (Albany NY)*, vol. 13, Article ID 23169, 2021.

[88] M. K. Atianand, W. Hu, A. T. Satpathy et al., "A long noncoding RNA lincRNA-EPS acts as a transcriptional brake to restrain inflammation," *Cell*, vol. 165, pp. 1672–1685, 2016.

[89] M. Ou, X. Li, S. Zhao, S. Cui, and J. Tu, "Long non-coding RNA CDKN2B-AS1 contributes to atherosclerotic plaque formation by forming RNA-DNA triplex in the CDKN2B promoter," *EBioMedicine*, vol. 55, Article ID 102694, 2020.

[90] C. Niespolo, J. M. Johnston, S. R. Deshmukh et al., "Tribbles-1 expression and its function to control inflammatory cytokines, including interleukin-8 levels are regulated by miRNAs in macrophages and prostate cancer cells," *Frontiers in Immunology*, vol. 11, Article ID 574046, 2020.

[91] H. Neuwirt, M. Puhr, F. R. Santer et al., "Suppressor of cytokine signaling (SOCS)-1 is expressed in human prostate cancer and exerts growth-inhibitory function through downregulation of cyclins and cyclin-dependent kinases," *American Journal Of Pathology*, vol. 174, pp. 1921–1930, 2009.

[92] J. Rong, L. Xu, Y. Hu et al., "Inhibition of let-7b-5p contributes to an anti-tumorigenic macrophage phenotype through the SOCS1/STAT pathway in prostate cancer," *Cancer Cell International*, vol. 20, no. 1, p. 470, 2020.

[93] Y. Yin, J. Long, Q. He et al., "Emerging roles of circRNA in formation and progression of cancer," *Journal of Cancer*, vol. 10, pp. 5015–5021, 2019.

[94] Y. Zhang, Y. Zhang, X. Li, M. Zhang, and K. Lv, "Microarray analysis of circular RNA expression patterns in polarized macrophages," *International Journal of Molecular Medicine*, vol. 39, pp. 373–379, 2017.

[95] C. Zhang, X. Han, L. Yang et al., "Circular RNA *circPPM1F* modulates M1 macrophage activation and pancreatic islet inflammation in type 1 diabetes mellitus," *Theranostics*, vol. 10, Article ID 10908, 2020.

[96] H. Song, Y. Yang, Y. Sun et al., "Circular RNA Cdyl promotes abdominal aortic aneurysm formation by inducing M1 macrophage polarization and M1-type inflammation," *Molecular Therapy*, vol. 30, pp. 915–931, 2022.

[97] X. Huang, J. Wang, J. Guan et al., "Exosomal Circsafb2 reshaping tumor environment to promote renal cell carcinoma progression by mediating M2 macrophage polarization," *Frontiers in Oncology*, vol. 12, Article ID 808888, 2022.

[98] O. M. Pello, R. Chevre, D. Laoui et al., "In vivo inhibition of c-MYC in myeloid cells impairs tumor-associated

macrophage maturation and pro-tumoral activities," *PLoS One*, vol. 7, no. 9, pp. e45399, Article ID e45399, 2012.

[99] O. M. Pello, M. De Pizzol, M. Mirolo et al., "Role of c-MYC in alternative activation of human macrophages and tumor-associated macrophage biology," *Blood*, vol. 119, pp. 411–421, 2012.

[100] O. M. Pello and V. Andres, "Role of c-MYC in tumor-associated macrophages and cancer progression," *OncoImmunology*, vol. 2, no. 2, pp. e22984, Article ID e22984, 2013.

[101] L. Zhong, Y. Zhang, M. Li et al., "E3 ligase FBXW7 restricts M2-like tumor-associated macrophage polarization by targeting c-Myc," *Aging (Albany NY)*, vol. 12, Article ID 24394, 2020.

[102] B. Dong, C. Wu, L. Huang, and Y. Qi, "Macrophage-related SPP1 as a potential biomarker for early lymph node metastasis in lung adenocarcinoma," *Frontiers in Cell and Developmental Biology*, vol. 9, Article ID 739358, 2021.

[103] T. Yu, S. Gan, Q. Zhu et al., "Modulation of M2 macrophage polarization by the crosstalk between Stat6 and Trim24," *Nature Communications*, vol. 10, p. 4353, 2019.

[104] S. Ren, X. Zhang, Y. Hu et al., "Blocking the Notch signal transduction pathway promotes tumor growth in osteosarcoma by affecting polarization of TAM to M2 phenotype," *Annals of Translational Medicine*, vol. 8, p. 1057, 2020.

[105] B. Cioni, A. Zaalberg, J. R. van Beijnum et al., "Androgen receptor signalling in macrophages promotes TREM-1-mediated prostate cancer cell line migration and invasion," *Nature Communications*, vol. 11, p. 4498, 2020.

[106] S. J. Lee, J. Y. Kim, R. Nogueiras et al., "Pkcζ-regulated inflammation in the nonhematopoietic compartment is critical for obesity-induced glucose intolerance," *Cell Metabolism*, vol. 12, pp. 65–77, 2010.

[107] M. Becerra-Diaz, A. B. Strickland, A. Keselman, and N. M. Heller, "Androgen and androgen receptor as enhancers of M2 macrophage polarization in allergic lung inflammation," *J immunol*, vol. 201, no. 10, pp. 2923–2933, 2018.

[108] S. O. Lee, E. Pinder, J. Y. Chun, W. Lou, M. Sun, and A. C. Gao, "Interleukin-4 stimulates androgen-independent growth in LNCaP human prostate cancer cells," *The Prostate*, vol. 68, pp. 85–91, 2008.

[109] F. N. Soki, A. J. Koh, J. D. Jones et al., "Polarization of prostate cancer-associated macrophages is induced by milk fat globule-EGF factor 8 (MFG-E8)-mediated efferocytosis," *Journal of Biological Chemistry*, vol. 289, Article ID 24560, 2014.

[110] H. R. Cha, J. H. Lee, J. A. Hensel et al., "Prostate cancer-derived cathelicidin-related antimicrobial peptide facilitates macrophage differentiation and polarization of immature myeloid progenitors to protumorigenic macrophages," *The Prostate*, vol. 76, pp. 624–636, 2016.

[111] H. H. Fan, L. Li, Y. M. Zhang et al., "PKCζ in prostate cancer cells represses the recruitment and M2 polarization of macrophages in the prostate cancer microenvironment," *Tumor Biology*, vol. 39, Article ID 101042831770144, 2017.

[112] J. Yang, C. Lu, J. Wei et al., "Inhibition of KPNA4 attenuates prostate cancer metastasis," *Oncogene*, vol. 36, pp. 2868–2878, 2017.

[113] Z. Z. Liu, Z. D. Han, Y. K. Liang et al., "TRIB1 induces macrophages to M2 phenotype by inhibiting IKB-zeta in prostate cancer," *Cellular Signalling*, vol. 59, pp. 152–162, 2019.

[114] R. Kalra, E. Bhagyaraj, D. Tiwari et al., "AIRE promotes androgen-independent prostate cancer by directly regulating IL-6 and modulating tumor microenvironment," *Oncogenesis*, vol. 7, p. 43, 2018.

[115] M. Huang, S. Narita, A. Koizumi et al., "Macrophage inhibitory cytokine-1 induced by a high-fat diet promotes prostate cancer progression by stimulating tumor-promoting cytokine production from tumor stromal cells," *Cancer Commun (Lond)*, vol. 41, no. 5, pp. 389–403, 2021.

[116] S. K. Biswas and A. Mantovani, "Orchestration of metabolism by macrophages," *Cell Metabolism*, vol. 15, pp. 432–437, 2012.

[117] E. Dai, L. Han, J. Liu et al., "Autophagy-dependent ferroptosis drives tumor-associated macrophage polarization via release and uptake of oncogenic KRAS protein," *Autophagy*, vol. 16, pp. 2069–2083, 2020.

[118] H. W. Nam, J. Bae, Y. W. Kim et al., "Anti-Cancer effects of RAW 264.7 cells on prostate cancer PC-3 cells," *Ann Clin Lab Sci*, vol. 50, no. 6, pp. 739–746, 2020.

[119] A. Erlandsson, J. Carlsson, M. Lundholm et al., "M2 macrophages and regulatory T cells in lethal prostate cancer," *The Prostate*, vol. 79, pp. 363–369, 2019.

[120] M. Lundholm, C. Hagglof, M. L. Wikberg et al., "Secreted factors from colorectal and prostate cancer cells skew the immune response in opposite directions," *Scientific Reports*, vol. 5, no. 1, Article ID 15651, 2015.

[121] P. Gu, X. Chen, R. Xie et al., "lncRNA HOXD-AS1 regulates proliferation and chemo-resistance of castration-resistant prostate cancer via recruiting WDR5," *Molecular Therapy*, vol. 25, pp. 1959–1973, 2017.

[122] S. Li, K. W. Fong, G. Gritsina et al., "Activation of MAPK signaling by CXCR7 leads to enzalutamide resistance in prostate cancer," *Cancer Research*, vol. 79, pp. 2580–2592, 2019.

[123] J. Escamilla, S. Schokrpur, C. Liu et al., "CSF1 receptor targeting in prostate cancer reverses macrophage-mediated resistance to androgen blockade therapy," *Cancer Research*, vol. 75, pp. 950–962, 2015.

[124] F. Liu, C. Wang, H. Huang et al., "SEMA3A-mediated crosstalk between prostate cancer cells and tumor-associated macrophages promotes androgen deprivation therapy resistance," *Cellular and Molecular Immunology*, vol. 18, pp. 752–754, 2021.

[125] P. Zhu, S. H. Baek, E. M. Bourk et al., "Macrophage/cancer cell interactions mediate hormone resistance by a nuclear receptor derepression pathway," *Cell*, vol. 124, pp. 615–629, 2006.

[126] T. Chandrasekar, J. C. Yang, A. C. Gao, and C. P. Evans, "Mechanisms of resistance in castration-resistant prostate cancer (CRPC)," *Transl Androl Urol*, vol. 4, no. 3, pp. 365–380, 2015.

[127] A. El-Kenawi, W. Dominguez-Viqueira, M. Liu et al., "Macrophage-Derived cholesterol contributes to therapeutic resistance in prostate cancer," *Cancer Res*, vol. 81, no. 21, pp. 5477–5490, 2021.

[128] H. Al-Janabi and C. E. Lewis, "Macrophage regulation of the development of castration-resistant prostate cancer," *Cancer Res*, vol. 81, no. 21, pp. 5399-5400, 2021.

[129] G. T. Lee, Y. S. Jung, Y. S. Ha, J. H. Kim, W. J. Kim, and I. Y. Kim, "Bone morphogenetic protein-6 induces castration resistance in prostate cancer cells through tumor infiltrating macrophages," *Cancer Science*, vol. 104, pp. 1027–1032, 2013.

[130] J. L. Owens, E. Beketova, S. Liu et al., "Targeting protein arginine methyltransferase 5 suppresses radiation-induced neuroendocrine differentiation and sensitizes prostate

cancer cells to radiation," *Molecular Cancer Therapeutics*, vol. 21, pp. 448–459, 2022.

[131] S. Natani, K. K. Sruthi, S. M. Asha, P. Khilar, P. S. V. Lakshmi, and R. Ummanni, "Activation of TGF-β - SMAD2 signaling by IL-6 drives neuroendocrine differentiation of prostate cancer through p38MAPK," *Cellular Signalling*, vol. 91, Article ID 110240, 2022.

[132] G. T. Lee, S. J. Kwon, J. H. Lee et al., "Macrophages induce neuroendocrine differentiation of prostate cancer cells via BMP6-IL6 Loop," *The Prostate*, vol. 71, pp. 1525–1537, 2011.

[133] I. Casaburi, A. Chimento, A. De Luca et al., "Cholesterol as an endogenous ERRα agonist: a new perspective to cancer treatment," *Frontiers in Endocrinology*, vol. 9, p. 525, 2018.

[134] C. Wilson, T. Wilson, P. G. Johnston, D. B. Longley, and D. J. Waugh, "Interleukin-8 signaling attenuates TRAIL- and chemotherapy-induced apoptosis through transcriptional regulation of c-FLIP in prostate cancer cells," *Molecular Cancer Therapeutics*, vol. 7, pp. 2649–2661, 2008.

[135] I. S. Hsieh, W. H. Huang, H. C. Liou, W. J. Chuang, R. S. Yang, and W. M. Fu, "Upregulation of drug transporter expression by osteopontin in prostate cancer cells," *Molecular Pharmacology*, vol. 83, pp. 968–977, 2013.

[136] Q. Liu, D. Tong, G. Liu et al., "Metformin inhibits prostate cancer progression by targeting tumor-associated inflammatory infiltration," *Clinical Cancer Research*, vol. 24, pp. 5622–5634, 2018.

[137] W. Guan, F. Li, Z. Zhao, Z. Zhang, J. Hu, and Y. Zhang, "Tumor-associated macrophage promotes the survival of cancer cells upon docetaxel chemotherapy via the CSF1/CSF1R–CXCL12/CXCR4 Axis in castration-resistant prostate cancer," *Genes*, vol. 12, no. 5, p. 773, 2021.

[138] J. Ma, F. Shayiti, J. Ma et al., "Tumor-associated macrophage-derived CCL5 promotes chemotherapy resistance and metastasis in prostatic cancer," *Cell Biology International*, vol. 45, pp. 2054–2062, 2021.

[139] R. Huang, S. Wang, N. Wang et al., "CCL5 derived from tumor-associated macrophages promotes prostate cancer stem cells and metastasis via activating β-catenin/STAT3 signaling," *Cell Death & Disease*, vol. 11, p. 234, 2020.

[140] L. Y. Fang, K. Izumi, K. P. Lai et al., "Infiltrating macrophages promote prostate tumorigenesis via modulating androgen receptor-mediated CCL4–STAT3 signaling," *Cancer Research*, vol. 73, pp. 5633–5646, 2013.

[141] D. G. Bostwick and L. Cheng, "Precursors of prostate cancer," *Histopathology*, vol. 60, pp. 4–27, 2012.

[142] J. Luo, K. Wang, S. Yeh et al., "LncRNA-p21 alters the antiandrogen enzalutamide-induced prostate cancer neuroendocrine differentiation via modulating the EZH2/STAT3 signaling," *Nature Communications*, vol. 10, p. 2571, 2019.

[143] T. Hayashi, K. Fujita, S. Nojima et al., "High-fat diet-induced inflammation accelerates prostate cancer growth via IL6 signaling," *Clinical Cancer Research*, vol. 24, pp. 4309–4318, 2018.

[144] T. Zheng, G. Ma, M. Tang, Z. Li, and R. Xu, "IL-8 secreted from M2 macrophages promoted prostate tumorigenesis via STAT3/MALAT1 pathway," *International Journal of Molecular Sciences*, vol. 20, no. 1, p. 98, 2018.

[145] K. Gollapudi, C. Galet, T. Grogan et al., "Association between tumor-associated macrophage infiltration, high grade prostate cancer, and biochemical recurrence after radical prostatectomy," *Am J Cancer Res*, vol. 3, no. 5, pp. 523–529, 2013.

[146] S. N. Sass, K. D. Ramsey, S. M. Egan, J. Wang, E. Cortes Gomez, and S. O. Gollnick, "Tumor-associated myeloid cells promote tumorigenesis of non-tumorigenic human and murine prostatic epithelial cell lines," *Cancer Immunology, Immunotherapy*, vol. 67, pp. 873–883, 2018.

[147] R. Solis-Martinez, M. Cancino-Marentes, G. Hernandez-Flores et al., "Regulation of immunophenotype modulation of monocytes-macrophages from M1 into M2 by prostate cancer cell-culture supernatant via transcription factor STAT3," *Immunol Lett*, vol. 196, pp. 140–148, 2018.

[148] C. P. Cheung, S. Yu, K. B. Wong et al., "Expression and functional study of estrogen receptor-related receptors in human prostatic cells and tissues," *Journal of Clinical Endocrinology and Metabolism*, vol. 90, pp. 1830–1844, 2005.

[149] S. Halin Bergstrom, S. Rudolfsson, M. Lundholm, A. Josefsson, P. Wikstrom, and A. Bergh, "High-grade tumours promote growth of other less-malignant tumours in the same prostate," *The Journal of Pathology*, vol. 253, pp. 396–403, 2021.

[150] V. Gocheva, H. W. Wang, B. B. Gadea et al., "IL-4 induces cathepsin protease activity in tumor-associated macrophages to promote cancer growth and invasion," *Genes & Development*, vol. 24, pp. 241–255, 2010.

[151] C. Lindahl, M. Simonsson, A. Bergh et al., "Increased levels of macrophage-secreted cathepsin S during prostate cancer progression in TRAMP mice and patients," *Cancer Genomics Proteomics*, vol. 6, no. 3, pp. 149–159, 2009.

[152] J. Wei, Z. Chen, M. Hu et al., "Characterizing intercellular communication of pan-cancer reveals SPP1+ tumor-associated macrophage expanded in hypoxia and promoting cancer malignancy through single-cell RNA-seq data," *Frontiers in Cell and Developmental Biology*, vol. 9, Article ID 749210, 2021.

[153] K. Izumi, L. Y. Fang, A. Mizokami et al., "Targeting the androgen receptor with siRNA promotes prostate cancer metastasis through enhanced macrophage recruitment via CCL2/CCR2-induced STAT3 activation," *EMBO Molecular Medicine*, vol. 5, pp. 1383–1401, 2013.

[154] S. Halin Bergstrom, M. Nilsson, H. Adamo et al., "Extra-tumoral heme oxygenase-1 (HO-1) expressing macrophages likely promote primary and metastatic prostate tumor growth," *PLoS One*, vol. 11, no. 6, pp. e0157280, Article ID e0157280, 2016.

[155] U. C. Dadwal, E. S. Chang, and U. Sankar, "Androgen receptor-CaMKK2 Axis in prostate cancer and bone microenvironment," *Frontiers in Endocrinology*, vol. 9, p. 335, 2018.

[156] H. Roca, J. D. Jones, M. C. Purica et al., "Apoptosis-induced CXCL5 accelerates inflammation and growth of prostate tumor metastases in bone," *Journal of Clinical Investigation*, vol. 128, pp. 248–266, 2018.

[157] X. Liao, N. Sharma, F. Kapadia et al., "Krüppel-like factor 4 regulates macrophage polarization," *Journal of Clinical Investigation*, vol. 121, pp. 2736–2749, 2011.

[158] S. Dubey, P. Vanveldhuizen, J. Holzbeierlein, O. Tawfik, J. B. Thrasher, and D. Karan, "Inflammation-associated regulation of the macrophage inhibitory cytokine (MIC-1) gene in prostate cancer," *Oncology Letters*, vol. 3, pp. 1166–1170, 2012.

[159] M. Masetti, R. Carriero, F. Portale et al., "Lipid-loaded tumor-associated macrophages sustain tumor growth and invasiveness in prostate cancer," *Journal of Experimental Medicine*, vol. 219, no. 2, Article ID e20210564, 2022.

[160] D. L. Adams, S. S. Martin, R. K. Alpaugh et al., "Circulating giant macrophages as a potential biomarker of solid tumors," *Proceedings of the National Academy of Sciences*, vol. 111, pp. 3514–3519, 2014.

[161] P. A. Osmulski, A. Cunsolo, M. Chen et al., "Contacts with macrophages promote an aggressive nanomechanical phenotype of circulating tumor cells in prostate cancer," *Cancer Research*, vol. 81, pp. 4110–4123, 2021.

[162] M. Fletcher, M. E. Ramirez, R. A. Sierra et al., "l-Arginine depletion blunts antitumor T-cell responses by inducing myeloid-derived suppressor cells," *Cancer Research*, vol. 75, pp. 275–283, 2015.

[163] R. Noy and J. W. Pollard, "Tumor-associated macrophages: from mechanisms to therapy," *Immunity*, vol. 41, pp. 49–61, 2014.

[164] J. Li, W. Feng, H. Lu et al., "Artemisinin inhibits breast cancer-induced osteolysis by inhibiting osteoclast formation and breast cancer cell proliferation," *Journal of Cellular Physiology*, vol. 234, Article ID 12663, 2019.

[165] J. Yokokawa, V. Cereda, C. Remondo et al., "Enhanced functionality of CD4+CD25highFoxP3+ regulatory T cells in the peripheral blood of patients with prostate cancer," *Clinical Cancer Research*, vol. 14, pp. 1032–1040, 2008.

[166] M. M. Tiemessen, A. L. Jagger, H. G. Evans, M. J. C. van Herwijnen, S. John, and L. S. Taams, "CD4 $^+$ CD25 $^+$ Foxp3 $^+$ regulatory T cells induce alternative activation of human monocytes/macrophages," *Proceedings of the National Academy of Sciences*, vol. 104, Article ID 19446, 2007.

[167] J. Cheng, L. Li, Y. Liu, Z. Wang, X. Zhu, and X. Bai, "Interleukin-1α induces immunosuppression by mesenchymal stem cells promoting the growth of prostate cancer cells," *Molecular Medicine Reports*, vol. 6, pp. 955–960, 2012.

[168] R. Tamura, T. Tanaka, Y. Akasaki, Y. Murayama, K. Yoshida, and H. Sasaki, "The role of vascular endothelial growth factor in the hypoxic and immunosuppressive tumor microenvironment: perspectives for therapeutic implications," *Medical Oncology*, vol. 37, p. 2, 2019.

[169] N. E. Brown, A. Jones, B. G. Hunt, and S. E. Waltz, "Prostate tumor RON receptor signaling mediates macrophage recruitment to drive androgen deprivation therapy resistance through Gas6-mediated Axl and RON signaling," *Prostate*, 2022.

[170] K. J. Pienta, J. P. Machiels, D. Schrijvers et al., "Phase 2 study of carlumab (CNTO 888), a human monoclonal antibody against CC-chemokine ligand 2 (CCL2), in metastatic castration-resistant prostate cancer," *Investigational New Drugs*, vol. 31, pp. 760–768, 2013.

[171] W. Guan, J. Hu, L. Yang et al., "Inhibition of TAMs improves the response to docetaxel in castration-resistant prostate cancer," *Endocrine-Related Cancer*, vol. 26, pp. 131–140, 2019.

[172] J. D. Jones, B. P. Sinder, D. Paige et al., "Trabectedin reduces skeletal prostate cancer tumor size in association with effects on M2 macrophages and efferocytosis," *Neoplasia*, vol. 21, pp. 172–184, 2019.

[173] F. Cortesi, G. Delfanti, A. Grilli et al., "Bimodal CD40/fas-dependent crosstalk between iNKT cells and tumor-associated macrophages impairs prostate cancer progression," *Cell Reports*, vol. 22, pp. 3006–3020, 2018.

[174] H. Xiao, Y. Guo, B. Li et al., "M2-Like tumor-associated macrophage-targeted codelivery of STAT6 inhibitor and IKKβ siRNA induces M2-to-M1 repolarization for cancer immunotherapy with low immune side effects," *ACS Central Science*, vol. 6, pp. 1208–1222, 2020.

[175] Y. W. Choo, M. Kang, H. Y. Kim et al., "M1 macrophage-derived nanovesicles potentiate the anticancer efficacy of immune checkpoint inhibitors," *ACS Nano*, vol. 12, pp. 8977–8993, 2018.

[176] T. Tanaka, A. Minami, J. Uchida, and T. Nakatani, "Potential of hyperbaric oxygen in urological diseases," *International Journal of Urology*, vol. 26, pp. 860–867, 2019.

[177] T. Satoh, T. Saika, S. Ebara et al., "Macrophages transduced with an adenoviral vector expressing interleukin 12 suppress tumor growth and metastasis in a preclinical metastatic prostate cancer model," *Cancer Res*, vol. 63, no. 22, pp. 7853–7860, 2003.

[178] C. W. Wanderley, D. F. Colon, J. P. M. Luiz et al., "Paclitaxel reduces tumor growth by reprogramming tumor-associated macrophages to an M1 profile in a TLR4-dependent manner," *Cancer Research*, vol. 78, pp. 5891–5900, 2018.

[179] N. Wang, S. Wang, X. Wang et al., "Research trends in pharmacological modulation of tumor-associated macrophages," *Clinical and Translational Medicine*, vol. 11, no. 1, p. e288, 2021 pp. e288.

[180] H. Jin, Y. He, P. Zhao et al., "Targeting lipid metabolism to overcome EMT-associated drug resistance via integrin β3/FAK pathway and tumor-associated macrophage repolarization using legumain-activatable delivery," *Theranostics*, vol. 9, pp. 265–278, 2019.

[181] F. Zhang, W. Lu, and Z. Dong, "Tumor-infiltrating macrophages are involved in suppressing growth and metastasis of human prostate cancer cells by INF-beta gene therapy in nude mice Clin Cancer Res," vol. 8, no. 9, pp. 2942–2951, 2002.

[182] H. Li, M. Y. Cao, Y. Lee et al., "Virulizin, a novel immunotherapy agent, activates NK cells through induction of IL-12 expression in macrophages," *Cancer Immunology, Immunotherapy*, vol. 54, pp. 1115–1126, 2005.

[183] C. Boibessot, O. Molina, G. Lachance et al., "Subversion of infiltrating prostate macrophages to a mixed immunosuppressive tumor-associated macrophage phenotype," *Clinical and Translational Medicine*, vol. 12, no. 1, p. e581, 2022 pp. e581.

[184] C. Y. Wu, Y. H. Yang, Y. Y. Lin et al., "Anti-cancer effect of danshen and dihydroisotanshinone I on prostate cancer: targeting the crosstalk between macrophages and cancer cells via inhibition of the STAT3/CCL2 signaling pathway," *Oncotarget*, vol. 8, Article ID 40246, 2017.

[185] D. Di Mitri, M. Mirenda, J. Vasilevska et al., "Re-Education of tumor-associated macrophages by CXCR2 blockade drives senescence and tumor inhibition in advanced prostate cancer," *Cell Reports*, vol. 28, pp. 2156–2168.e5, 2019.

[186] Z. Guo, Z. Xing, X. Cheng et al., "Somatostatin derivate (smsDX) attenuates the TAM-stimulated proliferation, migration and invasion of prostate cancer via NF-κB regulation," vol. 10, no. 5, Article ID e0124292, 2015.

[187] S. Malekghasemi, J. Majidi, B. Baradaran, and L. Aghebati-Maleki, "Prostate cancer cells modulate the differentiation of THP-1 cells in response to etoposide and TLR agonists treatments," *Cell Biology International*, vol. 44, pp. 2031–2041, 2020.

[188] H. Arora, K. Panara, M. Kuchakulla et al., "Alterations of tumor microenvironment by nitric oxide impedes castration-resistant prostate cancer growth," *Proceedings of the National Academy of Sciences*, vol. 115, Article ID 11298, 2018.

[189] A. I. Peltomaa, P. Raittinen, K. Talala et al., "Prostate cancer prognosis after initiation of androgen deprivation therapy among statin users. A population-based cohort study," *Prostate Cancer and Prostatic Diseases*, vol. 24, pp. 917–924, 2021.

[190] G. Jia, X. Wang, W. Wu et al., "LXA4 enhances prostate cancer progression by facilitating M2 macrophage polarization via inhibition of METTL3," *International Immunopharmacology*, vol. 107, Article ID 108586, 2022.

Research Article

Discovery of Lipid Metabolism-Related Genes for Predicting Tumor Immune Microenvironment Status and Prognosis in Prostate Cancer

Ying Zhang [ID],[1] **Xiangyu Kong** [ID],[2] **Shiyong Xin** [ID],[3] **Liangkuan Bi** [ID],[1] **and Xianchao Sun** [ID][1,3]

[1]*Department of Urology, The Second Affiliated Hospital of Anhui Medical University, Hefei 230032, China*
[2]*Center of Gallbladder Disease, Shanghai East Hospital, School of Medicine, Tongji University, Shanghai 200120, China*
[3]*Department of Urology, Shanghai East Hospital, School of Medicine, Tongji University, Shanghai 200120, China*

Correspondence should be addressed to Liangkuan Bi; blk_uro@126.com and Xianchao Sun; ahmusxc@163.com

Ying Zhang and Xiangyu Kong contributed equally to this work.

Background. Reprogramming of lipid metabolism is closely associated with tumor development, serving as a common and critical metabolic feature that emerges during tumor evolution. Meanwhile, immune cells in the tumor microenvironment also undergo aberrant lipid metabolism, and altered lipid metabolism also has an impact on the function and status of immune cells, further promoting malignant biological behavior. Consequently, we focused on lipid metabolism-related genes for constructing a novel prognostic marker and evaluating immune status in prostate cancer. *Methods.* Information about prostate cancer patients was obtained from TCGA and GEO databases. The NMF algorithm was conducted to identify the molecular subtypes. The least absolute shrinkage and selection operator (Lasso) regression analysis was applied to establish a prognostic risk signature. CIBERSORT algorithm was used to calculate immune cell infiltration levels in prostate cancer. External clinical validation data were used to validate the results. *Results.* Prostate cancer samples were divided into two subtypes according to the NMF algorithm. A six-gene risk signature (PTGS2, SGPP2, ALB, PLA2G2A, SRD5A2, and SLC2A4) was independent of prognosis and showed good stability. There were significant differences between risk groups of patients with respect to the infiltration of immune cells and clinical variables. Response to immunotherapy also differed between different risk groups. Furthermore, the mRNA expression levels of the signature genes were verified in tissue samples by qRT-PCR. *Conclusion.* We constructed a six-gene signature with lipid metabolism in prostate cancer to effectively predict prognosis and reflect immune microenvironment status.

1. Introduction

Prostate cancer (PCa) has become the second most common malignant tumor in men worldwide in terms of incidence and mortality, which seriously endangers men's health [1]. PCa is the most diagnosed cancer in men in more than half of the countries in the world, especially in developed countries and regions [2]. A large number of epidemiological studies have been conducted to confirm that age, race, and family genetic history are recognized risk factors [3]. In particular, along with the change in people's lifestyle and diet habits, obesity and the consequent disorder of blood lipid levels have been noticed. High-calorie food and saturated animal fat intake are associated with increased PCa incidence [4, 5].

Lipids, as important active molecules in cellular life activities, play an important role in adaptive changes in cancer cell metabolism [6]. Altered lipid metabolism is one of the most significant metabolic changes in tumorigenesis. Enhanced lipid synthesis or uptake contributes to the rapid growth of cancer cells and tumor formation [7, 8]. Lipids are a highly complex class of biomolecules that not only form the structural basis of biological membranes but also act as signaling molecules and energy sources. Although most somatic cells derive their lipids from food sources or hepatic synthesis, various cancers reactivate fatty acids (FA)

synthesis from scratch, making them more independent of externally supplied lipids [9]. Consequently, blocking lipid supply might have a significant impact on bioenergetics, membrane biosynthesis, and intracellular signaling processes in cancer cells. In addition, altered lipid effectiveness would also affect cancer cell migration, induction of angiogenesis, metabolic symbiosis, evasion of immune surveillance, and cancer drug resistance [10, 11]. However, targeting this aspect of cancer cell metabolism remains challenging given the complexity of cellular lipid species and the dynamic nature of their synthesis, remodeling, and catabolism.

Currently, immune cells in the tumor microenvironment (TME) also undergo lipid reprogramming, which has a significant impact on T cell function [12, 13]. Through continuous exploration and in-depth analysis, there are many new advances in the understanding of the complexity of lipid metabolism in different tumor immune cells, and the molecular mechanisms of lipid metabolism on cell function [14]. Targeting genes and enzymes related to tumor and immune lipid metabolism may have different effects on cancer prevention and treatment [15]. Therefore, abnormal lipid metabolism and tumor immunity are gaining widespread attention and enthusiasm from researchers.

In this study, the expression of lipid metabolism-related genes in PCa was examined in order to recognize hub genes that are predictive of patient outcome and immune microenvironment status. We constructed and validated a six-gene signature that accurately predicts PCa patient prognosis, along with immune infiltration cell patterns. Clinical application of this prognostic signature may be possible and reflects the immune status of PCa patients.

2. Materials and Methods

2.1. Data Collection. Human lipid metabolism pathways were downloaded from the Molecular Signature Database (MSigDB) [16], and 776 genes (Supplementary Table S1) were obtained from six lipid metabolism pathways (Supplementary Table S2). PCa samples and corresponding clinicopathological information were obtained from TCGA database and GEO database (GSE116918). The sample information in TCGA dataset was shown in Supplementary Table S3.

2.2. Molecular Subtype Identification. A total of 776 genes from TCGA dataset were extracted and genes with significant differential expression were selected. PCa samples were clustered using nonnegative matrix factorization (NMF) clustering algorithm [17]. We set the number of clusters k from 2 to 10, and determined the average contour width of the common member matrix using the R package "NMF."

2.3. Gene Set Variation Analysis (GSVA). The GSVA enrichment score of the signaling pathway in each PCa sample was calculated using the "GSVA" R package. The correlation between the different risk subgroups and clinical variables was analyzed by the chi-square test. Kaplan–Meier survival

analysis was applied to analyze the difference in progression-free survival (PFS) between the two subgroups.

2.4. A Comprehensive Analysis of Immune Characteristics. PCa samples were examined for their immune profiles by importing their expression data into CIBERSORT and iterating 1000 times to estimate the relative proportions of immune cells. Our results were displayed as a landscape map showing the proportion of immune cells and clinicopathological factors. An immunophenoscore (IPS) was used to represent tumor immunogenicity on a scale from 0 to 10. Higher IPS scores represent increased immunogenicity. The IPS of TCGA patients was obtained from the Cancer Immunome Atlas (TCIA) (https://tcia.at/home).

2.5. Clinical Patients and Prostate Specimens. Sixty paired normal and tumor tissues were collected from PCa patients who underwent surgery at the Second Affiliated Hospital of Anhui Medical University (Hefei, China). They had diagnostic criteria according to the WHO classification and received no preoperative treatment. Informed consent was obtained from each patient before inclusion in the study, and ethical approval was obtained from the Ethics Committee of the Second Affiliated Hospital of Anhui Medical University.

2.6. RNA Extraction and qRT-PCR. TRIzol (Invitrogen, USA) was used to extract the total RNA. qRT-PCR was conducted based on the manufacturer's instruction. GAPDH was an internal control. Fold-changes were calculated by the $2^{-\Delta\Delta Ct}$ method. Primer information is shown in Supplementary Table S4.

2.7. Statistical Analysis. Bioinformatic analyses were conducted using R version 4.1.1. For comparing continuous data, Student's t or Wilcoxon test were used. The chi-square test and Fisher test were used for comparing clinical and pathological parameters. Spearman correlation analysis was used to analyze the correction between the risk signature and immune cells. All statistical p-values were two-sided and $p < 0.05$ was considered statistically significant.

3. Results

3.1. Different Subtypes Were Classified Based on Lipid Metabolism-Related Genes. Six lipid metabolism-related gene sets were selected from MSigDB. The gene expression of PCa was investigated using RNA-seq data from TCGA prostate cancer cohort (TCGA-PRAD). To identify genes with differential expression, the "limma" R package was used. The differential expression of 56 lipid metabolism-related genes were found on PCa ($p < 0.05$, Figure 1(a), Supplementary Table S5). After that, PCa samples were clustered by the NMF method. Cophenetic, dispersion, and silhouette all indicate that $k = 2$ is an optimal number of clusters (Figures 1(b) and 1(c)). PFS prognostic relationships between Cluster 1 (C1) and Cluster 2 (C2) show that
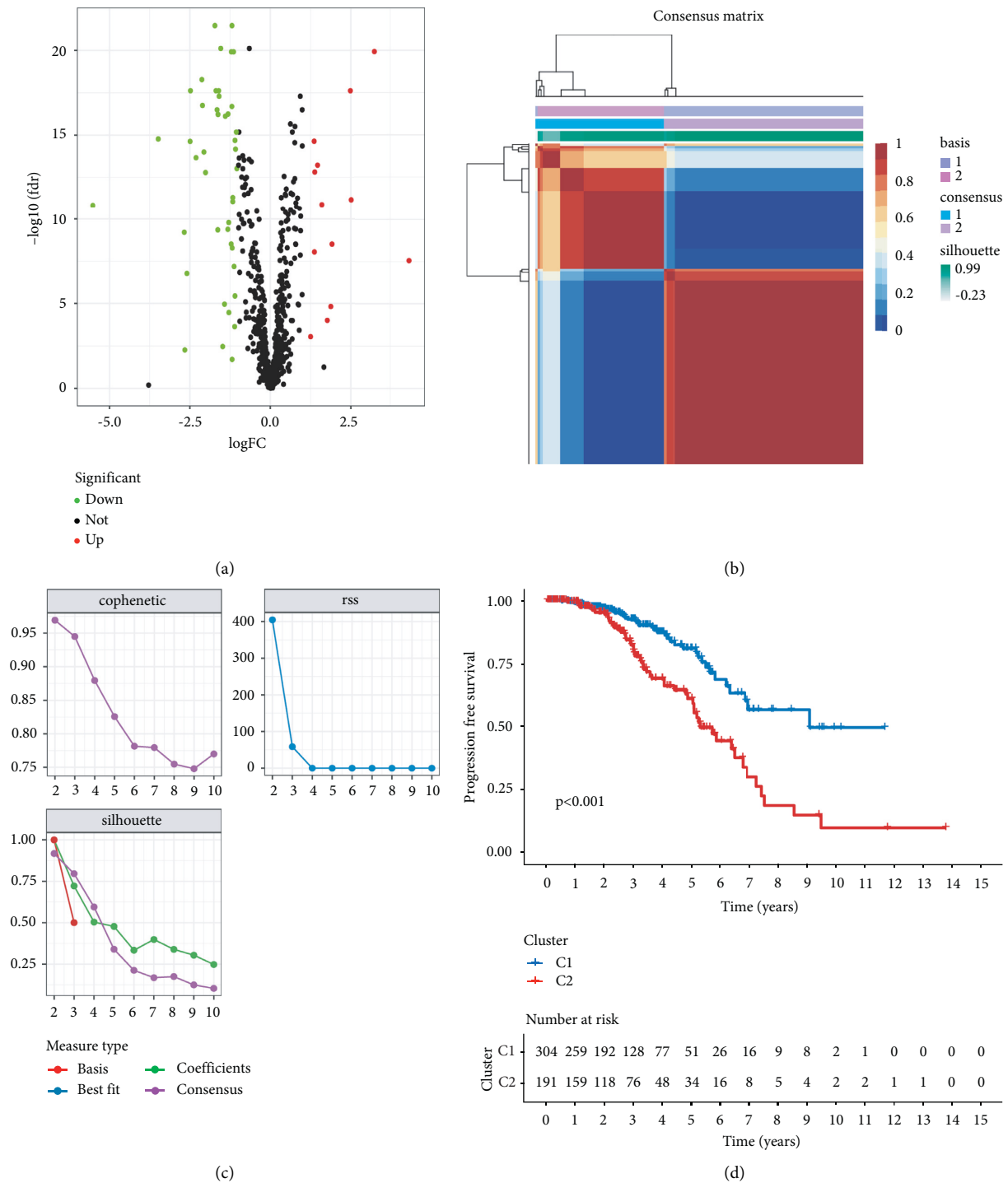
(a)

(b)

(c)

(d)

FIGURE 1: Classification was based on different subtypes. (a) Volcano map displaying the differentially expressed lipid metabolism-related genes in TCGA-PRAD. Red: up-regulation, blue: down-regulation. (b) NMF clustering consensus map. (c) NMF distributions when rank = 2–10. (d) Progression-free survival analysis of two subtypes in TCGA-PRAD.

subgroup C1 has a better prognosis than subgroup C2 (Figure 1(d)), log-rank $p < 0.001$).

3.2. Establishment of the Prognostic Risk Model.
To screen for significant genes associated with prognosis in TCGA-PRAD cohort, we performed a Cox proportional hazard analysis. On the basis of a p-value of less than 0.05, 11 genes showed significant prognostic differences (Supplementary Table S6). In order to develop a highly accurate prognostic model and to narrow the list of genes, Lasso regression analysis was used to identify hub genes (Figures 2(a) and 2(b)). Combining the analysis, six target genes were selected. The six-gene signature formula was as follows: Risk
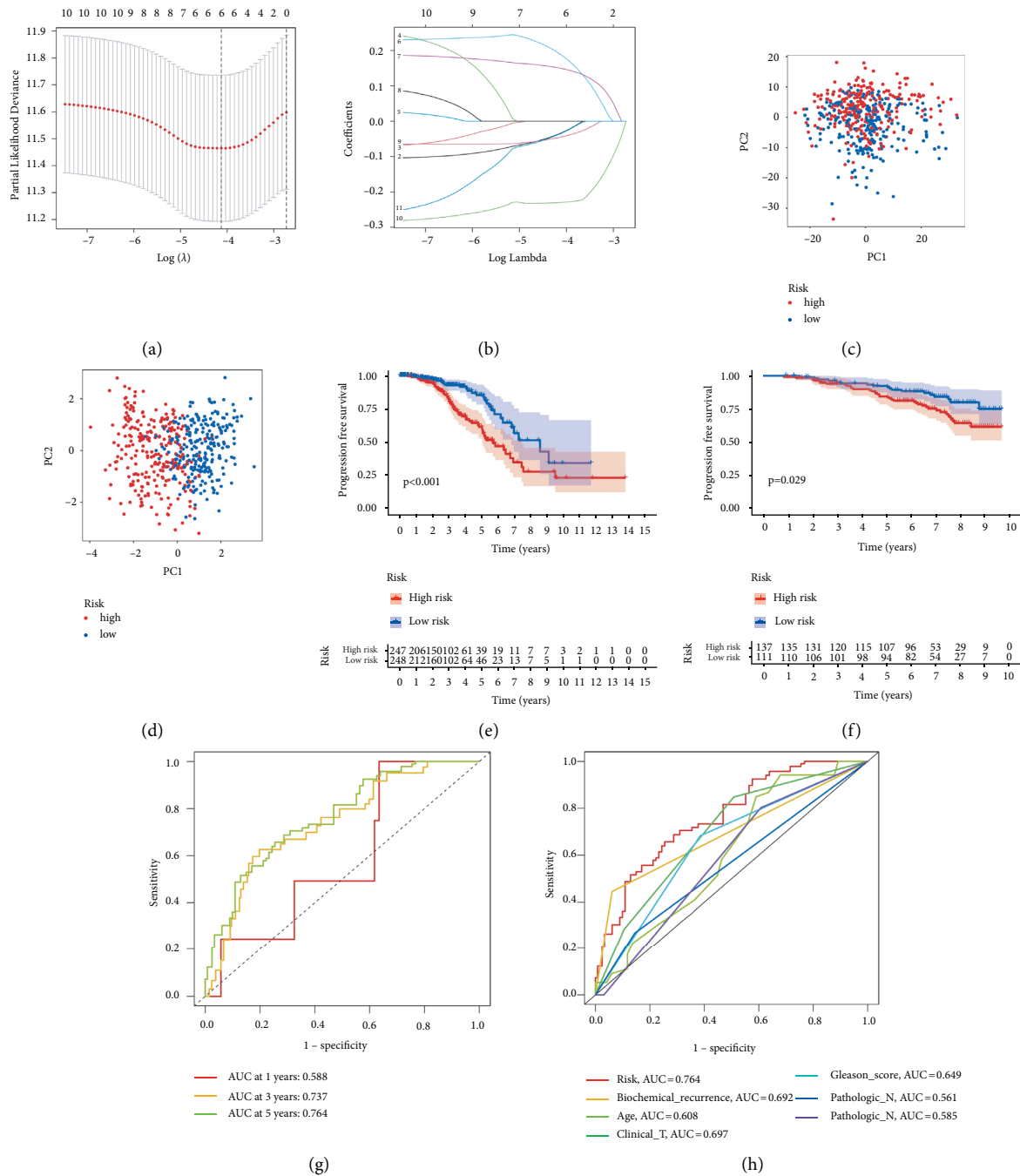
(a)

(b)

(c)

(d)

(e)

(f)

(g)

(h)

FIGURE 2: Establishment of the prognostic risk model. (a) LASSO coefficient profile plot. (b) The values of lambda in the model. (c) PCA plot in the two risk groups with lipid metabolism-related genes. (d) PCA plot in the two risk groups with risk signature genes. (e) Survival curves of the groups in TCGA-PRAD cohort. (f) Survival curves of the groups in the GSE116918 cohort. (g) ROC curve of the model in TCGA-PRAD cohort. (h) The accuracy of the risk model was tested with other clinical variables.

score = expression level of PTGS2 × (−0.033) + expression level of SGPP2 × (0.188) + expression level of ALB × (0.149) + expression level of PLA2G2A × (−0.045) + expression level of SRD5A2 × (−0.229) + expression level of SLC2A4 × (−0.035). PCA plot analysis demonstrated that samples in two risk groups were distributed in two directions with the six genes in our risk model compared with lipid metabolism-related gens (Figures 2(c) and 2(d)). The K-M curves for the two subgroups of the risk score were shown in

Figure 2(e), and there was a significant difference between them ($p < 0.001$). We then used the same coefficients in GSE116918 as an independent validation cohort and significantly different results were observed (Figure 2(f), $p = 0.029$). The area under the curve (AUC) values for 1, 3, and 5 years, respectively, were 0.588, 0.737, and 0.764 (Figure 2(g)). Furthermore, we compared the 5-year ROC curve with some clinicopathological variables. We found that the risk model exhibited satisfactory prognostic
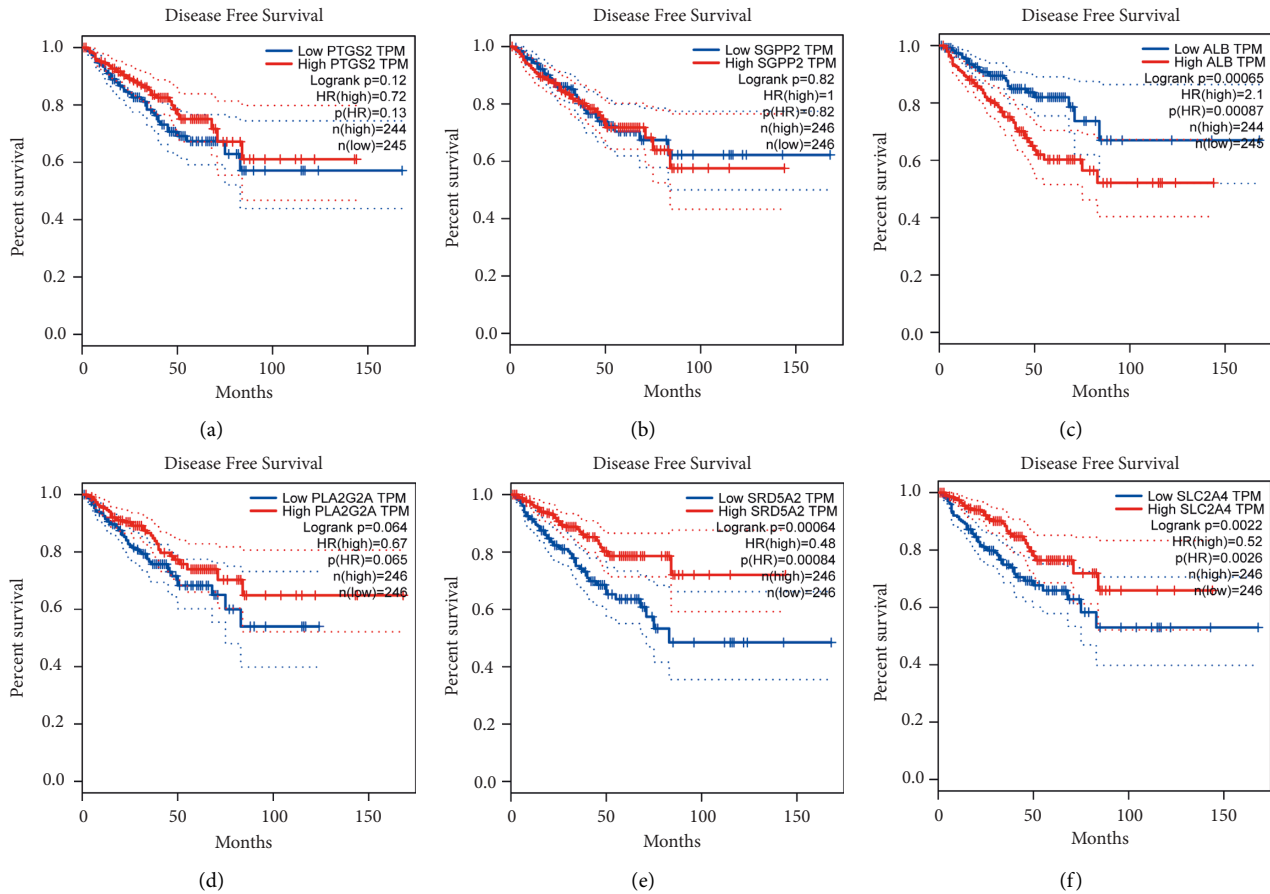
Figure 3: GEPIA survival analysis of PTGS2, SGPP2, ALB, PLA2G2A, SRD5A2, and SLC2A4.

accuracy with regards to age, biochemical recurrence, clinical T stage, Gleason score, pathological N stage, and pathological T stage (Figure 2(h)). Gene Expression Profiling Interactive Analysis (GEPIA) database was applied to analyze the associations between the six signature genes and PFS in PCa [18]. Low expressions level of PLA2G2A, SRD5A2, and SLC2A4 as well as high expression level of ALB were closely correlated with poorer survival outcomes of PCa patients (Figure 3).

3.3. Independent Prognostic Analysis and Construction of the Nomogram.
Univariate Cox regression analysis indicated that biochemical recurrence, clinical T stage, Gleason score, pathological N stage, pathological T stage. and risk were closely related to PFS (Figure 4(a)). According to multivariate analysis, only biochemical recurrence (HR = 5.059, 95% CI = [2.831–9.041], $p < 0.001$), clinical T stage (HR = 1.546, 95% CI = [1.051–2.275], $p = 0.027$), and risk score (HR = 2.475, 95% CI = [1.540–3.977], $p < 0.001$) were significantly related to PFS (Figure 4(b)). These results demonstrated that this six-gene signature was an independent factor predicting prognosis. The clinicopathological features and risk were combined to construct a nomogram to assess the clinical utility of the prognostic model (Figure 4(c)). Moreover, the nomogram displayed the

highest accuracy in predicting survival (AUC = 0.843) compared with other independent factors (Figure 4(d)).

3.4. Association between the Risk Model with Clinical Characteristics.
Correlation analysis of the risk score and clinical variables such as biochemical recurrence, clinical T stage, Gleason score, pathological N stage, and pathological T stage indicated a statistically significant association (Figures 5(a)–5(f)). Based on the risk score, PCa patients can also be distinguished by age, clinical T stage, pathologic T stage, and N stage (Supplementary Figure S1). In addition, GSVA further confirmed that a high-risk subgroup was significantly enriched in porphyrin and chlorophyll metabolism and pyrimidine metabolism (Figure 5(g)).

3.5. Correlation between the Risk Model and Immunity.
A 33 diverse cancer immune subtype classification has described the immune landscape of PCa according to the immune expression characteristics of four representative signatures: C1 (wound healing), C2 (IFN-γ dominant), C3 (inflammatory), and C4 (lymphocyte depleted) [19]. We found that a higher proportion of C1, C2, and C4 was distributed in the high-risk subgroup, while a higher proportion of C3 in the low-risk subgroup ($p = 0.001$, chi-square test;
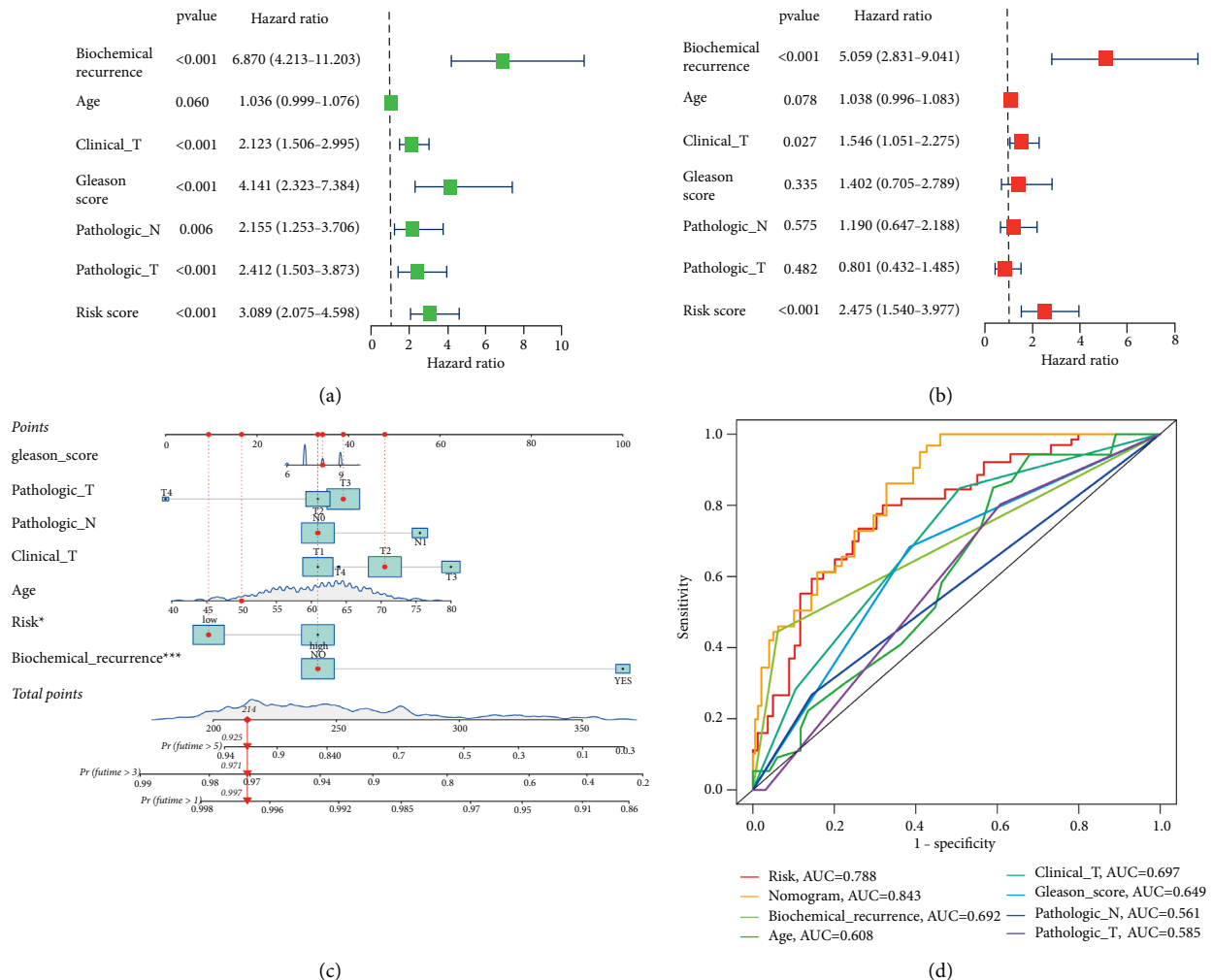
(a)

(b)

(c)

(d)

Figure 4: Independent prognostic analysis and construction of the nomogram. Univariate (a) and multivariate (b) cox analysis indicate that this risk signature was an independent risk factor for predicting prognosis. (c) A nomogram to predict survival. (d) AUC for the nomogram, risk, and clinical variables.

Figure 6(a)). CIBERSORT was applied to evaluate the relative proportions of 22 kinds of immune cells in the TME to examine the indicative roles of this risk model [20]. A significant correlation was found between high-risk subgroups and CD4 memory-activated T cells, regulatory T cells (Tregs), M0 macrophages, and M1 macrophages, while the low-risk subgroup was significantly associated with monocytes and mast resting cells (Figure 6(b)). Figure 6(c) illustrated the relationship between clinical and immunological characteristics of different subgroups at risk.

As well, we investigated the potential of the risk model for predicting the response to immune checkpoint inhibitors (ICIs). The expression of PD-1, PD-L1, LAG3, and CD40 was markedly higher in the low-risk subgroup, indicating a negative correlation with risk (Figures 7(b)–7(h)). A quantification of enrichment scores of immune-related pathways was also performed. Antigen presentation functions, such as APC co-inhibition, CCR, and HLA, tended to favor the low-risk group (Figure 7(a)).

3.6. Role of the Risk Signature in Immunotherapeutic Responses. Next, the ESTIMATE algorithm was used to investigate the correlation between the two groups in immune scores and stromal scores [21]. We found that the low-risk subgroup showed higher immune scores, stromal scores, and estimate scores than the high-risk subgroup (Figure 8(a)). These results further demonstrate that the risk model can affect the immune activity of the TME in PCa. For investigating the capacity of risk predicting response to immunotherapeutic, immunophenogram analysis was undertaken to investigate the association between immunophenoscore (IPS) and different risk subgroups [22]. Findings showed that the low-risk subgroup exhibited higher IPS compared with the high-risk subgroup, which implied that low-risk score patients exhibited a higher positive response to immunotherapy (Figures 8(b)–8(e)). Chemotherapy is an effective strategy for cancer treatment. We further analyzed the correlation between risk score and chemotherapeutic efficacy. We found that the low-risk subgroup was positively associated with a lower IC50 of Docetaxel,
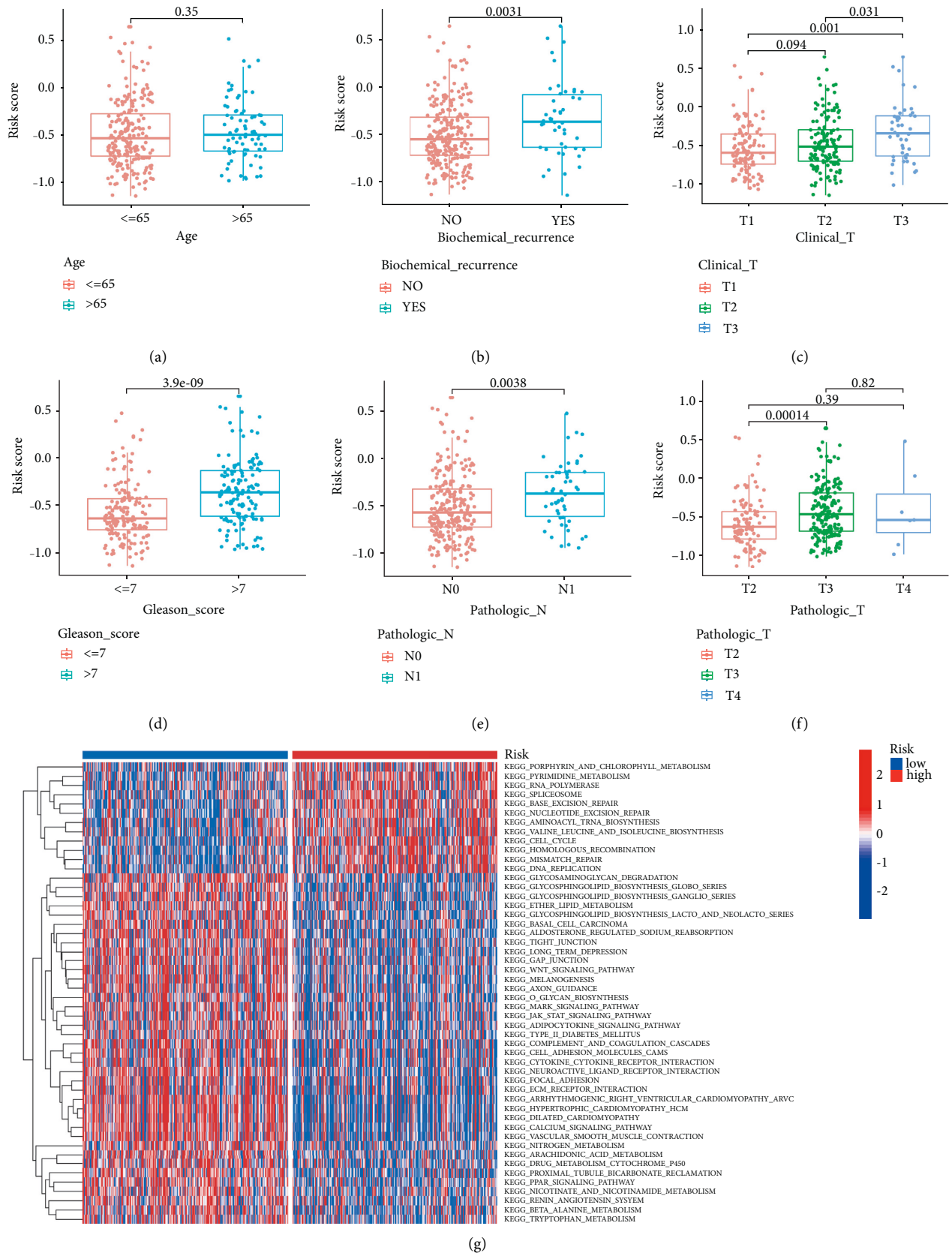
Figure 5: Association between the risk model with different clinical characteristics. Correlation analysis of risk with age (a), biochemical recurrence (b), clinical T stage (c), Gleason score (d), pathological N stage (e), and pathological T stage (f). (g) GSVA enrichment analysis of biological activities between the two risk groups.
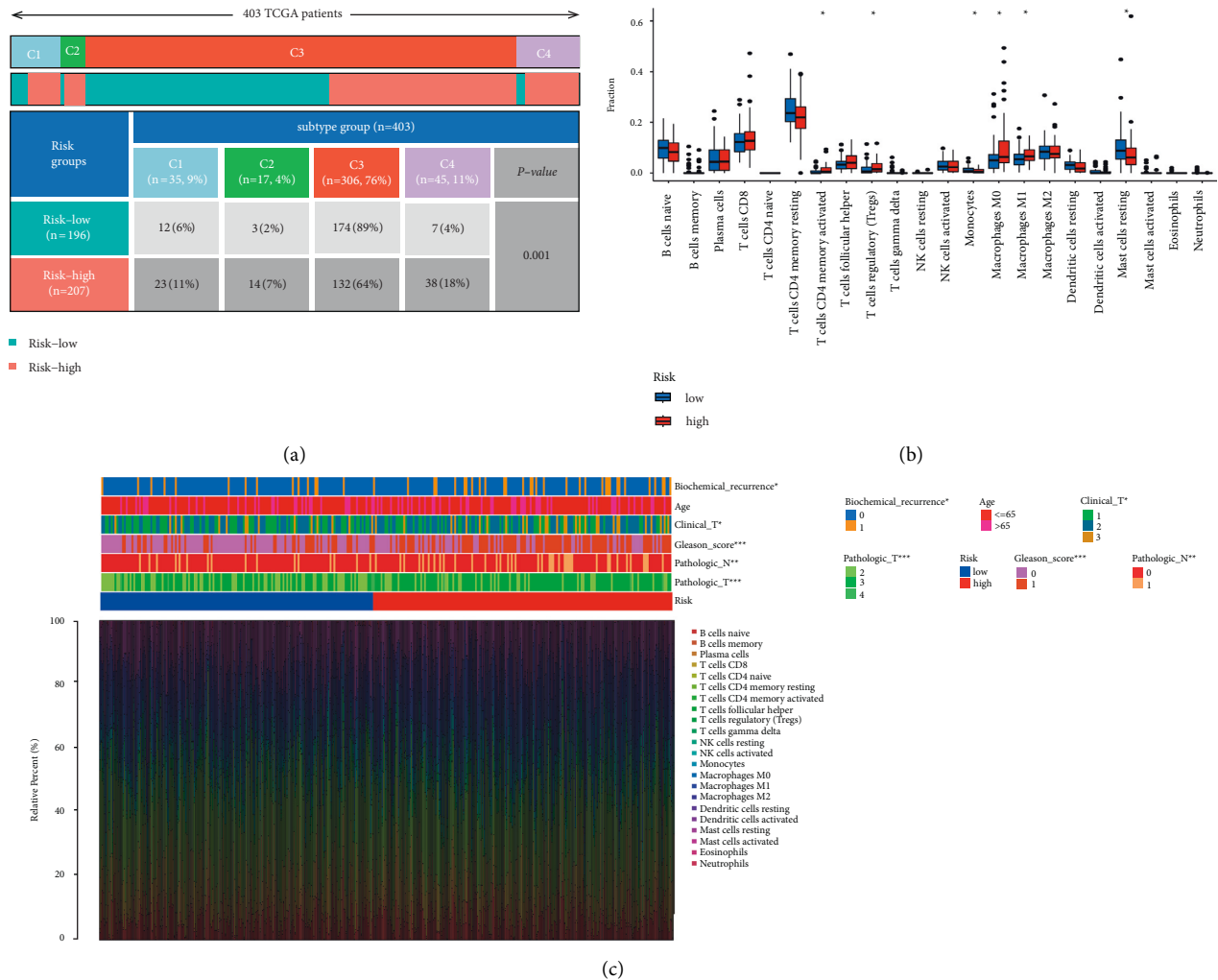
(a)

(b)

(c)

FIGURE 6: Correlation between the risk model and immunity. (a) Different immune subtypes are distributed in the two risk groups. (b) Two risk subgroups with different proportions of immune cells. (c) Clinical features of two risk subgroups with the immune landscape. $^*p < 0.05$, $^{**}p < 0.01$, $^{***}p < 0.001$.

Bleomycin, and Trametinb, while a higher IC50 of 5-Fluorouracil and Mitomycin C, indicating a different distribution of targeted IC50 agents in low- and high-risk subgroups (Figures 8(f)–8(j)).

3.7. Clinical Validation of this Risk Model. In addition to the above results, 60 cases of tissue specimens of PCa were analyzed. We verified the mRNA expression of three signature genes in cancer and normal tissues by qRT-PCR. The findings also showed that the mRNA expression of SGPP2 was higher in tumor tissues, whereas the mRNA expression of SRD5A2 was higher in normal tissues (Figure 9). These results confirmed the significant role of these genes in PCa. The workflow of the present study was shown in Supplementary Figure S2.

4. Discussion

PCa is becoming a growing problem among men worldwide. Its treatment is mainly divided into endocrine therapy and surgery [23]. For patients with advanced PCa,

androgen resistance usually occurs, resulting in castration-resistant prostate cancer (CRPC), which severely affects the life expectancy and quality of patients [24]. Additionally, its tendency to invade surrounding tissues and cause local adhesion greatly increases the difficulty of surgery [25]. Hence, studies are continuously conducted to address the progression and aggressiveness of PCa in order to explain the pathogenesis and explore new therapeutic targets.

In terms of metabolic studies, PCa has remarkable heterogeneity. On the one hand, its metabolic pattern is different from other tumors, and on the other hand, its own metabolic form has significant phenotypic changes as the disease progresses [26, 27]. It has been clearly suggested that in prostate malignancy cells, β-oxidation of FA becomes one of the most important forms of energy supply [28]. Lipid accumulation and disorders of lipid metabolism in PCa cells increase the pathological process, CRPC, and aggressiveness [29]. Further understanding of the energy metabolism of PCa will enable us to design and find better drugs to prevent the development of CRPC.
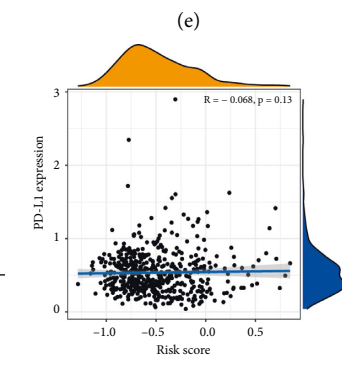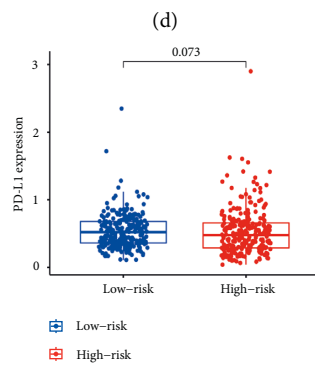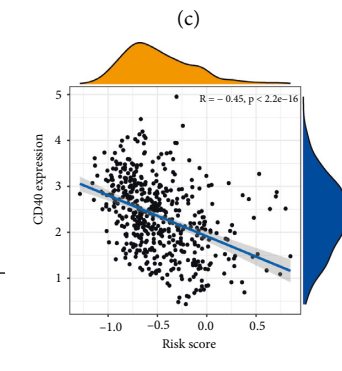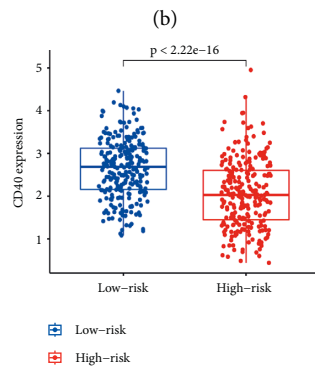
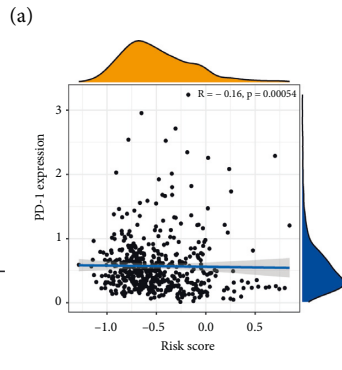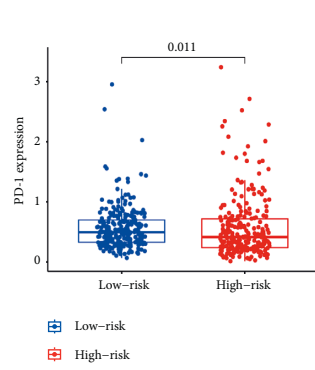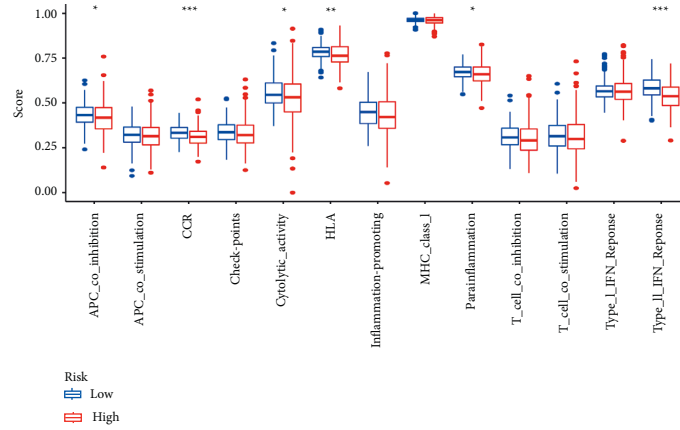(a)

(b)

(c)

(d)
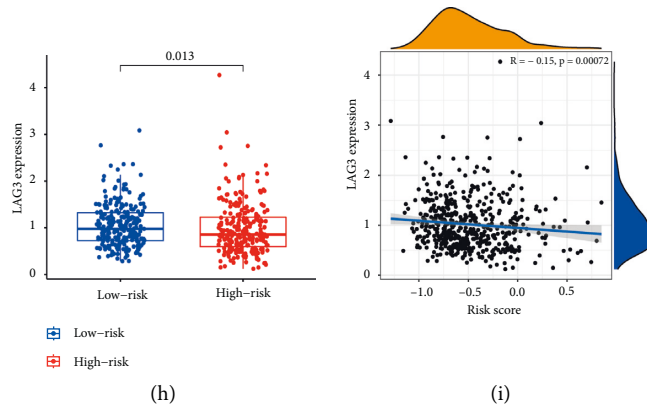

(e)

(f)

(g)

Figure 7: Continued.

(h)

(i)

FIGURE 7: Correlation between the risk model and ICIs. (a) Immune-related pathways were quantified in different risk subgroups. Correlation between risk and PD-1 (b, c), CD40 (d, e), PD-L1 (f, g), and LAG3 (h, i). $^*p < 0.05$, $^{**}p < 0.01$, $^{***}p < 0.001$.

(a)

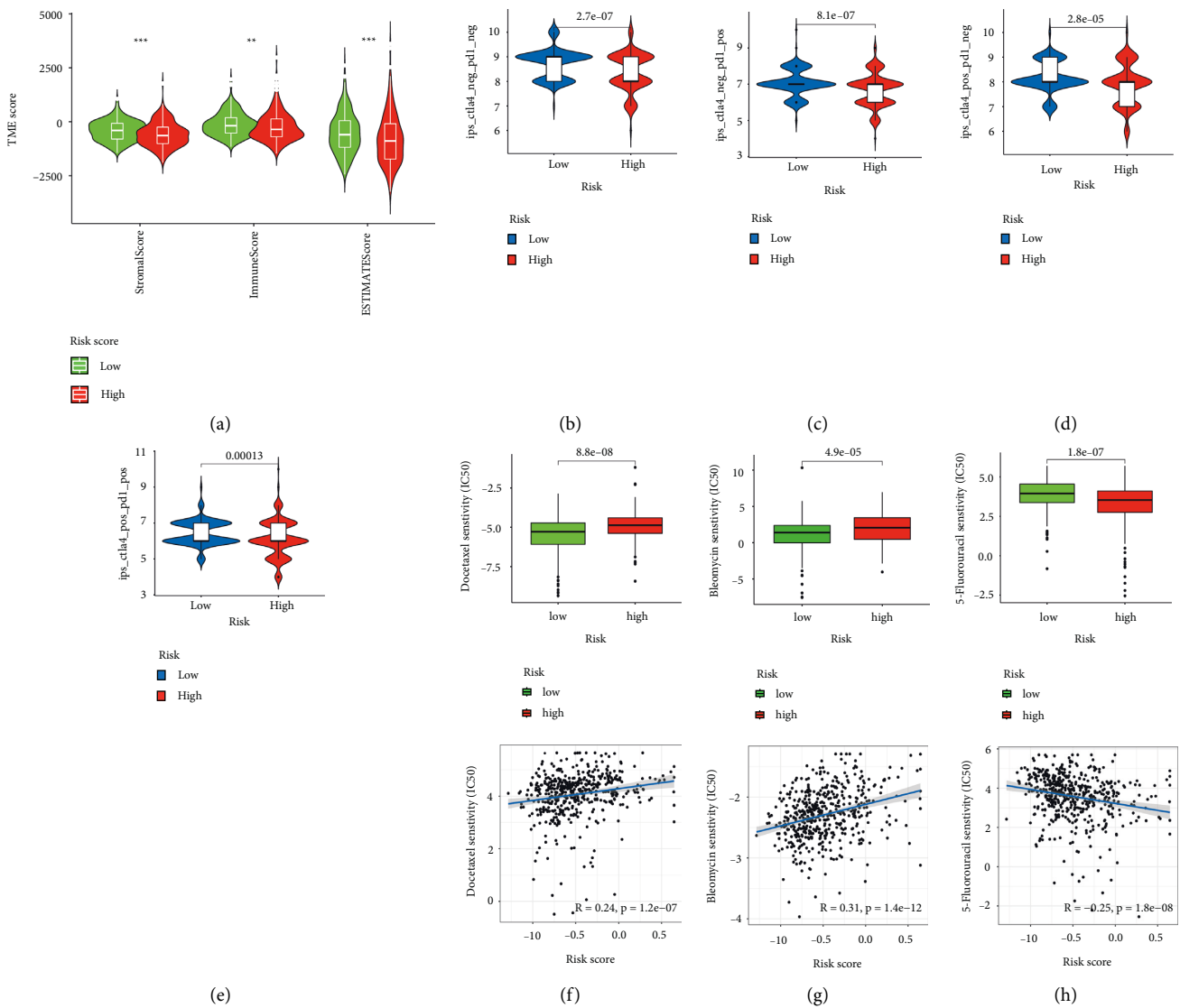(b)

(c)

(d)

(e)

(f)
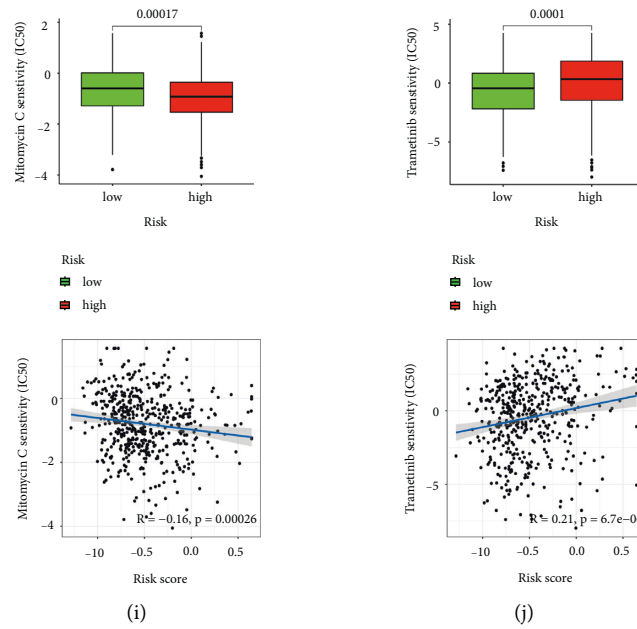

(g)

(h)

FIGURE 8: Continued.

(i)

(j)

FIGURE 8: Role of the risk signature in immunotherapeutic responses. (a) ESTIMATE algorithm was used to investigate the correlation between the two groups in immune scores and stromal scores. (b)–(e) The correlation between immunophenoscore and different risk groups. Low-risk subgroup was positively correlated with a lower IC50 of Docetaxel (f), Bleomycin (g), and Trametinb (j), while a higher IC50 of 5-Fluorouracil (h) and Mitomycin C (i). $^{**} p < 0.01$, $^{***} p < 0.001$, ns $p > 0.05$.
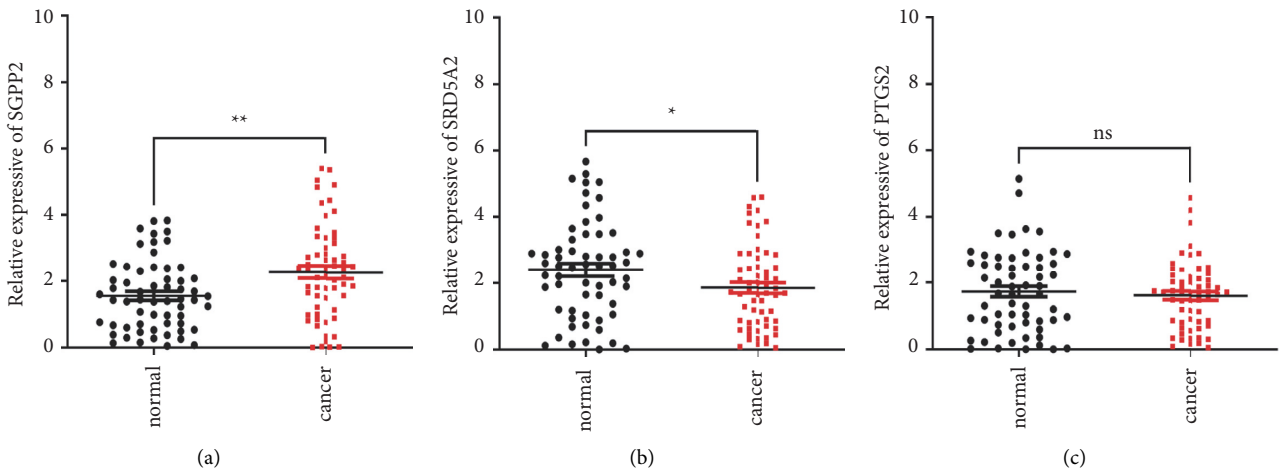

(a)

(b)

(c)

FIGURE 9: Clinical validation of this risk model. qRT-PCR analysis of SGPP2, SRD5A2, and PTGS2 mRNA levels in tissue samples (a)–(c). $^{*} p < 0.05$, $^{**} p < 0.01$, ns $p > 0.05$.

Alterations in lipid metabolism affect a variety of cellular functions, which in turn affect downstream signaling pathways, associated with cell proliferation, adhesion, and motility. These alterations in the tumor can be closely related to enhanced oncogene signaling pathways and alterations in related metabolic enzymes. Moreover, the interaction between parenchyma and mesenchyme in the malignant development of tumor continuously remodels TME, and a unique tumor-associated lipid microenvironment gradually forms around it, which can have complex interactions with tumor cells through bioactive molecules such as hormones and adipokines [30, 31].

Lipid metabolism reprogramming can significantly affect immune cell fate and function. Under normal conditions, FA synthesis and uptake are key features of effector T cells. To survive in a hostile environment, immune cells undergo metabolic reprogramming, using FA as a secondary resupply station for energy [32]. FA catabolism also improves CD8^{+} T cell function through alternative pathways [33]. The normal function of immune cells is dependent on cholesterol and membrane cholesterol levels control the number of T cell receptor nanoclusters and affect their immune recognition function. Hossain et al. found that increased FA uptake and oxidation in tumor-infiltrated MDSC were

accompanied by increased oxygen consumption rates and mitochondrial mass [34]. There is a potential impact of altered lipid metabolism in tumor immunity on natural killer T cell (NKT) nondependent and dependent immune function [35]. Both the M1 and M2 phenotypes of macrophages are dependent on specific lipid mediators [36].

The present study identified two subtypes of PCa based on genes that were associated with lipid metabolism using the NMF algorithm. Next, Lasso regression analysis was performed to construct a six-gene prognostic risk model. According to our study, this model performed well in predicting survival in PCa patients and correlated with both clinical features and immune microenvironment. The risk model was established with PTGS2, SGPP2, ALB, PLA2G2A, SRD5A2, and SLC2A4. Based on the corresponding coefficients, a risk score was calculated. Samples were grouped according to their risk levels. Discrepancies between the survival analyses for different risk subgroups were significant. Additionally, we found that the risk score was an independent factor for survival. CIBERSORT confirmed that patients in the high-risk subgroup had higher proportions of CD4 memory-activated T cells, regulatory T cells, M0 macrophages, and M1 macrophages, while monocytes and mast resting cells were upregulated in the low-risk group, suggesting different patterns of infiltration among the subgroups. We also demonstrated that the low-risk subgroup was correlated with immune checkpoints such as PD-1, PD-L1, CD40, and LAG3, indicating that patients with different risks respond differently to immunotherapy and low-risk patients may have a better response to immunotherapy. Next, we further validated the expression of the risk signature genes in PCa tissue specimens. The qRT-PCR results suggested that the expression of SGPP2 was significantly elevated in tumor tissue specimens, while the expression of SRD5A2 was significantly increased in normal tissue. Comparison with other relevant published studies, we comprehensive analysis and explanation of the association between the lipid metabolism-related genes with the immune microenvironment and the prognosis of PCa. We revealed the role of lipid metabolism-related genes in PCa and validated the target genes in clinical samples. Nevertheless, the specific biological functions of these genes in PCa need to be further explored.

Reprogramming of lipid metabolism is a prevalent and crucial metabolic feature that emerges during tumor evolution, allowing them to survive and further evolve in a hostile environment [37]. Through extensive exploration of aberrant lipid metabolism and tumor immunity, new breakthroughs have been made in the discovery of molecular mechanisms and metabolic adaptations, generating significant changes in antitumor therapeutic strategies [38]. Consequently, we sought to fill the gap between lipid metabolism gene status and PCa prognosis prediction. We believe these genes were involved in lipid metabolism processes, and this model may serve as a prognostic biomarker for PCa and immune microenvironment evaluation.

In conclusion, we constructed a six-gene signature associated with lipid metabolism, which was an independent prognostic factor in PCa. This six-gene signature could be recognized as a prognostic marker to reflect the lipid metabolism and immunity status of PCa.

Abbreviations

PCa:	Prostate cancer
NMF:	Nonnegative matrix factorization
TCGA:	The cancer genome atlas
GEO:	Gene expression omnibus
ROC:	Receiver-operating characteristic
PFS:	Progression-free survival
LASSO:	Least absolute shrinkage and selection operator
AUC:	Areas under curve
TME:	Tumor microenvironment
GSVA:	Gene set variation analysis
ICIs:	Immune checkpoint inhibitors
IPS:	Immunophenoscore
FA:	Fatty acid
qRT-PCR:	Quantitative real time polymerase chain reaction
TCGA-PRAD:	The cancer genome atlas-prostate adenocarcinoma.

Data Availability

The authors declare that the data supporting the findings of the current study are provided in the article. Datasets analyzed for this work can be obtained from TCGA(https://portal.gdc.cancer.gov/), GEO (https://www.ncbi.nlm.nih.gov/geo/), MSigDB (https://www.gsea-msigdb.org/gsea/msigdb), and CIBERSORT (https://cibersort.stanford.edu/).

Ethical Approval

This study was approved by the Ethics Committee of the Second Affiliated Hospital of Anhui Medical University.

Conflicts of Interest

The authors declare that they have no conflicts of interest.

Authors' Contributions

Supplementary Materials

Figure S1. A stratified survival basis of two risk subgroups in age (a)–(b), N stage (c)–(d), clinical T stage (e)–(f), and pathologic T stage (g)–(h). Figure S2. The workflow of the present study. Table S1. Lipid metabolism-related genes. Table S2. Six pathways involved in lipid metabolism. Table S3. Clinical characteristics of prostate cancer patients from TCGA cohort. Table S4. Primer information. Table S5. 56

genes with significant prognostic differences. Table S6. 11 genes showed significant prognostic differences by cox proportional hazard analysis. (*Supplementary Materials*)

References

[1] R. L. Siegel, K. D. Miller, H. E. Fuchs, and A. Jemal, "Cancer statistics, 2022," *CA: A Cancer Journal for Clinicians*, vol. 72, no. 1, pp. 7–33, 2022.

[2] D. A. Siegel, M. E. O'Neil, T. B. Richards, N. F. Dowling, and H. K. Weir, "Prostate cancer incidence and survival, by stage and race/ethnicity—United States, 2001–2017," *Morbidity and Mortality Weekly Report*, vol. 69, no. 41, pp. 1473–1480, 2020.

[3] R. A. Sabol, E. M. Ledet, E. Jaeger et al., "Family history and pathogenic/likely pathogenic germline variants in prostate cancer patients," *The Prostate*, vol. 81, no. 7, pp. 427–432, 2021.

[4] M. Matsushita, K. Fujita, and N. Nonomura, "Influence of diet and nutrition on prostate cancer," *International Journal of Molecular Sciences*, vol. 21, no. 4, p. 1447, 2020.

[5] J. R. Marshall, "Diet and prostate cancer prevention," *World Journal of Urology*, vol. 30, no. 2, pp. 157–165, 2012.

[6] X. Bian, R. Liu, Y. Meng, D. Xing, D. Xu, and Z. Lu, "Lipid metabolism and cancer," *Journal of Experimental Medicine*, vol. 218, no. 1, Article ID e20201606, 2021.

[7] L. A. Broadfield, A. A. Pane, A. Talebi, J. V. Swinnen, and S. M. Fendt, "Lipid metabolism in cancer: new perspectives and emerging mechanisms," *Developmental Cell*, vol. 56, no. 10, pp. 1363–1393, 2021.

[8] C. W. Fhu and A. Ali, "Fatty acid synthase: an emerging target in cancer," *Molecules*, vol. 25, no. 17, p. 3935, 2020.

[9] P. Morigny, J. Boucher, P. Arner, and D. Langin, "Lipid and glucose metabolism in white adipocytes: pathways, dysfunction and therapeutics," *Nature Reviews Endocrinology*, vol. 17, no. 5, pp. 276–295, 2021.

[10] H. Li, Z. Feng, and M. L. He, "Lipid metabolism alteration contributes to and maintains the properties of cancer stem cells," *Theranostics*, vol. 10, no. 16, pp. 7053–7069, 2020.

[11] H. Iwamoto, M. Abe, Y. Yang et al., "Cancer lipid metabolism confers antiangiogenic drug resistance," *Cell Metabolism*, vol. 28, no. 1, pp. 104–117, 2018.

[12] K. C. Corn, M. A. Windham, and M. Rafat, "Lipids in the tumor microenvironment: from cancer progression to treatment," *Progress in Lipid Research*, vol. 80, Article ID 101055, 2020.

[13] C. S. Field, F. Baixauli, R. L. Kyle et al., "Mitochondrial integrity regulated by lipid metabolism is a cell-intrinsic checkpoint for treg suppressive function," *Cell Metabolism*, vol. 31, no. 2, pp. 422–437, 2020.

[14] X. Liu, C. L. Hartman, L. Li et al., "Reprogramming lipid metabolism prevents effector *i* cell senescence and enhances tumor immunotherapy," *Science Translational Medicine*, vol. 13, no. 587, Article ID eaaz6314, 2021.

[15] Y. Hao, D. Li, Y. Xu et al., "Investigation of lipid metabolism dysregulation and the effects on immune microenvironments in pan-cancer using multiple omics data," *BMC Bioinformatics*, vol. 20, no. S7, p. 195, 2019.

[16] A. Liberzon, C. Birger, H. Thorvaldsdottir, M. Ghandi, J. P. Mesirov, and P. Tamayo, "The molecular signatures database hallmark gene set collection," *Cell Systems*, vol. 1, no. 6, pp. 417–425, 2015.

[17] S. Akcay, E. Guven, M. Afzal, and I. Kazmi, "Non-negative matrix factorization and differential expression analyses identify hub genes linked to progression and prognosis of glioblastoma multiforme," *Gene*, vol. 824, Article ID 146395, 2022.

[18] Z. Tang, C. Li, B. Kang, G. Gao, C. Li, and Z. Zhang, "GEPIA: a web server for cancer and normal gene expression profiling and interactive analyses," *Nucleic Acids Research*, vol. 45, 2017.

[19] V. Thorsson, D. L. Gibbs, S. D. Brown et al., "The immune landscape of cancer," *Immunity*, vol. 48, no. 4, pp. 812–830, 2018.

[20] J. I. Kawada, S. Takeuchi, H. Imai et al., "Immune cell infiltration landscapes in pediatric acute myocarditis analyzed by CIBERSORT," *Journal of Cardiology*, vol. 77, no. 2, pp. 174–178, 2021.

[21] J. Wu, L. Li, H. Zhang et al., "A risk model developed based on tumor microenvironment predicts overall survival and associates with tumor immunity of patients with lung adenocarcinoma," *Oncogene*, vol. 40, no. 26, pp. 4413–4424, 2021.

[22] Q. Xu, S. Chen, Y. Hu, and W. Huang, "Landscape of immune microenvironment under immune cell infiltration pattern in breast cancer," *Frontiers in Immunology*, vol. 12, Article ID 711433, 2021.

[23] M. Y. Teo, D. E. Rathkopf, and P. Kantoff, "Treatment of advanced prostate cancer," *Annual Review of Medicine*, vol. 70, no. 1, pp. 479–499, 2019.

[24] K. H. Stopsack, S. Nandakumar, A. G. Wibmer et al., "Oncogenic genomic alterations, clinical phenotypes, and outcomes in metastatic castration-sensitive prostate cancer," *Clinical Cancer Research*, vol. 26, no. 13, pp. 3230–3238, 2020.

[25] P. Rescigno, C. Buonerba, J. Bellmunt, G. Sonpavde, S. De Placido, and G. Di Lorenzo, "New perspectives in the therapy of castration resistant prostate cancer," *Current Drug Targets*, vol. 13, no. 13, pp. 1676–1686, 2012.

[26] G. E. Stoykova and I. R. Schlaepfer, "Lipid metabolism and endocrine resistance in prostate cancer, and new opportunities for therapy," *International Journal of Molecular Sciences*, vol. 20, no. 11, p. 2626, 2019.

[27] J. Dlubek, J. Rysz, Z. Jablonowski, A. Gluba-Brzozka, and B. Franczyk, "The correlation between lipid metabolism disorders and prostate cancer," *Current Medicinal Chemistry*, vol. 28, no. 10, pp. 2048–2061, 2021.

[28] Y. Liu, "Fatty acid oxidation is a dominant bioenergetic pathway in prostate cancer," *Prostate Cancer and Prostatic Diseases*, vol. 9, no. 3, pp. 230–234, 2006.

[29] D. A. Bader and S. E. McGuire, "Tumour metabolism and its unique properties in prostate adenocarcinoma," *Nature Reviews Urology*, vol. 17, no. 4, pp. 214–231, 2020.

[30] T. Motohara, K. Masuda, M. Morotti et al., "An evolving story of the metastatic voyage of ovarian cancer cells: cellular and molecular orchestration of the adipose-rich metastatic microenvironment," *Oncogene*, vol. 38, no. 16, pp. 2885–2898, 2019.

[31] G. Deep and I. R. Schlaepfer, "Aberrant lipid metabolism promotes prostate cancer: role in cell survival under hypoxia and extracellular vesicles biogenesis," *International Journal of Molecular Sciences*, vol. 17, no. 7, p. 1061, 2016.

[32] Y. Zhang, R. Kurupati, L. Liu et al., "Enhancing CD8 (+) *T* cell fatty acid catabolism within a metabolically challenging tumor microenvironment increases the efficacy of melanoma immunotherapy," *Cancer Cell*, vol. 32, no. 3, pp. 377–391.e9, 2017.

[33] M. L. Balmer, E. H. Ma, G. R. Bantug et al., "Memory CD8 (+) *T* cells require increased concentrations of acetate induced by stress for optimal function," *Immunity*, vol. 44, no. 6, pp. 1312–1324, 2016.

[34] F. Hossain, A. A. Al-Khami, D. Wyczechowska et al., "Inhibition of fatty acid oxidation modulates immunosuppressive functions of myeloid-derived suppressor cells and enhances cancer therapies," *Journal for ImmunoTherapy of Cancer*, vol. 3, no. S2, pp. O18–O47, 2015.

[35] S. Fu, K. He, C. Tian et al., "Impaired lipid biosynthesis hinders anti-tumor efficacy of intratumoral iNKT cells," *Nature Communications*, vol. 11, no. 1, p. 438, 2020.

[36] S. Wang, R. Liu, Q. Yu, L. Dong, Y. Bi, and G. Liu, "Metabolic reprogramming of macrophages during infections and cancer," *Cancer Letters*, vol. 452, pp. 14–22, 2019.

[37] W. Yu, Q. Lei, L. Yang et al., "Contradictory roles of lipid metabolism in immune response within the tumor microenvironment," *Journal of Hematology & Oncology*, vol. 14, no. 1, p. 187, 2021.

[38] B. I. Reinfeld, M. Z. Madden, M. M. Wolf et al., "Cell-programmed nutrient partitioning in the tumour microenvironment," *Nature*, vol. 593, no. 7858, pp. 282–288, 2021.